

# Design, Characterization and Development of Various Plasmonic Optical Sensors for Biomedical Applications

*A thesis submitted  
in partial fulfillment for the degree of*

Doctor of Philosophy

by

Niteshkumar Subhash Agrawal



Department of Avionics  
INDIAN INSTITUTE OF SPACE SCIENCE AND TECHNOLOGY  
Thiruvananthapuram - 695547

July 2021

# CERTIFICATE

This is to certify that the thesis titled **Design, Characterization and Development of Various Plasmonic Optical Sensors for Biomedical Applications**, submitted by **Niteshkumar Subhash Agrawal**, to the Indian Institute of Space Science and Technology, Thiruvananthapuram, for the award of the degree of **Doctor of Philosophy**, is a bonafide record of the research work done by him under our supervision. The contents of this thesis, in full or in parts, have not been submitted to any other Institute or University for the award of any degree or diploma.

**Dr. Chinmoy Saha,**  
Associate Professor  
Department of Avionics,  
Indian Institute of Space Science and  
Technology (IIST), Thiruvananthapuram

**Dr. Chandrakanta Kumar,**  
Scientist/Engineer-'SG',  
U R Rao Satellite Centre,  
Indian Space Research  
Organization (ISRO), Bangalore

**Dr. Deepak Mishra**  
Head of the Department  
Department of Avionics,  
Indian Institute of Space Science and  
Technology (IIST), Thiruvananthapuram

Place: Thiruvananthapuram  
July 2021

## DECLARATION

I declare that this thesis titled **Design, Characterization and Development of Various Plasmonic Optical Sensors for Biomedical Applications** submitted in fulfillment of the Degree of Doctor of Philosophy is a record of original work carried out by me under the supervision of **Dr. Chinmoy Saha (IIST, Thiruvananthapuram)** and **Dr. Chandrakanta Kumar (URSC, ISRO, Bangalore)**, and has not formed the basis for the award of any other degree, diploma, associateship, fellowship or other titles in this or any other Institution or University of higher learning. In keeping with the ethical practice in reporting scientific information, due acknowledgments have been made wherever the findings of others have been cited.

Place: Thiruvananthapuram  
July 2021

Niteshkumar Subhash Agrawal  
Research Scholar  
Department of Avionics  
Roll No.: SC18D047

## ACKNOWLEDGEMENTS

I have been engaged in doctoral research at the Indian Institute of Space Science and Technology (IIST), and U R Rao Satellite Centre (URSC- ISRO), under the AICTE-INAE-TRF fellowship scheme of ISRO/DoS-INAE. It was a great opportunity, honor, and privilege to work at Shandong Key Laboratory of Optical Communication, School of Physics Science and Information Technology, Liaocheng University (LCU), China for carrying out experimental studies of my research work. I am indeed indebted to all these organizations for providing me with the necessary supports and facilities during the period of my research work.

Firstly, I express my most sincere gratitude towards my research supervisors **Dr. Chinmoy Saha of IIST** and **Dr. Chandrakanta Kumar of URSC- ISRO** for their continuous guidance, support, and encouragement during my entire Ph.D. work. It was a real joy to work with them and I must say that without their whole-hearted support and care, it was not possible to complete my Ph.D. work successfully. I am greatly indebted to **Dr. V. K. Dadhwal, Director, IIST**, **Dr. Niveditha B K, Deputy Director, ISRO Headquarters, Bangalore**, **Dr. Y. V. N. Krishna Murthy, Registrar, IIST**, and **Dr. Raju K. George, Dean (R&D), IIST** for their support and kind approval on foreign collaboration for the experimental work. I am also thankful to **Dr. Deepak Mishra, HoD Dept. of Avionics**, and **Prof. B S Manoj, Dept. of Avionics** for the fruitful and timely advice, comments that constantly kept me inspired and encouraged at various stages of Ph.D. endeavor.

I take this opportunity to thank my doctoral committee members - **Dr. Basudev Majumder, Dr. Sooraj R**, and **Dr. Resmi L** for their regular and valuable inputs, comments, and suggestions, and for steering the Ph.D. thesis towards the proper path. I would like to express my

gratitude to **Dr. Santosh Kumar, Associate Professor, School of Physics Science and Information Technology, Liaocheng University, China,** and **Dr. Bingyuan Zhang, Vice-Dean, School of Physics Science and Information Technology, Liaocheng University, China** for providing a wonderful research platform and unfailing guidance and support.

I am highly grateful to Mr. Pramod M, Mr. Jeeva B, Mr. Avinash C, Dr. Lokendra Singh, Mr. Guo Zhu, Mr. Qing Shan Yang, Ms. Elizabeth G, and Ms. Gopika R who in their own way made my Ph.D. experience joyful and easy-going.

I would like to thank my family members, friends, and well-wishers for their support. After all, I am indebted to the Almighty for giving me the health, wisdom, and strength to pursue my passion.

Niteshkumar Subhash Agrawal

## ABSTRACT

In the recent past, rapid development and globalization have brought healthcare issues to the fore. Nowadays, healthcare has become the most essential and challenging matter worldwide. Because of that, demands for fast and low-cost detecting methods and devices in biomedical industries have been growing rapidly. Plasmonics has attracted a lot of attention in the arena of medical diagnostic due to the unique optical properties of plasmon resonant nanostructures (NSs). Enough attention has been given to the development, preparation, and durability of plasmon materials. A variety of materials, structures, and functionalities are closely related to the basic structure of plasmonics, which allows for the development of biosensors that can be used in real-life situations. The proposed localized surface plasmon resonance (LSPR) phenomenon-based optical fiber sensors (OFSs), thoroughly investigated in the present thesis, have great potential and can contribute immensely to biosensing field in coming days, both on research and application fronts. Owing to the diversity and nature of the work requiring complementary skills and expertise, many scientists and researchers from the multidisciplinary fields/ areas are increasingly getting involved in this area of LSPR based OFSs. These sensors have the special ability to detect molecules associated with events in real-time. Advances in nanotechnology and nanoscience have allowed the development of plasmonic NSs, thin films, and highly sensitive methods for the determination of optical properties. Advances in nanotechnology and nanoscience have made it possible to develop plasmon NSs, thin films, and development of a highly sensitive optical characterization technique. Different aspects of LSPR based OFSs like, detection schemes, realization, configuration, component, and application of sensors have been reported here. Moreover, advantages and challenges related to several practical aspects, synthesis of nanomaterials (NMs), detection mechanisms, and innovative methodologies to enhance the sensitivity, selectivity, and limit of detection (*LoD*) is thoroughly studied and highlighted. The latest challenges in engineering and role of different NMs (metallic, magnetic, carbon-based NMs, latex nanoparticles (NPs), etc.) to enhance the performance of optical sensors are discussed as well. Such information should provide useful insight needed for further development of future plasmonic biosensors.

The present thesis deals with the design, characterization, and development of various LSPR phenomenon-based OFSS for various biomedical applications. These include different configurations of the sensors and activation methodologies aimed at detection and measurements of some of the very important analytes present in human body fluids. These arrays of newly developed sensors are briefly mentioned below:

1. *Dopamine Sensor*: Dopamine (DA) biosensor using silver NPs (AgNPs) nanocoated tapered optical fiber probe has been successfully designed and developed. The important sensing parameter such as linear range, *LoD*, sensitivity, and correlation coefficient (CC) that could be achieved are 10 nM - 1  $\mu$ M, 0.058  $\mu$ M, 9.7 nm/  $\mu$ M, and 0.992, respectively. Typical challenges and concerns of these types of LSPR sensors have been considered thoroughly in this work.

2. *Ascorbic Acid Sensor*: Periodically tapered optical fiber structure with gold NPs (AuNPs), and graphene oxide (GO) nanocoated ascorbic acid (AA) sensor probe has been developed. Comparative performance for four, five, and eight sections periodically tapered structures-based AA sensor have also been investigated. The results such as *LoD*, sensitivity, and CC for proposed AA sensor (Probe-2) are recorded as 51.94  $\mu$ M, 8.3 nm/mM, and 0.9724, respectively.

3. *L-Cysteine Sensor*: Development of LSPR phenomenon-based L-Cysteine (L-Cys) biosensors have been demonstrated successfully. Structural advancements such as tapering and hetero-core design are employed in the development of proposed L-Cys sensor. Nanomaterials such as AgNPs and GO are used to improve the sensitivity. The combined features of two different structural modifications (i.e., tapered and hetero-core), results in significantly increased linearity range, CC, sensitivity, and *LoD* and their values are recorded as 10 nM- 1 mM, 99.04%, 7.0 nm/mM, and 63.25  $\mu$ M, respectively.

4. *Cholesterol Sensor*: LSPR phenomenon-based Cholesterol (Cho) sensor has been investigated and realized. An improvised and a new combination of multimode fiber (MMF), photosensitive fiber (PSF), and single-mode fiber (SMF) based core mismatch MMF-PSF-MMF (MPM) and SMF-PSF-SMF (SPS) structure has been proposed for the first time. Moreover, NMs such as AuNPs, and zinc-oxide NPs (ZnO-NPs) are deposited over the proposed bare fiber structure for improving the performance. The measured sensing parameters of proposed Cho sensor (Probe-1) like *LoD*, CC, and sensitivity are found to be 0.6161 mM, 0.9754, and 0.6898 nm/mM, respectively.

5. *Uric acid Sensor*: SMF-MMF-SMF-MMF-SMF (SMSMS) structure-based hetero-core design for the effective detection of uric acid (UA) has also been carried out. The requirement of sensing devices with a wide measurement range is fulfilled with these hetero-core structures. The performance of one of such sensor developed for the measurement of UA available with serum, with respect to *LoD*, sensitivity, and correlation correlator are observed as 69.26  $\mu\text{M}$ , 6.15 nm/mM, and 0.9439, respectively, whereas those parameters for detection of UA available with urine, are observed as 0.35 mM, 1.23 nm/mM, and 0.9695, respectively.

# TABLE OF CONTENTS

<b>CERTIFICATE</b>		<b>i</b>
<b>DECLARATION</b>		<b>ii</b>
<b>ACKNOWLEDGEMENT</b>		<b>iii</b>
<b>ABSTRACT</b>		<b>v</b>
<b>LIST OF TABLES</b>		<b>xi</b>
<b>LIST OF FIGURES</b>		<b>xii</b>
<b>ABBREVIATIONS</b>		<b>xvi</b>
<b>CHAPTER 1</b>	<b>Introduction</b>	<b>1</b>
1.1	Plasmonic Optic Fiber Sensors: An Overview	2
1.1.1.	Biosensing	2
1.1.2	Plasmonic Sensors	2
1.1.3	Advantages of Optic Fiber Sensors	3
1.2	Motivation, Scope, and Objective	4
1.3	Thesis Contribution	5
1.4	Thesis Outline	6
<b>CHAPTER 2</b>	<b>Literature Survey, Design Methodology and Role of Nanomaterials</b>	<b>8</b>
2.1	Introduction	9
2.2	Plasmonic Sensors	9
2.2.1	Surface Plasmon Resonance Phenomenon	10
2.2.2	Localized Surface Plasmon Resonance Phenomenon	10
2.3	Structural Developments	12
2.4	Nanomaterials and Their Significant Role	13
2.5	Characterization of Nanomaterial and Sensor Probes	13
2.6	Sensor Development and Applications	14
2.7	Major Instruments Used for the Investigation	18
2.8	Summary	21
<b>CHAPTER 3</b>	<b>Development of Dopamine Sensor using Tapered Optical Fiber</b>	
	<b>Sensor Probe</b>	<b>22</b>

3.1	Introduction	23
3.2	Experimental Methodology	24
3.2.1	Sensor Fabrication and Design Consideration	24
3.2.2	Synthesis of Silver Nanoparticles	26
3.2.3	Silver Nanoparticles Nanocoating and PEG Functionalization	27
3.3	Characterization and Measurement	28
3.4	Results and Discussion	29
3.4.1	Performance of Dopamine Sensor	29
3.4.2	Selectivity, Reproducibility and Reusability Test	33
3.5	Summary	35
<b>CHAPTER 4</b>	<b>Development of Ascorbic Acid Sensor using Periodically Tapered Optical Fiber Sensor Probe</b>	<b>36</b>
4.1	Introduction	37
4.2	Experimental Methodology	38
4.2.1	Sensor Fabrication and Design Consideration	38
4.2.2	Synthesis of Nanomaterials	38
4.2.3	Nanocoating and Enzyme Functionalization	40
4.3	Characterization and Measurement	40
4.4	Results and Discussion	44
4.4.1	Performance of Ascorbic Acid Sensor Probe	44
4.4.2	Selectivity Test	45
4.5	Summary	48
<b>CHAPTER 5</b>	<b>Development of L-Cysteine Sensor using Tapered SMS Structure based Optical Fiber Sensor Probe</b>	<b>49</b>
5.1	Introduction	50
5.2	Experimental Methodology	51
5.2.1	Sensor Fabrication and Design Consideration	51
5.2.2	Nanomaterial Synthesis and Immobilization Process	53
5.3	Characterization and Measurement	53
5.4	Results and Discussion	55

5.5	Summary	60
<b>CHAPTER 6</b>	<b>Development of Cholesterol Sensor using Core Mismatch MPM/SPS Structure based Optical Fiber Sensor Probe</b>	<b>61</b>
6.1	Introduction	62
6.2	Experimental Methodology	63
	6.2.1 Sensor Fabrication and Design Consideration	63
	6.2.2 Nanomaterial Realization, Nanocoating, and Functionalization Process	65
6.3	Characterization and Measurement	65
6.4	Results and Discussion	70
	6.4.1 Performance of Cholesterol Sensor	70
	6.4.2 Reusability, Reproducibility, and Selectivity test	73
6.5	Summary	76
<b>CHAPTER 7</b>	<b>Development of Uric Acid Sensor using SMSMS-MZI Structure based Optical Fiber Sensor Probe</b>	<b>78</b>
7.1	Introduction	79
7.2	Experimental Methodology	80
	7.2.1 Sensor Fabrication and Design Consideration	80
	7.2.2 Nanomaterial Realization, Immobilization, and Functionalization Process	80
7.3	Characterization and Measurement	81
7.4	Results and Discussion	84
	7.4.1 Performance of Uric Acid Sensor	84
	7.4.2 Reproducibility, Reusability, and Selectivity Test	85
7.5	Summary	90
<b>CHAPTER 8</b>	<b>Conclusion and Future Scope</b>	<b>91</b>
8.1	Conclusion	92
8.2	Future Scope	94
	REFERENCES	96
	LIST OF PUBLICATIONS	112

## LIST OF TABLES

1.1:	Advantages of optical fiber-based sensors	4
2.1:	Summary of plasmonic phenomenon-based optical fiber sensors	17
3.1:	Comparative study of dopamine sensors	32
4.1:	Comparative study of ascorbic acid sensor	47
5.1:	Comparative study of L-Cysteine sensors	59
6.1:	Performance of proposed cholesterol sensors	73
6.2:	Comparative study of cholesterol sensors	76
7.1:	Performance of proposed uric acid sensor	87
7.2:	Comparative study of uric acid sensors	89

# LIST OF FIGURES

2.1: (a) Fusion splicer, and (b) combiner manufacturing system (CMS)	18
2.2: (a) Vacuum drying oven, (b) fume hood, (c) dry nitrogen gas cylinder, (d) plasma centrifuge machine, (e) ultrasonic cleaning machine, and (f) ultrasonic homogenizer sonicator	19
2.3: (a) SEM and EDS, and (b) AFM	20
2.4: (a) High resolution (HR) spectrometer, and (b) tungsten halogen light source	20
3.1: (a) Sensor configuration, and (b) SEM images of proposed DA sensor probe	25
3.2: Schematic of sensor probe nanocoating procedure	26
3.3: Schematic of dopamine sensor measurement setup	27
3.4: Analysis of AgNPs (a) absorbance spectrum, (b) HR-TEM image, (c) histogram to analyze the size, (d) EDS image	29
3.5: SEM images of dopamine sensor probe at (a) lower magnification, (b) higher magnification	30
3.6: Results of dopamine detection (a) LSPR spectra, and (b) Linearity plot	31
3.7: Selectivity test for dopamine sensor (a) test 1 (in presence of other analytes), and (b) test 2 (in presence of ascorbic acid coexist with dopamine)	33
3.8: Reproducibility and (b) reusability test of dopamine sensor	34

4.1: Schematic of (a) four tapered structure, and (b) experimental setup and different configurations of AA sensor	39
4.2: Schematic of nanocoating, and functionalization process	41
4.3: The fiber length vs. diameter analysis of (a) Probe-1, (b) Probe-2, and (c) Probe-3; and (d) SEM image of the multi-tapered probe	41
4.4: Absorbance spectrum of (a) AuNPs, and (b) GO; HR-TEM image of (c) AuNPs, and (d) GO; and (e) histogram of AuNPs	42
4.5: SEM image at lower magnification of (a) Probe-1, (b) Probe-2, and (c) Probe-3; (d) SEM image at higher magnification, and (e) EDS image of proposed Probe-2	43
4.6: Analysis of tapered MMF vs. tapered SMF optical fiber probe	45
4.7: (a) LSPR spectra, and (b) linearity plot of Probe-1; (c) LSPR spectra, and (d) linearity plot of Probe-2; (e) LSPR spectra, and (f) linearity plot of Probe-3	46
4.8: Selectivity test of the ascorbic acid sensor	47
5.1: Graphical abstract of plasmonic sensors for detection of L-Cysteine	51
5.2: (a) Schematic view of bare fiber probe, and (b) wave propagation through sensor probe	52
5.3: Schematic view of a nanocoating process	54
5.4: Absorbance spectrum of (a) silver NPs, and (b) graphene oxide; HR-TEM image of (c) silver NPs, and (d) graphene oxide	55

5.5: SEM image of Probe-2 recorded at (a) lower magnification, and (b) higher magnification, and (c) EDS image of Probe-2	56
5.6: Schematic of experimental setup for measurement of L-Cysteine	57
5.7: LSPR spectra of (a) Probe-1, (b) Probe-2	58
5.8: Linearity plot of L-Cysteine sensor	59
5.9: (a) Reproducibility and (b) reusability test for Probe-2	60
6.1: Schematic of different configurations and design considerations of proposed P-OFSs (a) MPM, and (b) SPS	64
6.2: Different configurations of cholesterol sensor, (a) Probe-1, (b) Probe-2, and (c) Probe-3	64
6.3: Schematic of nanocoating process	66
6.4: Schematic of enzyme functionalization process	66
6.5: Absorbance spectrum of (a) 10 nm and 30 nm AuNPs, and (b) ZnO-NPs; HR-TEM image of (c) 10nm_ AuNPs, (d) 30nm_ AuNPs, and (e) ZnO-NPs; (f) AFM of ZnO-NPs, histogram analysis of (g) 10nm_ AuNPs, and (h) 30nm_ AuNPs	68
6.6: SEM image of (a) 10nm_AuNPs and ZnO-NPs nanocoated probe, (b) 30nm_AuNPs and ZnO-NPs nanocoated probe, and (c) sensor probe at higher magnification, and (d) EDS image	69
6.7: Schematic of an experimental setup for the measurement of cholesterol	69

6.8: Structural optimization of (a) MPM Vs. MSM structure, (b) calibration curve of PSF length used in proposed SPS/ MPM structure, (c) calibration plot to analyze the etching time of probe, and (d) etching time Vs. waist diameter calibration plot	70
6.9: LSPR spectra for (a) Probe-1, (b) Probe-2, and (c) Probe-3	71
6.10: (a) Linearity plot of Probe-1 and -2, and linearity plot of (b) Probe-1 and -3	72
6.11: (a) Reusability, and (c) reproducibility test for Probe-1	74
6.12: Selectivity test for (a) Probe-1, and (b) Probe-2	75
7.1: Schematic of optical signal propagation via. proposed structure	81
7.2: Absorbance spectrum of (a) AgNPs, and (b) CuO-NPs; HR-TEM image of (c) AgNPs, and (d) CuO-NPs; SEM image at (e) lower magnification, and (f) higher magnification; (g) EDS image	83
7.3: Schematic of a measurement setup for the detection of uric acid and enlarge view of sensor	83
7.4: LSPR spectra for (a) Probe-1, and (b) Probe-2	85
7.5: Linearity plot of uric acid sensor for (a) serum sample, and (b) urine sample	86
7.6: Reproducibility test for (a) Probe-1, and (b) Probe-2; reusability test for (c) Probe-1 (d) Probe-2	87
7.7: Selectivity test of Probe-2 with (a) serum biomolecules, and (b) urine biomolecules	88

## ABBREVIATIONS

AA	Ascorbic Acid
AFM	Atomic Force Microscope
AgNPs	Silver Nanoparticles
AOx	Ascorbate Oxidase
AuNPs	Gold Nanoparticles
BNPs	Bimetallic Nanoparticles
CC	Correlation Coefficient
Cho	Cholesterol
CMS	Combiner Manufacturing System
CuO-NPs	Copper Oxide Nanoparticles
DA	Dopamine
$D_p$	Penetration Depth
EDS	Energy Dispersive X-Ray Spectroscopy
EMI	Electromagnetic Interference
EWs	Evanescent Waves
FBG	Fiber Bragg Grating
GO	Graphene Oxide
HCF	Hollow-core fiber
HR-TEM	High Resolution - Transmission Electron Microscope
L-Cys	L-Cysteine
<i>LoD</i>	Limit of Detection

LPG	Long Period Grating
LSPR	Localized Surface Plasmon Resonance
LSPs	Localized Surface Plasmons
MCF	Multicore fiber
MMF	Multimode fiber
MMI	Multimode Interference
MZI	Mach Zehnder Interferometer
NA	Numerical Aperture
NIR	Near-Infrared
NMs	Nanomaterials
NPs	Nanoparticles
NSs	Nanostructures
PCF	Photonic crystal fiber
Pd	Palladium
PEG	Polyethylene Glycol
P-OFSs	Plasmonic-Optical Fiber Sensors
PSF	Photosensitive fiber
PSPs	Propagating Surface Plasmons
Pt	Platinum
RI	Refractive Index
SCW	Series Combiner Workstation
SD	Standard Deviation
SEM	Scanning Electron Microscope

SESS	Surface-Enhanced Spectroscopies
SMF	Single-mode fiber
SPP	Surface Plasmon Polariton
SPR	Surface Plasmonic Resonance
SPs	Surface Plasmons
SPWs	Surface Plasmon Waves
TEM	Transmission Electron Microscope
TIR	Total Internal Reflection
UA	Uric Acid
ZnO-NPs	Zinc Oxide Nanoparticles

# **Chapter 1**

## **Introduction**

## **1.1 Plasmonic Optic Fiber Sensors: An Overview**

### **1.1.1 Biosensing**

The biosensors engendered the research community owing to their boundless and versatile applications. This includes medical diagnostic (e.g. glucose biosensor or other biological analytes targets), environmental monitoring (e.g. detection of pesticides and heavy metal ions in river water contaminants), remote monitoring (e.g. airborne bacteria monitoring, ozone biosensors), DNA biosensing, monitoring of water qualities in remote areas, toxic level determination, food safety, and gas detection [1], etc. For the effective detection and measurement of biological analytes, various biosensing techniques, like, electrochemical, amperometric, piezoelectric, gravimetric, potentiometric, pyroelectric, thermometric, luminescent, magnetic, and optical methods are reported in past studies [2]. The rapid expansion of accurate and cost-effective biosensing devices has increased their use for medical diagnostic and other commercial applications. Moreover, the research community is immensely attracted to an optical technique-based sensor mainly in the area of biomedical applications. Plasmonic-optical fiber sensors (P-OFSs) proposed in this study belong to such a category. P-OFSs are extensively functional in various key areas viz. environmental monitoring, physical parameter sensing, medical diagnostics (analytes/virus/bacteria/DNA/RNA/cells detection), chemical sensing, and telemedicine [3]. Further, they have enhanced performance compared to conventional sensors in terms of many important sensing parameters which include sensitivity, passiveness, range of detection, limit of detection (*LoD*), data accuracy, and multiplexing capabilities [4]. P-OFSs also provide features like immunity to electromagnetic interference (EMI), light-weight, small size, low cost, flexibility, and stability under extraordinary circumstances like extreme temperature or pressures [5]. Due to all these advantages, nowadays P-OFSs are used in several research as well as commercial applications.

### **1.1.2 Plasmonic Sensors**

In this technique, biomolecules are unlabeled and traced in their innate forms. Specifically, it targets the optical biosensors that make use of the refractive index (RI) change as a sensing transduction signal [6, 7]. Assorted unlabeled optical bio-sensing platforms are established like

surface plasmon resonance (SPR), localized SPR (LSPR), ring resonators, fiber gratings, and photonic crystals [8]. Mostly, sensing performance of each optical configuration is assessed and compared in respect of sensitivity and  $LoD$ . In SPR phenomena, the resonance transpires when the wave vector of the excitation light (evanescent waves (EWs)) matches with the wave vector of the surface plasmons, causing a reflectance spectrum/ sharp dip transmittance [9].

Presently, various bio-sensing devices are designed based on extremely potent LSPR optical sensing techniques. The LSPR phenomenon is a combined electron charge oscillation in metal nanoparticles (NPs) which are energized by input optical signal, and extremely sensitive to the local dielectric environment. When an electromagnetic wave links with the metallic NPs, plasmons begin to oscillate in the vicinity of NPs with a specific frequency, and resonance arises when the frequency of excitation light matches with the oscillating frequency of plasmons followed by extinction (i.e. scattering, and absorption) of light [10]. This technique has various key benefits such as portability, label-free detection, multiplexing ability, biocompatibility, high data accuracy, remote sensing, and real-time monitoring [11]. This is among the most effective, label-free detection plasmonic techniques and provides a kinetic resolution of bimolecular binding reaction [12]. As a result, LSPR is also used widely for chemical, physical, and bio-sensing applications [9]. Further, LSPR has several potent applications in the area of biomedical engineering like diagnosing, metabolites, and hormone revealing [13]. These sensors are developed using plasmonic nanostructures (NSs) having an exceptional capacity of enhancing the photoluminescence, caused by the interaction among the optical signal and metal NSs [14]. During the fabrication, nanomaterials (NMs) are deposited over the surface of bare fiber probe, which acts as a metal-dielectric interface, and consequently produces oscillation owing to free-electrons, when an optical signal passes through it [15]. These sensors are designed by varying the, i) type of fibers, ii) core diameter, iii) shape, and iv) alignment [16].

### **1.1.3 Advantages of Optic Fiber Sensors**

The advantages of OFSs are summarized in Table 1.1 as per different categories. Various optical fibers like single-mode fiber (SMF), photonic crystal fiber (PCF), photosensitive fiber (PSF), multimode fiber (MMF), multi-core fiber (MCF), hollow-core fiber (HCF), and other types of special fibers are used for designing P-OFSs. The use of optical fiber in sensing applications

yields a plethora of advantages [17] as summarized below:

- i. **Biocompatibility:** Inert materials, such as silica and plastic are used in the fabrication of optical fiber. These materials do not have any side effects when exposed to or absorbed by biological substances.
- ii. **EMI immunity:** Unlike electrochemical sensors, OFSs remain unaffected by EMI.
- iii. **Compact size, low weight, and flexibility:** This feature allows probes to be inserted inside the organism to enlighten its inner cavities with a catheter. This allows the diagnostic devices to reach remote body parts of an individual without open surgery.
- iv. **Multi-parameter sensing:** Optical fiber can multiplex as well as integrate the signals from diverse OFSs in optical networks, in time or wavelength domain.
- v. **Low cost:** Optical fiber-based communication has facilitated the reduction of development expenditures of optical devices. Therefore, the production of medical devices using this technology is cheaper.
- vi. **Range of light propagation configurations:** An optical fiber guides the light, and it is possible to mould the internal light flux by modifying the fiber structure with different arrangements.
- vii. **Ability to work in hazardous media:** An optical fiber can offer improved performance in extreme situations like working near nuclear environments or the ocean [17].

## 1.2 Motivation, Scope, and Objective

Healthcare problems and associated technologies have now become the most essential and challenging area worldwide. Demands for fast, reliable, accurate, and low-cost detecting methods

Table 1.1  
Advantages of optical fiber-based sensors

Design	Environment	Others
Inert material	Chemical resistant	Biocompatible and sterilization
Robust packaging	Cryogenic to high temp.	Lightweight
Light power	EMI insensitive	Intrinsically safe
Small size	In situ monitoring	Cheaper
Less attenuation	Remote monitoring	Multiplexing

and devices in biomedical industries have been growing rapidly in recent years, particularly in the underdeveloped regions of the world [18]. According to Dr. Joy Adamson, a renowned scientist, “More than 95% of innovations in the field of medical science are yet to come” [19]. In the field of health monitoring and diagnosis, the P-OFSs have shown extraordinary capabilities in realizing highly sensitive and accurate sensors for the measurement of biological analytes. This serves as a motivation for our current research work.

### **1.2.1 Objective of the work**

The key objective of this thesis is to design and develop simplified yet effective P-OFSs for the detection and measurement of biological analytes and urinary proteins. The work reported in this thesis was taken up with the following objectives:

- Theoretical understanding of the fundamentals of plasmonic and biosensing.
- Theoretical and practical understanding of plasmonic sensing methods.
- To study the chemical and biological processes involved in nanocoating of probe.
- Analysis of probe functionalization process.
- To study the development of different optical fiber structures.
- To study the development of plasmonic OFSs and their applications
- To study the utilization of OFSs for biomolecules monitoring
- Analysis of developed P-OFSs in presence of different biomolecules.

### **1.3 Thesis Contributions**

The primary contributions of our research work revolve around design of an efficient sensor for detection and measurement of the level of the analytes found in body fluid using P-OFSs. For this, multiple combinations of fiber structure along with different NMs are analyzed. Though the basic configuration of the sensor can remain the same, depending on the activation process of the sensor, it becomes sensitive to a particularly targeted analyte. In this thesis, five different sensors specific

to five different analytes are investigated. Detailed design, realization, and experimental results of these sensors are thoroughly reported in five exclusive chapters:

- Dopamine Sensor: Development of LSPR sensor using silver NPs (AgNPs) along with polyethylene glycol (PEG) immobilized/ functionalized optical tapered structure-based sensor probe to detect and measure dopamine (DA) concentration in serum is reported in chapter 3.
- Ascorbic Acid (AA) Sensor: A periodically tapered gold NPs (AuNPs) and graphene oxide (GO) – nanocoated OFSs is proposed to detect ascorbic acid (AA). It is reported in chapter 4 along with a comparative study over four, five, and eight tapered structure-based AA sensors.
- L-Cysteine Sensor: Features of hetero-core and tapered optical-fiber configuration are used in the development of novel types of P-OFSs. These feature-based tapered SMF-MMF-SMF (SMS) P-OFSs are projected for L-Cysteine (L-Cys) detection and are reported in chapter 5.
- Cholesterol Sensor: The ultra-sensitive AuNPs and zinc oxide NPs (ZnO-NPs) nanocoated sensor probes are investigated for the rapid, reliable, and accurate measurement of cholesterol (Cho) concentration. For this, various designs such as MMF-PSF-MMF (MPM) and SMF-PSF-SMF (SPS), also termed as core-mismatch configuration are proposed in chapter 6.
- Uric Acid (UA) Sensor: Uric acid (UA) sensor with copper oxide-NPs (CuO-NPs) and AgNPs immobilized SMF-MMF-SMF-MMF-SMF (SMSMS) core-mismatch sensor probe is proposed in chapter 7.

## 1.4. Thesis Outline

The plasmonic phenomenon and different OFSs based on this have broadly been distributed under eight chapters of this thesis.

The background information/knowledge in the form of literature survey, preliminary and basic concepts related to structural designing, and methodologies are discussed in **chapter-2**. It also describes the role of NMs in the development of P-OFSs and major findings over it. Moreover, the

tradeoffs associated with several research aspects, synthesis of NPs and the detection mechanisms, with innovative methodologies which were established to improve the sensitivity, selectivity, and *LoD* are highlighted.

**Chapter-3** is dedicated to the key advancement over tapered structured-based P-OFSs. The single tapered structure-based LSPR sensors for accurate and valuable detection of DA are proposed and discussed in this chapter.

The comparative study over periodically tapered optical fiber structure-based AA sensors is presented in **chapter-4**. For this single tapered SMF/ MMF, four tapered SMF, five tapered SMF, and eight tapered SMF/ MMF optical fiber-based designs are proposed and studied in different sections.

In a step of structural development, tapered and hetero-core design-based fiber optic-LSPR sensor is studied in **chapter 5**. A tapered SMS fiber structure-based LSPR sensor is designed and presented here for the detection of L-Cys, a urinary protein available with human body fluids.

**Chapter 6** involves the major development of hetero-core structure-based LSPR sensors. The emphasis of hetero-core structure on recent advances in P-OFSs and the approaches to overcome the limitations, future possibilities in sensing field are discussed in detail. Two major development over hetero-core structure-based sensors are deliberated in this part i.e., i) core mismatch SPS structure, and ii) core mismatch MPM structure-based Cho sensor.

In **chapter-7**, SMSMS design based In-line Mach Zehnder Interferometer (MZI) hetero-core arrangement is proposed for UA detection available with body fluid. This type of design greatly helps to mitigate the narrow range measurement issue with other LSPR sensors.

**Chapter 8** summarizes the study over different NMs, structural designs, characterization of NMs and probes, and analytes measurement using P-OFSs. Future trends and research areas are also summed up in this chapter, indicating the scope and potentials of rapid growth in biomedical applications.

# **Chapter 2**

## **Literature Survey, Design Methodology and Role of Nanomaterials**

## 2.1 Introduction

In recent times, biosensors are applied to a variety of applications like environmental monitoring, disease detection, point-of-care monitoring, drug discovery, forensics, ensuring food safety, and biomolecule detections [20, 21]. Especially, optical fiber-based LSPR sensors have great potential in contributing different kinds of sensing applications in biomedical industries [22]. A wide range of LSPR phenomenon-based OFSs is designed and developed for biomolecules, gas, pressure, chemicals, bacteria, DNA/ RNA, cells, and virus detection. These sensors are also applicable for food safety, point-of-care application, and environmental monitoring. In near future, this is going to be extended to pathogenic microorganisms (mycobacteria, fungi, and protozoa) detection. Because of their unique features, like, label-free detection, ease of fabrication, remote monitoring, biocompatibility, and immunity to electromagnetic interference, LSPR sensors are becoming more popular for versatile applications in biomedical fields. In addition to this, setup cost in LSPR phenomenon based sensing is relatively higher but due to low material cost and long durability the effective cost remains on the lower side. Synthesis of more effective NMs (metallic NPs, bi-metallic NMs, 2D NMs, nanorods, and other unique NMs), structural advancements (tapering, bending, micro-ball, hetero-core, core-mismatch, and other structural development), and different measurement techniques, have been employed to advance the sensing performance of P-OFSs. A review of latest developments and present state of the art in LSPR phenomenon-based OFSs are discussed in this chapter. The study includes an in-depth literature survey on structural development, synthesis of NMs, nanocoating processes, detection mechanism, and biosensing applications. Further, important stages and key challenges in development of LSPR sensors are also presented.

## 2.2 Plasmonic Sensors

Surface plasmons (SPs) are coherent oscillations of free electrons on the metallic surface excited by electromagnetic radiation at metal-dielectric interface [23]. SPs are usually classified into two classes i.e., propagating SPs (PSPs), and localized SPs (LSPs). Here, PSPs, and LSPs are excited on the metallic films, and NPs, respectively. Here, the term "plasmonic sensor" refers to a sensor that uses the spectral properties of the plasmon to act as a transducer of the sensor signal [14]. The

research community is greatly influenced by plasmonic sensors in last decade, due to its wide range of applications in clinical diagnostics, biomolecules detection, gas sensing, detection of physical parameters (temperature, pressure, etc.), medicine, security, food safety, and chemical sensing [24]. The various plasmonic sensing methods, such as SPR (based on PSPs), and LSPR (based on LSPs) were reported in past studies [25]. The phenomenon relevant in the present studies is discussed in brief in the following sections.

### **2.2.1 Surface Plasmon Resonance Phenomenon**

SPR is basically the oscillation of free electrons, in conduction band, that gradually increases due to the exchange of energy from the electromagnetic interaction at the metal-dielectric interface [26]. The evanescent field is very sensitive to any change in the RI of the surrounding environment. Eventually, when the RI of sensing medium changes, the SPR excitation will change consequently and the characteristics (viz. angle, wavelength, phase, etc.) of any incident wave get changed due to the interaction. Thus, the wave coming out of the active interaction zone will carry the information about the type of the SPR resonance i.e., about the surrounding medium [27].

### **2.2.2 Localized Surface Plasmon Resonance Phenomenon**

In principle of LSPR sensor, surface plasmon waves (SPWs) are optically excited by the EWs which are present in total internal reflection (TIR) of normal fiber region [28]. SPWs is a transverse electromagnetic wave, traveling along with the interfaces of two different mediums such as metal and dielectric [29]. Due to the real-time monitoring, label-free detection, and non-aggressive behavior of LSPR sensors, many of the plasmonic studies reported in last few years are based on LSPR phenomenon [30]. The SPR phenomenon becomes localized due to the use of nanometer-sized ( $\leq 100$  nm) metallic NPs and is termed LSPR [27]. In LSPR, resonance occurs when frequency of light matches exactly to the natural frequency of free electrons [31]. Overall, LSPR phenomenon is a collective oscillation of free electron charges in metallic NMs that are excited by light [32, 33]. This oscillation enhances the near-field amplitude at resonance wavelength and field is greatly localized and decays rapidly away from the dielectric interface of NPs [34]. Inter-particle coupling is identified by investigating the LSPR shift of metallic NPs [35]. The metallic NPs such as AuNPs and AgNPs exhibits unique optical extinction properties at visible and near-infrared

(NIR) regions, which greatly supports the LSPR phenomenon [36]. At the LSPR sensor output, wavelength shifts are directly related to the increase in the RI [37]. The use of optical fiber in LSPR based sensing shows a range of benefits viz. remote sensing, portability, immunity to electromagnetic interference, small size, lightweight, and multiplexing ability [38]. These sensors are developed using plasmonic NSs having an exceptional capacity of enhancing the photoluminescence, due to the interaction among the optical signal and metal NSs [39]. In LSPR, prime sensing parameters like sensitivity, *LoD*, and dynamic range are greatly dependent on the roughness, shape, and antibacterial behavior of metallic NPs [40]. LSPR concept within the context of OFSSs was proposed for the first time in 1980s. The development of sensors based on LSPR phenomenon is interdisciplinary and have greatly attracted many physicists, biologists, chemists, and material scientists. This enabled the creation of a large footprint in the world of sensors due to its numerous applications [41]. As a result, a large volume of research in different aspects of realization of more effective sensors is being carried out across the world. In this context, the contribution of the proposed work is briefed into following sections.

### 2.2.2.1 Theoretical Analysis

We assume that the NPs are spherical in shape with radius  $a$ , and z-polarized light of wavelength ' $\lambda$ '. The radius ' $a$ ' is much smaller than the wavelength of light i.e.  $a / \lambda < 0.1$ ). The resulting solution for the EM field outside the NPs are indicated by [42]:

$$E_{out}(x, y, z) = E_0 \hat{z} - \left[ \frac{\epsilon_{in} - \epsilon_{out}}{\epsilon_{in} + 2\epsilon_{out}} \right] a^3 E_0 \left[ \frac{\hat{z}}{r^3} - \frac{3z}{r^5} (x\hat{x} + y\hat{y} + z\hat{z}) \right] \quad 2.1$$

Here,  $\epsilon_{in}$  and  $\epsilon_{out}$  shows the dielectric constant of metal NPs, and external environment, respectively. Because  $\epsilon_{in}$  is highly dependent on wavelength, the first term in square brackets determines the dielectric resonance condition for NPs. When the dielectric constant of the metal is roughly equal to  $-2\epsilon_{out}$ , the EM field is enhanced relative to the incident field. In the case of AgNPs and AuNPs, this condition is met in the visible spectrum, which has important implications for surface-enhanced spectroscopies. The radius ' $a$ ' and external dielectric constant ( $\epsilon_{out}$ ) also play key roles in determining the EM field outside the NPs, consistent with experimental results. Further, extinction spectrum of the metal sphere is indicated as:

$$E(\lambda) = \frac{24\pi^2 N a^2 \epsilon_{out}^{3/2}}{\lambda \ln(10)} \left[ \frac{\epsilon_i(\lambda)}{(\epsilon_r(\lambda) + \chi \epsilon_{out})^2 + \epsilon_i(\lambda)^2} \right] \quad 2.2$$

Here,  $\epsilon_r$  and  $\epsilon_i$  are the real and imaginary components of the metal-dielectric function, respectively. Again, we note the wavelength dependence of the metal dielectric function of additional interest is the factor of  $\chi$  that appears in front of  $\epsilon_{out}$ . The value of  $\chi$  is 2 for the case of a sphere, but it takes on values as large as 20 to account for particle geometries with high aspect ratios. Because we can only solve the value of  $\chi$  analytically for spheres and spheroids, and we must approximate it for all other geometries.

There are several equations available in open source, which define the changes in a local environment. For example, the LSPR excitation wavelength maximum,  $\lambda_{max}$  is sensitive to the refractive index ( $n$ ) or dielectric constant ( $\epsilon$ ). These both terms are related by  $\epsilon = n^2$ . This leads to following relationship:

$$\Delta\lambda_{max} = m\Delta n \left[ 1 - \exp\left(\frac{-2d}{l_d}\right) \right] \quad 2.3$$

where  $m$  is the bulk RI response of the NPs;  $\Delta n$  is the change in RI induced by the adsorbate;  $d$ , and  $l_d$  are indicates the effective adsorbate layer thickness and characteristic EM-field-decay length, respectively. This relationship is the basis of LSPR wavelength-shift reported in the sensing experiments [42].

## 2.3 Structural Developments

Different types of standard optical fibers like PCF, SMF, PSF, MMF, HCF, MCF, and other special fibers are used for the development of P-OFSs. The special fiber such as PSF are sensitive to the UV radiations. At the same instance, the lower diameter of fiber core is responsible for the excitation of lower order modes due to mode squeezing phenomenon, which basically occurs on the excretion of EWs. This fiber reveals distinct properties such as withstanding up to 300 - 400°C (applicable in a harsh environment), less attenuation (allows to be used in longer lengths), and a larger difference in core/cladding index [43-45]. Due to these exceptional features, it is well suited for hydrophones, temperature sensing, FBG, strain sensing, geophones, biomedical sensing applications [46]. To improve the LSPR phenomenon, various structural advancements such as splicing of fiber, tapering, fiber bending, micro-ball, hetero-core, long-period grating (LPG), core-mismatch design, etc., are presented in past studies. Sophisticated instruments, such as, fusion splicer, series combiner workstation (SCW), and combiner manufacturing system (CMS) are used

in realizing different structures of the sensor. Various unique sensor designs, such as multi-tapered structure, tapered SMS- multimode interference (MMI) structure, in-line SPS and MPM structure, and SMSMS-MZI structure with improved range of detection and sensitivity are presented in this study.

## **2.4 Nanomaterials and Their Significant Role**

The detection in plasmonic sensors are influenced by, i) dielectric properties of the neighboring medium [47], and ii) composition, shape, and nature of NMs [10]. Various NSs shapes (spherical, triangles, octahedrons, prisms, cubes, bipyramids, nanorods, nanoshells, nanostars, etc.), and bimetallic NPs are reported and used for development of plasmonic sensors [48]. The unique feature of NPs helps in different aspects; e.g. large surface area allows them to bind with a wide range of functional ligands [49]. The latest challenge in developing and synthesizing different NMs (metallic, magnetic, carbon-based NMs, bimetallic-NPs, novel-NPs, etc.) to enhance the performance of plasmonic sensors are discussed herein. Nanotechnology is associated with synthesis, characterization, and application of NMs in the Nano range (1–100 nm). NMs are widely used in the field of science and technology in general. Specifically, over the last decade, application of nanotechnology in the field of Nano-medicine has enhanced significantly. Due to small size of NPs, it is widely used for the creation of new devices that are used in pharmaceutical companies. In recent years, due to quantum size effect, large surface area, and unique properties of metallic NPs, NMs such as AgNPs, AuNPs, ZnO-NPs, CuO-NPs, Platinum (Pt), and Palladium (Pd) have been extensively studied. These NMs are deposited over the sensor surface acts as a metal-dielectric interface, which is necessary for LSPR when an optical signal pass through it. These metallic NPs are used in diagnostic, drug regulation, labeling, and biosensors because of their high compatibility with biological system.

## **2.5 Characterization of Nanomaterials and Sensor Probes**

Characterization is the crucial process required to fully comprehend the behavior of NMs [50]. To check the behavior and physical aspects of synthesized NMs and sensor probe, various characterization instruments are used during the development of the proposed P-OFSs. The

physical aspects focus on the confirmation of formation of NPs and determining their dimension, shape, degree of homogeneity, using sophisticated instruments like ultraviolet-visible spectroscopy (UV-Vis-spectroscopy), atomic force microscope (AFM), and high resolution-transmission electron microscope (HR-TEM) [51]. Further, energy dispersive X-ray spectroscopy (EDS), and scanning electron microscope (SEM) are generally engaged to characterize the surface of immobilized probes [52, 53]. UV-Vis-spectroscopy is used to check the spectral absorption of the prepared NMs solution, whereas AFM and HR-TEM are used to check the morphology of the synthesized NMs. In next step of characterization, SEM, and EDS are used to check the uniformity of NMs coatings and NMs present over the immobilized sensor probes.

## **2.6 Sensor Development and Applications**

The biosensor market has developed significantly over the last two decades, especially in the biomedical industry [54]. However, the application of biosensors is not restricted only to the healthcare sector [55], rather it is also useful in controlling an industrial process (11 %), animal husbandry and agricultural testing (8 %), defense and safety (6 %), environmental monitoring (5 %), research and development (R&D) (3 %), and automation (2 %) [56]. Since 1960 thousands of studies were reported for the development of biosensors most of which are related to medical applications [57]. This contribution is intended to increase the accuracy, safety, and rapid testing capabilities of the device [58, 59]. The current developments in nanotechnology show that the surface plasmons can be used for a specific application by varying the properties of different types of NMs [60, 61].

Various processes are involved in the development of LSPR-OFSs. These are: i) synthesis of NMs, ii) characterization of NMs, iii) fabrication of bare fiber probe, iv) cleaning of bare fiber probe, v) salinization of bare fiber probe, vi) immobilization of NMs, vii) characterization of nanocoated probe, and viii) enzyme functionalization [62]. The NMs, such as AuNPs, AgNPs, GO, CuO-NPs, platinum (Pt), ZnO-NPs, and palladium (Pd), have been extensively studied in past. Among these, AuNPs and AgNPs attracted remarkable attention, because of their unique chemical and physical properties. To synthesize different metallic NPs, various standard methods, such as wet chemical reduction method [63-65], lithography [66], and vapor deposition method [67-69] are adopted.

In fabrication process, several structural advancements are well investigated and proposed for the development of P-OFSs such as tapering [70, 71], bending [72, 73], chemical etching [74], splicing of different fibers [75], addition of highly sensitive dielectric layer [76], micro-ball structure [77], hetero-core structure [43], fiber Bragg grating (FBG) structure, etc. Among these processes, uncontrolled fabrication, surface irregularity, and uncertainty in outcomes are reported in bending and chemical etching methods [78, 79]. In P-OFSs, the EWs interact with the surrounding dielectric medium, for which tapering is the best choice [80]. Tapering is amongst the finest options to increase the penetration depth and allows the EWs to interact with outer medium [81]. It has been observed that tapered structure-based LSPR-OFSs helps to enhance the sensitivity and provides promising performance [82]. Post tapering, the core nearly gets merged with cladding and end configuration begins to support the multimode configurations [83]. Most of the optical fiber tapered structures are developed with the hydrogen flame-brushing method [84], thermally stabilized plasma technique [38], and sweep arc technique [85] to achieve a uniform waist. The hetero-core-based sensor design also grabs remarkable attention. In this technique propagating light waves might leak in cladding layer and will suit for LSPR phenomenon [86].

Various preparatory processes follow next. The bare sensor is cleaned using acetone and Piranha treatment to take out the unwanted elements from the surface. This process helps to improve surface density of reactive OH<sup>-</sup> groups [87]. This is followed by salinization with MPTMS or APTMS solution using a coupling agent to improve the connection of the metal NPs over the surface of sensor [88]. The immobilization process follows next in which synthesized NPs are deposited over a surface of sensor probe.

This plasmonic sensing is a highly evolving research field in last few years and extended to the areas like single-photon imaging, optical antennas, and treatment of cancer [72, 89]. Nowadays, LSPR phenomenon is comprehensively used to detect and diagnose different physical parameters in various fields and for diagnostics applications.

### **2.6.1 Biosensing Applications**

Medical diagnostics and bio-sensing are a few of the apt fields for applying the optical effect of LSPR [90]. Biosensing *in-vivo* and *in-vitro* detection, such as, analytes detection [70, 91, 92], bacteria detection [93-95], virus detection [96, 97], DNA/ RNA detection [98, 99], and cell detection [100, 101] using P-OFSs are largely investigated in last few years. However, some

challenges have to be addressed for accurate and sensitive measurement using LSPR sensors [102]. Following major observations were reported based on the investigation over the plasmonic-based optical sensing: (i) P-OFSs are used for the wide range of applications by observing the wavelength shift caused by the change in local RI, (ii) LSPR-OFSs techniques offers a higher sensitivity performance as that of SPR-OFSs with additional advantages of wavelength tenability, smaller sensing volume, and lower cost of instrumentation, (iii) LSPR-OFSs are single nanoparticle system providing higher sensitivity to RI than nanoparticle array or nanosheet, and (iv) electronic resonance enhances the wavelength shift as that of conventional RI based technologies [103-105]. To improve the performance of P-OFSs, some futuristic advancement can be expected in the following aspects: (i) investigation over high sensitivity and accurate sensors which can be used for commercial application, (ii) analysis using different nanoparticles, nanoclusters, and nanosheets on sensor surface to improve the performance of sensors, (iii) investigation on the multi-channel P-OFSs which can improve the sensing efficiency and correlation coefficient (CC), (iv) possible enhancement of the specificity of a sensor (selectivity) through the functionalization process over the NPs layer, and (v) investigation and realization of the improvement based on structural advancement. The research works that are studied and analyzed in present study will greatly contribute to the development and understanding of the plasmonic phenomenon-based sensing methods [106, 107]. The flexible design allows development of optical sensors with plasmonic metallic NSs. Hence, plasmon-enhanced optical sensors add to the applications in biomedical industries [108, 109].

The reports on LSPR-based OFSs to detect the various biomolecules such as Cho, UA, AA, DA, IgG, L-Cys, etc., are available in open literature. A summary of plasmonic phenomenon-based OFSs, reported in past for the detection of various analytes is provided in Table 2.1. It can be observed that various NMs such as AuNPs, AgNPs, GO, Glucose capped AgNPs and other NMs are utilized to boost the sensitivity of sensors. In last decade, plasmonics is getting embraced by biosensing due to the unique optical properties of plasmon resonant NSs, and significant attention has been given to the development, preparation, and durability of plasmon materials. A variety of materials, structures, and functionality is closely related to the basic structure of plasmonics, which allows us to develop practical biosensors that can be used in real-life situations.

Table 2.1  
Summary of Plasmonic Phenomenon based Fiber Optic Sensors

Material used	Detection	Mechanism	Structure used	Linear range	LoD	Sensitivity	Ref.
AuNPs	IgG	SPR/ LSPR		n.r <sup>a</sup>	37 ng/mL	3915 nm/RIU	[110]
AuNPs	Uric acid	LSPR	Micro-ball-SMF	50 $\mu$ M - 1 mM	n.r <sup>a</sup>	0.005 %/mM	[111]
AuNPs/ GO				10 $\mu$ M - 1 mM	65.60 $\mu$ M	2.1 %/mM	
AuNPs	Sulphide Ions	LSPR		4.16 - 41.63 $\mu$ M	0.54 ppm	n.r <sup>a</sup>	[112]
AuNPs	Cholesterol	LSPR	SMF-HCF	50 nM - 1 $\mu$ M	25.5 nM	16.149 nm/ $\mu$ M	[92]
AgNPs/GO	Cholesterol	LSPR	Simple SMF	0 - 10 mM	1.131 mM	5.14 nm/mM	[113]
AuNPs	Cholesterol	LSPR	Simple SMF	10 nM - 1 $\mu$ M	53.1 nM.	0.125 %/mM	[114]
AuNPs (10 nm)	Uric acid	LSPR	Tapered SMF	10 - 800 $\mu$ M	175.89 $\mu$ M	0.0073 nm/ $\mu$ M	[70]
AuNPs (30 nm)					280.07 $\mu$ M	0.0131 nm/ $\mu$ M	
AuNPs	Heavy metal lead ions	LSPR	Simple MMF	n.r <sup>a</sup>	n.r <sup>a</sup>	0.28 nm/mM,	[115]
AuNPs	Glucose	LSPR	Tapered SMF	0 - 10 mM	322 $\mu$ M	0.9261 nm/mM	[116]
GO/AuNPs /GO <sub>x</sub>	Glucose	LSPR	Tapered SMF	0 - 11 mM	2.26 mM	1.06 nm/mM	[117]
AuNPs/GO <sub>x</sub>	Glucose	SPR	TFBG (SMF)	1 - 500 $\mu$ M	N.R.	2.61 dB/ $\mu$ M	[118]
AuNPs	Glucose	SPR	Tapered SMF	n.r <sup>a</sup>	n.r <sup>a</sup>	~2180 nm/RIU	[119]
Silver and silicon	Ethanol	SPR	Simple SMF	n.r <sup>a</sup>	15.34 $\mu$ M	21.70 nm/mM	[120]
AuNPs	Thrombin	SPR/ LSPR	Tilted FBG	1- 35 nM	1 nM	3.21 $\times$ 10 <sup>7</sup> dB/M	[121]
Glucose capped AgNPs	Mercury	LSPR	Simple SMF	n.r <sup>a</sup>	2 ppb	n.r <sup>a</sup>	[122]
AuNPs	Glyphosate in Water	LSPR	LPG	n.r <sup>a</sup>	0.02 $\mu$ M	n.r <sup>a</sup>	[123]
GO	Uric acid	LSPR	SMS structure	10 - 800 $\mu$ M	259 $\mu$ M	0.0089 nm/ $\mu$ M	[124]
GO/AuNPs					206 $\mu$ M	0.0082 nm/ $\mu$ M	

<sup>a</sup> not reported.

## 2.7 Major Instruments Used for the Investigation

As mentioned earlier, this investigation needs many sophisticated tools and instruments. The photographs of various instruments used in fabrication of probe, characterization of NMs and sensor probe, and measurement are shown in Figs. 2.1-2.4. For realization of the basic structure from optical fibers by splicing and tapering, the combiner manufacturing systems (CMS, 3SAE, Japan), and fusion splicer (FSM:100P+, Fujikura, Japan) as shown in Fig. 2.1, are used. For further processing of the probe and preparing the NMs, many different processes are used. A

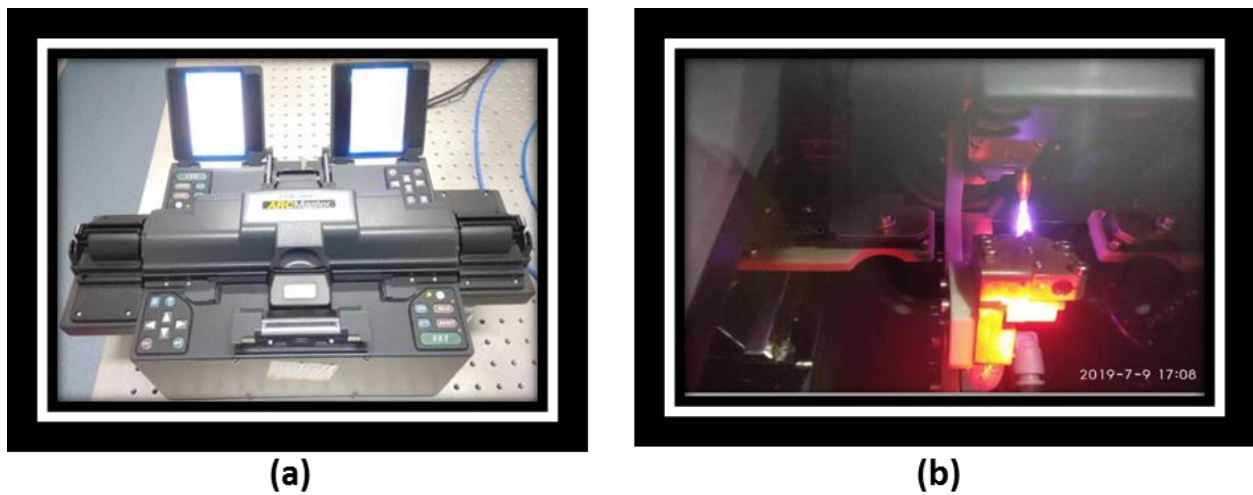
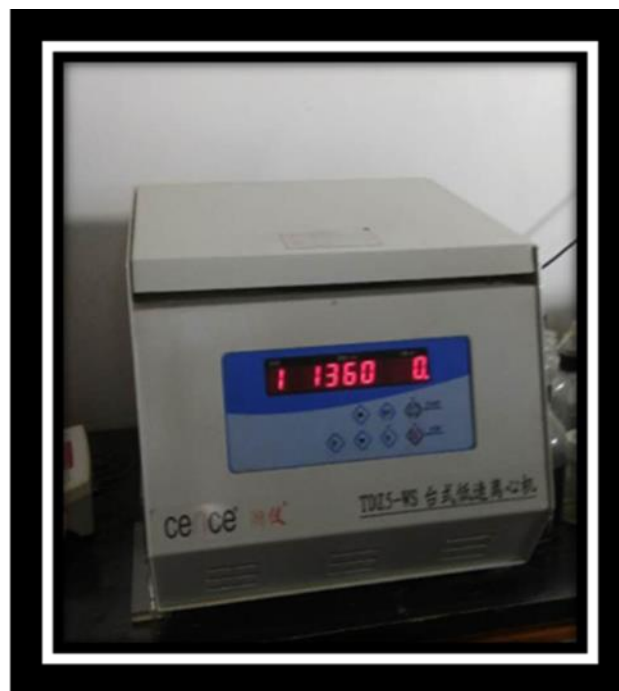


Figure 2.1: (a) Fusion splicer, and (b) combiner manufacturing system (CMS).





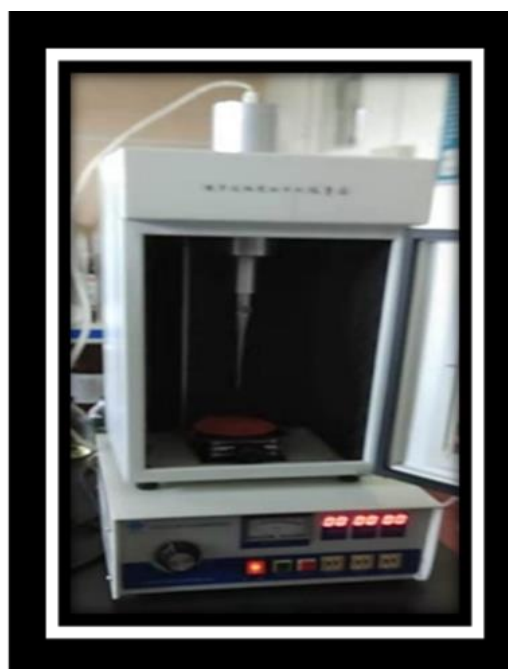
(c)



(d)



(e)



(f)

Figure 2.2: (a) Vacuum drying oven, (b) fume hood, (c) dry nitrogen gas cylinder, (d) plasma centrifuge machine, (e) ultrasonic cleaning machine, and (f) ultrasonic homogenizer sonicator.



(a)



(b)

Figure 2.3: (a) SEM and EDS, and (b) AFM.



(a)



(b)

Figure 2.4: (a) High resolution (HR) spectrometer, and (b) tungsten halogen light source.

vacuum drying oven and nitrogen gas cylinder are used during delicate drying processes, and for removing flammable solvents. To limit the exposure to hazardous or vapors, toxic fumes, and dusts fume hood is used. The plasma centrifuge machine was used for the separation of mixtures with close densities. On the other hand, for extraction of multiple compounds ultrasonic homogenizer sonicator is used. An ultrasonic cleaning machine is employed for high-quality cleaning. The photographs of all these instruments are presented in Fig. 2.2. The realized NMs and their coating on the sensor are characterized using HR-TEM (Talos-L120C), AFM (SPA 300 HV), and SEM/EDS (Gemini Carl Zeiss Microscopy) as shown in Fig. 2.3. For the final

measurement of analytes using proposed sensors, optical source (tungsten halogen- HL1000), and spectrometer (Ocean-Optics: HR 2000+) are used. The photographs of these instruments are presented in Fig. 2.4.

## 2.8 Summary

The plasmonic sensing area is widely explored in recent years and is considered to be among a few top emerging technologies. As mentioned above, LSPR phenomenon-based OFSs offers many potential applications in key areas including prospective, health monitoring and diagnostics, medicine, biotechnology, drug treatment, and nutrition monitoring. This chapter presents an overview of the existing work done by other researchers in the field of plasmonics sensing. The following major observations are recorded in this survey:

- i. Among various available configurations, tapered and hetero-core-based designs are best suited with regards to sensitivity, *LoD*, and range of linearity.
- ii. The metal NPs are in high demand in various sensing devices because of strong absorption bands available in the visible and NIR regions.
- iii. The primary NMs, such as AuNPs and AgNPs are synthesized using a wet-chemical method. It may leave some toxic content on the surface of probe during nanocoating process.
- iv. Due to this, AuNPs and AgNPs immobilized probes can further be coated with other NMs such as CuO-NPs, ZnO-NPs, 2D materials, GO, etc.
- v. The nanocoating material with a large surface area and higher biocompatibility are applicable for biosensing applications.
- vi. Many of the plasmonic phenomenon-based OFSs suffer from a narrow measurement range.

The plasmonic-OFSs has the potential to provide the platform for multiplexed analysis and specificity towards detection, which is crucial for medical diagnostics.

# **Chapter 3**

## **Development of Dopamine Sensor using Tapered Optical Fiber Sensor Probe**

### 3.1 Introduction

In chapter 2, basic concepts related to plasmonic sensors, plasmonic methodologies (i.e., SPR and LSPR) to detect different biomolecules, structural development, and design considerations of LSPR sensors, NMs, and their significant role in the development of P-OFSs were discussed. It also described the effective characterizations of NMs and sensor probes, past developments and biosensing applications of P-OFSs, background information in the form of literature surveys, and major instruments used during the development of sensor probes.

This chapter deals with tapered design-based P-OFSs for the measurement of Dopamine (DA) concentration. DA found in the central nervous system in human body is responsible for communication of nerve cells and is known as a messenger molecule. It controls locomotion, cognition, and neuroendocrine secretion and is a very vital indicator of human health [125]. Hence the detection and the measurement of DA are very crucial as it plays a major role in controlling the hormone and a neurotransmitter and thus the peripheral system in the human body [126]. The concentration of DA typically lies in the 10 nM to 1  $\mu$ M range in human body system. An abnormal DA level leads to severe diseases such as neurosis, deficit hyperactivity disorder, and parkinsonism [127]. This chapter explains about fabrication of proposed single tapered sensor probe and their design considerations DA detection present in central nervous system. This includes synthesis of AgNPs, nanocoating, and functionalization, characterization of synthesized AgNPs, and immobilized probe. The performance of proposed DA sensor is checked over the preliminary sensing parameters viz. sensitivity, *LoD*, linearity range, and *CC*. In addition, results of selectivity, reproducibility, and reusability test are presented below sections.

LSPR phenomenon-based sensor has shown great potential in biosensors development and is used for the detection of various biomolecules, hormones, and metabolites. In past, to improve the LSPR phenomenon, several modifications of the optical fiber structures, such as, tapering, bending, chemical etching, splicing the different fibers, and addition of a highly sensitive dielectric layer, etc., have been introduced during the development and fabrication of probes. Among these, as indicated in past studies, tapering method is found to be highly effective [128]. The tapered fiber structure is mostly distributed in three sections, namely, i) normal fiber section, ii) transition section, and iii) tapered section. Realization of single tapered structure-based P-OFSs comprises following steps: The proposed tapered optical fiber structure is immobilized with highly

biocompatible NMs such as AgNPs. In functionalization process, PEG is deposited over the AgNPs nanocoated probe. This helps to reduce the protein absorbance, which is best suited for LSPR phenomenon and enhances the sensitivity. The Ag (silver) is the most frequently used NMs for metal NPs productions. The LSPR phenomenon-based sensor is very sensitive to the variation in size, and shape of NPs, separation distance of NPs, compositions, geometry, and local dielectric environment [129].

## 3.2 Experimental Methodology

The experimental investigation involves different stages such as i) fabrication and design consideration of probe, ii) synthesis of AgNPs, and iii) characterization and the measurement of probes. Specific developments for the LSPR phenomenon-based DA sensors are presented below.

### 3.2.1 Sensor Fabrication and Design Consideration

The proposed LSPR phenomenon-based OFSs is proposed to detect the DA concentration available in serum. The tapered OFSs used in this study offers several attractive merits, including flexibility, compactness, and a higher evanescent field. This offers access to EWs of the mode propagating over the tapered section, easing exposure towards neighboring elements. The proposed sensor is designed with step-index SMF (8.2/125  $\mu\text{m}$ ), and a CMS machine is used during the development of probe with a tapered section. In the design of a bare tapered probe, the important fabrications parameters such as waist length, waist diameter, and transition region are considered as 4 mm, 40  $\mu\text{m}$ , and 5 mm, respectively. There is a possibility of fast drop in transmitted power and mode squeezing, also difficult to handle a fiber of too small waist-diameter (mechanically weaker) [130]. Therefore, proposed sensor is realized with a waist diameter of 40  $\mu\text{m}$  or more. The sensor configuration and SEM images of proposed sensor probe are presented in Fig. 3.1(a)-(b), respectively. The sensor is further immobilized with AgNPs, which offers more advantages for probes such as higher extinction coefficients, antimicrobial, sharper extinction bands, high field enhancements, high electrical conductivity, stability, and low sintering temperatures. The EWs have a vital role in LSPR based sensors. The distance traveled by the EWs at the core-clad boundary known as penetration depth ( $d_p$ ) is given by [20]:

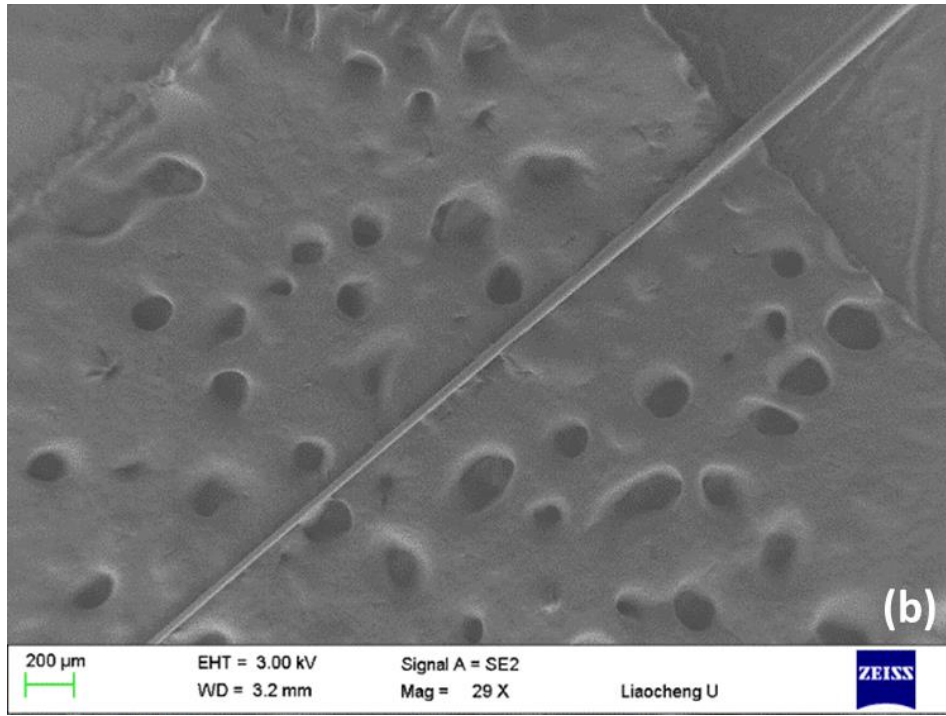
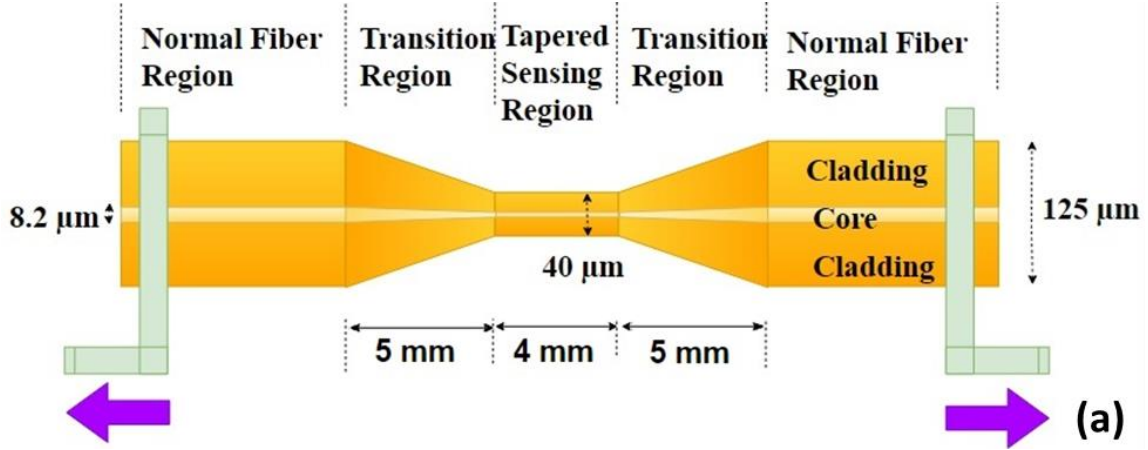


Figure 3.1: (a) Sensor configuration, and (b) SEM images of proposed DA sensor probe [131] © 2019 IEEE.

$$d_p = \frac{\lambda}{2\pi \sqrt{n_{co}^2 \sin^2 \theta_i - n_{cl}^2}} \quad (3.1)$$

where,  $n_{co}$ , and  $n_{cl}$  indicates the core, and cladding RI whereas  $\lambda$  and  $\theta_i$  are the optical signal wavelength, and angle of incidence of the light, respectively. In general, on disturbing TIR of SMF, two different kind of mode sustains i.e. two symmetric and two asymmetric modes. The symmetric modes propagate within the core whereas asymmetric modes propagate in the cladding.

The interaction of asymmetric modes with external medium causes the phase and wavelength variation in symmetric modes of core. In reported work, we prefer to call the asymmetric modes as the super-modes [132].

### 3.2.2 Synthesis of Silver Nanoparticles

A well-established electrochemical process [131] is used for the synthesis of AgNPs in present study. The reagents include silver nitrate ( $\text{AgNO}_3$ ), and reducing agent sodium borohydride ( $\text{NaBH}_4$ ), used during synthesis process. Ice-cooled  $\text{AgNO}_3$  (20 mL, 1 mM) solution is added dropwise in prepared  $\text{NaBH}_4$  (14 mL, 1 mM) solution and stirred vigorously for about an hour. As a result, the solution turns greenish-yellow that indicates the formation of the AgNPs in the solution. The formation of AgNPs was confirmed with absorbance spectrum using UV-spectrophotometer which was observed at 392 nm. Further morphology of AgNPs was observed using HR-TEM characterization machine.

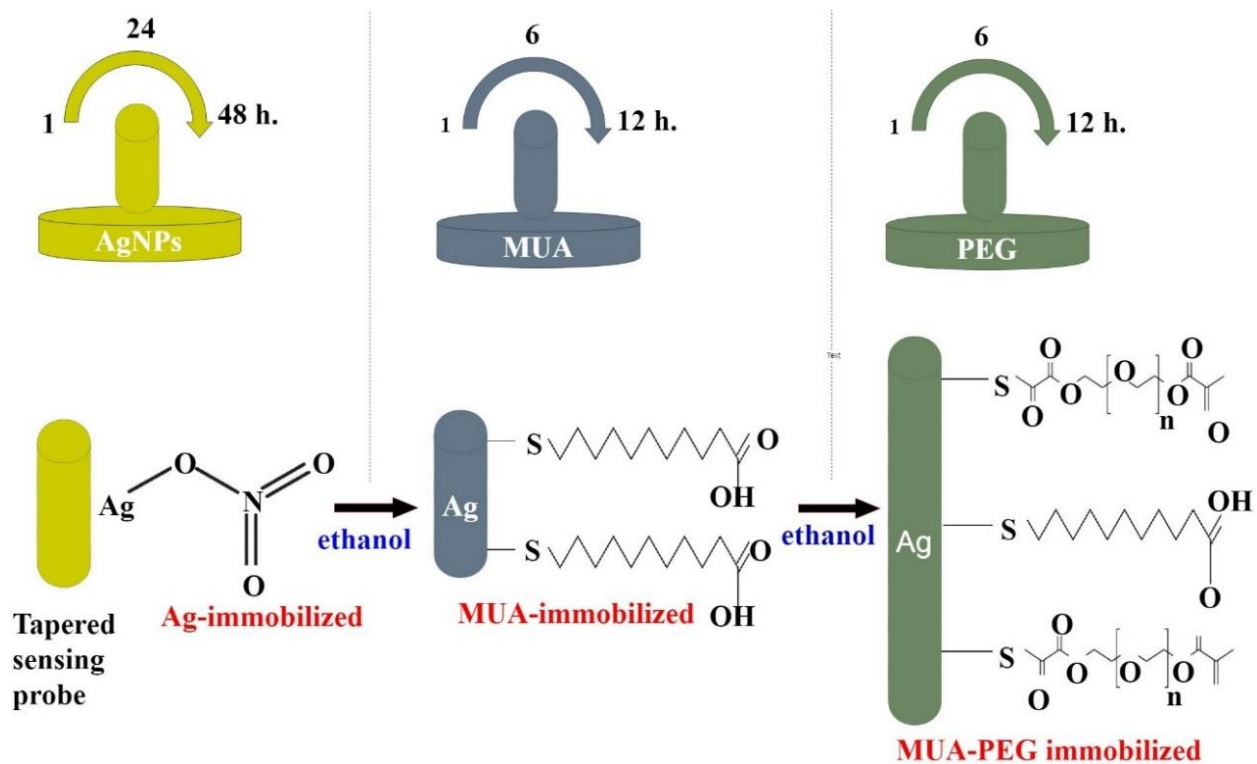


Figure 3.2: Schematic of sensor probe nanocoating procedure [131] © 2019 IEEE.

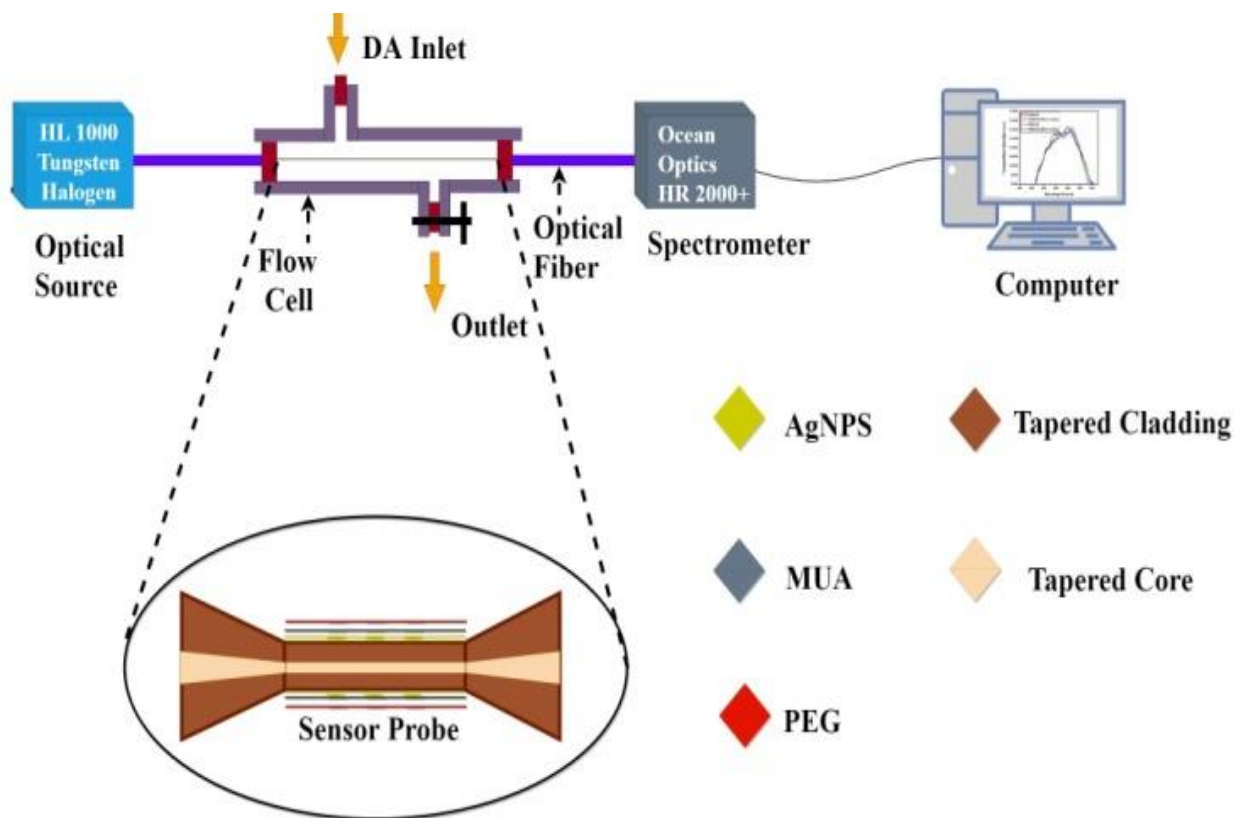


Figure 3.3: Schematic of dopamine sensor measurement setup [131] © 2019 IEEE.

### 3.2.3 Silver Nanoparticles Nanocoating and PEG Functionalization

The AgNPs/ PEG immobilization process, and measurement setup are elaborated in Fig. 3.2, and Fig. 3.3, respectively. The reagents such as 11-mercaptoundecanoic acid (MUA), PEG, hydrogen peroxide ( $H_2O_2$ ), sulfuric acid ( $H_2SO_4$ ), 3-mercaptopropyl trimethoxysilane (MPTMS), chloroform and phosphate-buffered saline (PBS) is used during the bare probe cleaning, salinization, and nanocoating process. Different cleaning and salinization steps are adopted before nanocoating over the bare fiber structure. The steps followed are, i) to remove the unwanted particles over the bare fiber sensor surface (sensing section) the fiber is dipped in acetone for 20 min, ii) subsequently to take away the resistant materials from sensor surface, bare fiber probe is kept in Piranha solution (contain  $H_2O_2$  and  $H_2SO_4$ ) for 30 min, and iii) for the salinization, the prepared MPTMS solution is deposited over bare fiber probe. Further, the salinized probe is rinsed and dried with ethanol and nitrogen gas, respectively to remove the uncoated elements. After that, a dip-coating process is used for the nanocoating of AgNPs over the salinized probe. It takes

around 48 hrs for uniform coating of AgNPs over the bare sensor structure, which is further confirmed with the SEM characterization. AgNPs are the most commonly used metal NMs during the development of LSPR phenomenon-based P-OFSs. AgNPs have many inherent advantages such as higher biocompatibility, extinction coefficients, field enhancements, and electrical conductivity, stability, and low sintering temperatures, these features have greatly benefited the development of highly sensitive DA sensors [131]. In the functionalization of AgNPs immobilized probe, MUA (10 ml, 10 mM) is first functionalized (it produces carboxyl groups which are found in acetic and amino acids that are used to build proteins). At the last, PEG is functionalized over the probe. PEG coating provides a range of advantages, such as i) low toxicity, ii) protection of lipoplexes from interaction with blood components, and iii) reduced protein absorption [133].

### **3.3 Characterization and Measurement**

The characterization and measurement of synthesized NPs and immobilized probes and techniques for effective DA detection have been discussed in this section. Instruments such as UV spectrophotometer, HR-TEM, SEM, and EDS are used during the experiment and the following important observations were recorded, i) sphericity of the synthesized AgNPs (with HR-TEM analysis), ii) absorbance spectrum at 392 nm (with UV spectrophotometer), iii) AgNPs mean diameter: around  $7.5 \pm 0.5$  nm (with histogram analysis- ImageJ software), iv) uniformity of the proposed AgNPs nanocoating over surface of a probe (using SEM analysis), and v) immobilized particles are silver (AgNPs) (confirmed with EDS analysis). All the observations are recorded from the NMs and NMs immobilized probes. Characterization results are indicated in Fig. 3.4, and Fig. 3.5, respectively. For the measurement of LSPR spectra, tungsten-halogen white light-source (emits the light with 300-1800 nm range) and optical spectrometer (detect the optical signal with 300-1000 nm range) is used. The different DA test sample is prepared in a range of 10 nM to 100  $\mu$ M for the experiment. The prepared test samples are stored at 2-8°C, when not in use. Spectrum is recorded only after the stabilization of output signal. Before injecting another test sample, the flow cell is cleaned with buffer solution (PBS).

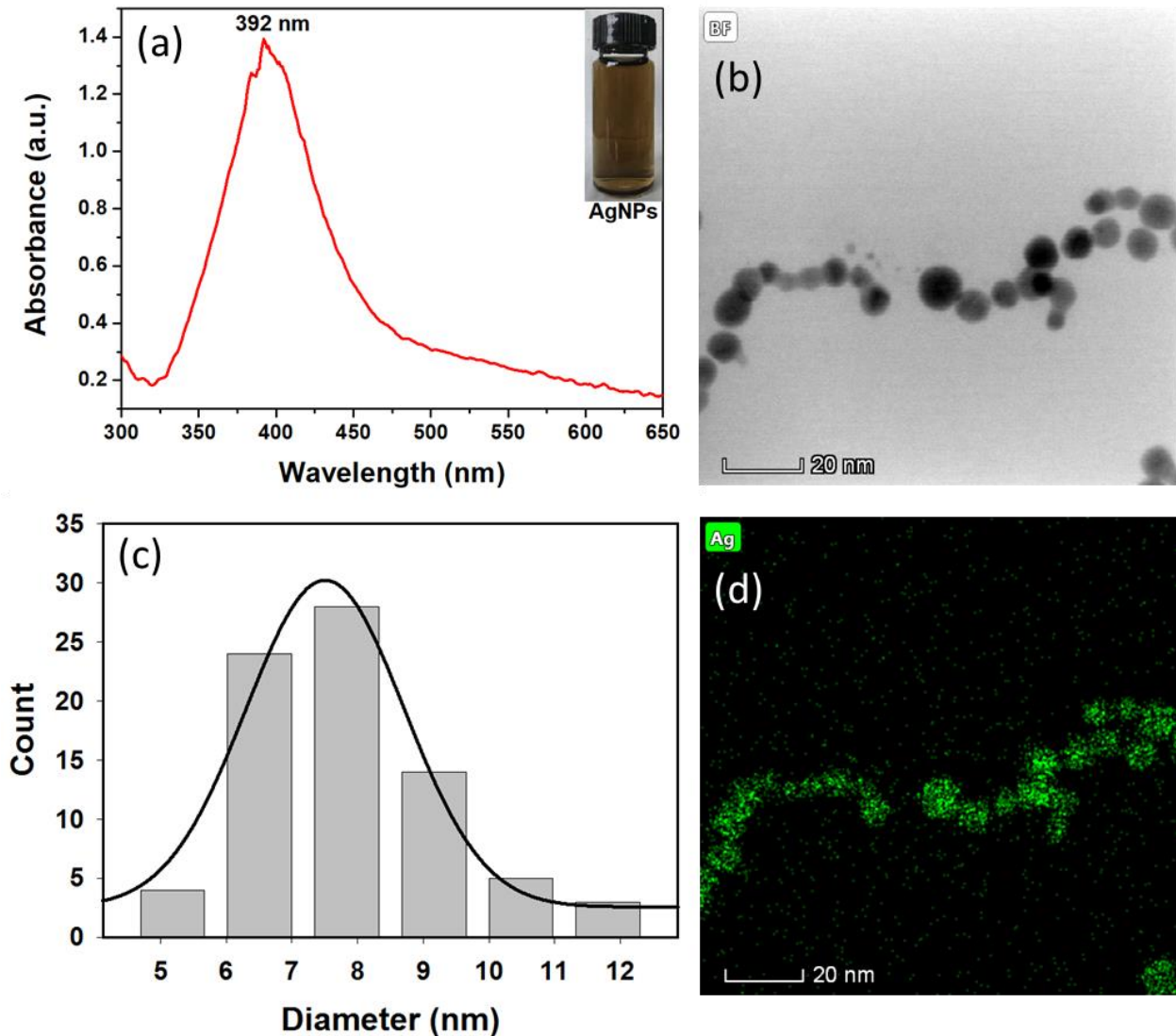


Figure 3.4: Analysis of AgNPs (a) absorbance spectrum, (b) HR-TEM-image, (c) histogram to analyze the size, (d) EDS image [131] © 2019 IEEE.

## 3.4 Results and Discussion

### 3.4.1 Performance of Dopamine Sensor

The performance of the newly developed DA sensor is analyzed based on the different prime sensing factors like sensitivity, selectivity, linearity range,  $CC$ ,  $LoD$ , reusability, and reproducibility. The spectral deviation is checked over the input light signal, LSPR spectra are observed over a large range of prepared DA samples. Figure 3.6 (a) indicates the LSPR spectra with different DA samples whereas, Fig. 3.6 (b) indicates the linearity curve for DA detection present in human body system. The prime indicators which help to check the ability of P-OFSs,

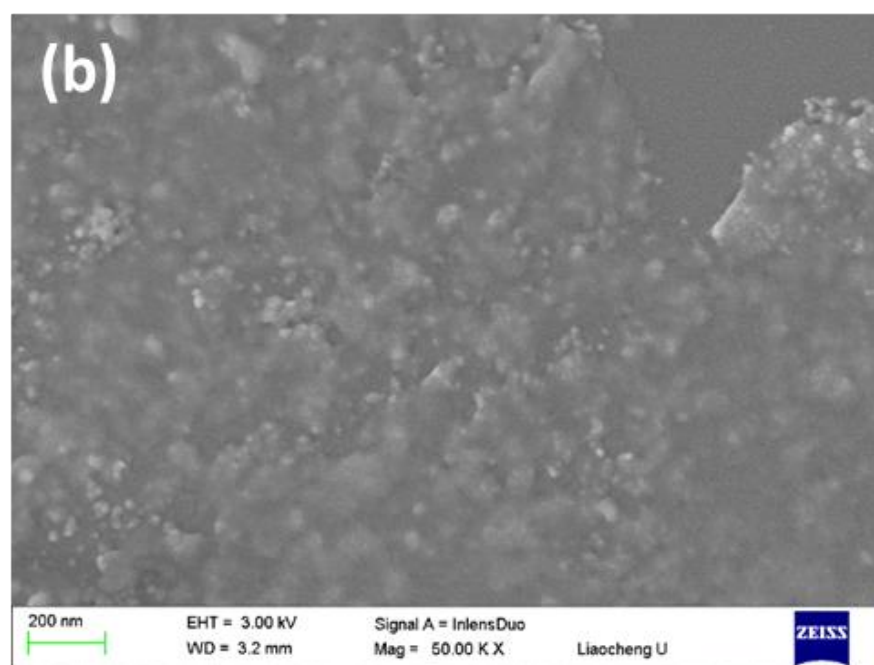
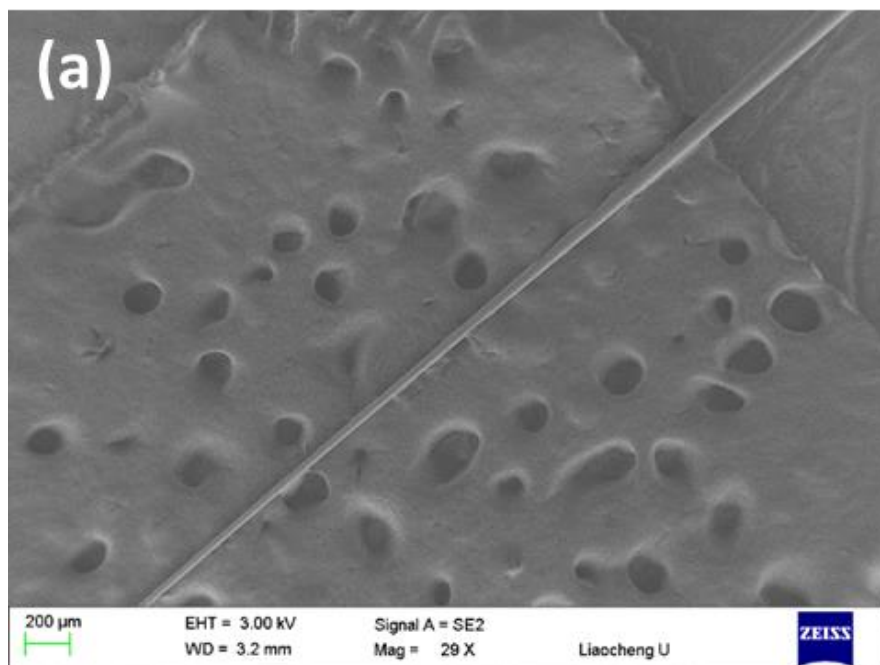


Figure 3.5: SEM images of dopamine sensor probe at (a) lower magnification, (b) higher magnification [131] © 2019 IEEE.

namely sensitivity ( $9.7 \text{ nm}/\mu\text{M}$ ),  $LoD$  ( $0.058 \mu\text{M}$ ), and linearity ( $10 \text{ nM}$ -  $1 \mu\text{M}$ ) are greatly enhanced. Different sensing mechanisms were adopted in past such as cyclic voltammetry, Amperometry, optical methods, and Voltammetric method to detect the DA concentration.

Different biosensors used for the detection of DA reported in open literature are compared in Table 3.1. The LSPR phenomenon (optical method) based DA sensor reveals great performance on all the sensing parameters. From the measured data, the linear equation that can be fit to the proposed DA sensor is:

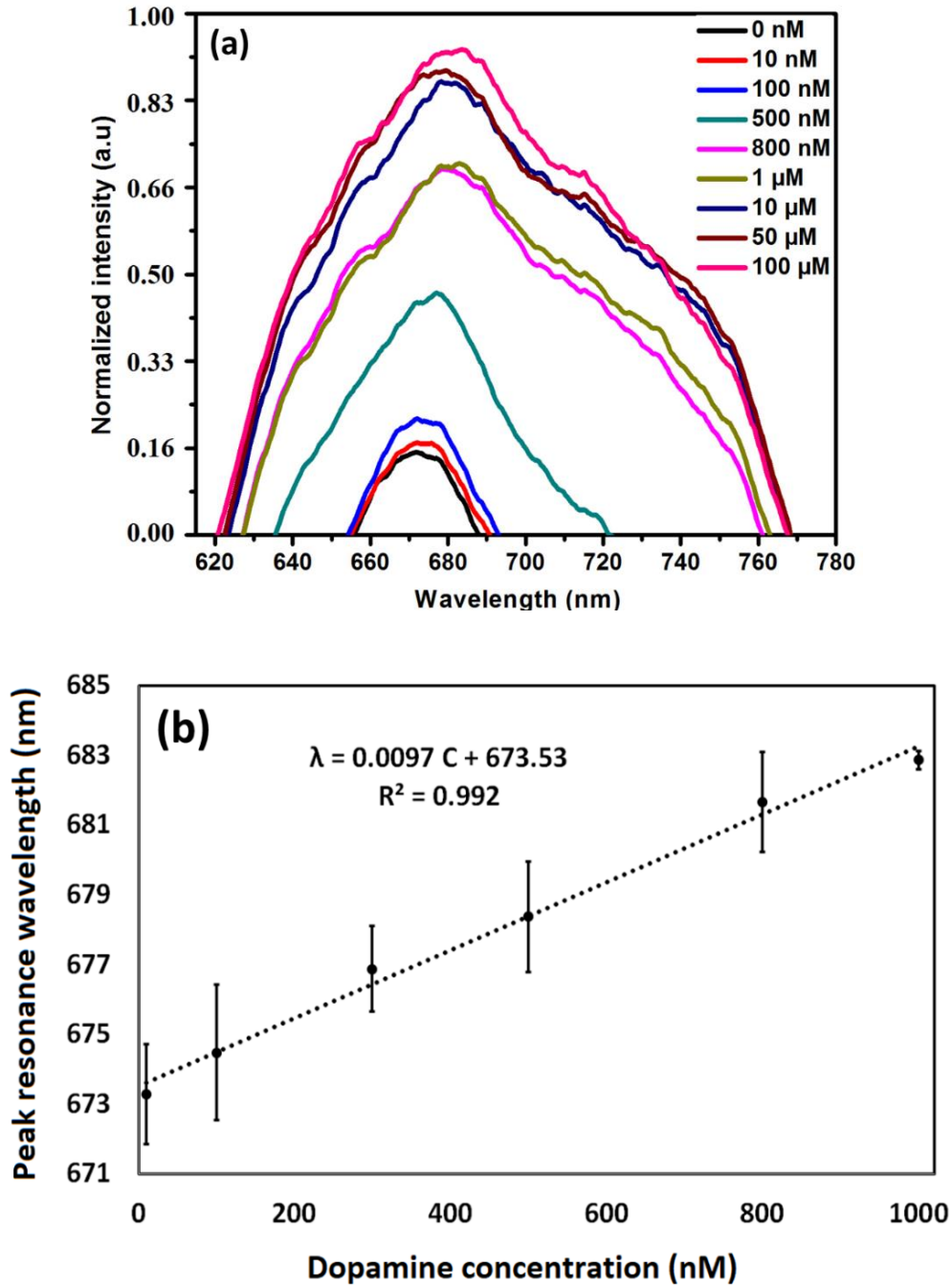


Figure 3.6: Results of dopamine detection (a) LSPR spectra, and (b) linearity curve [131] © 2019 IEEE.

Table 3.1  
Comparative study of dopamine sensors [131] © 2019 IEEE.

Material	Method	Linearity	LoD	Sensitivity	Ref.
Ag/MoS <sub>2</sub>	Cyclic Voltammetry	0.2 μM to 50 μM	0.2 μM	1.0 μA/ μM	[134]
AgNPs	Cyclic Voltammetry	1 μM to 10 μM.	0.41 V	n.r. <sup>a</sup>	[110]
AuNPs	Cyclic Voltammetry	1 μM to 100 μM	5.83 μM	n.r. <sup>a</sup>	[135]
Graphene-AuNPs	Amperometry	1 μM to 125 μM.	0.07 μM	0.124 μA/ μM	[119]
AuNPs	Differential Pulse Voltammetric Method	10 μM to 100 μM	0.7 ± 0.18 μM	0.1 mA/ mM/ cm <sup>2</sup>	[136]
AgNPs	LSPR	10 nM to 1 μM	0.058 μM	9.7 nm/ μM	This work

n.r.<sup>a</sup>: not reported

$$\lambda = 0.0097 C + 673.53 \quad (3.2)$$

whereas  $C$  is a DA concentration and linearity exists between 10 nM - 1 μM as revealed from linearity curve. In next step, to calculate the  $LoD$  of proposed DA sensor, the standard equation is used as indicated below:

$$LoD = (3 \times \text{Standard Deviation (SD)}) / \text{Sensitivity} \quad (3.3)$$

Here  $LoD$  indicates the ability to measure lowest concentration of analyte (DA). To calculate the value of SD, ten reference samples (peak resonance wavelength) are taken into consideration. To calculate the SD, the standard equation is used as indicated below:

$$\sigma = \sqrt{\frac{\sum(x_i - \mu)^2}{N}} \quad (3.4)$$

whereas,  $N$  is the size of reference samples,  $\mu$  is a mean of peak resonance wavelength of reference samples, and  $x_i$  is the peak resonance wavelength of reference sample.

### 3.4.2 Selectivity, Reproducibility and Reusability Test

The reagents like Cho, L-Cys, Glucose, D-Galactose, Urea, and AA were used in selectivity tests. To test the selectivity of a projected probe in existence of other analytes, the DA sensor probe

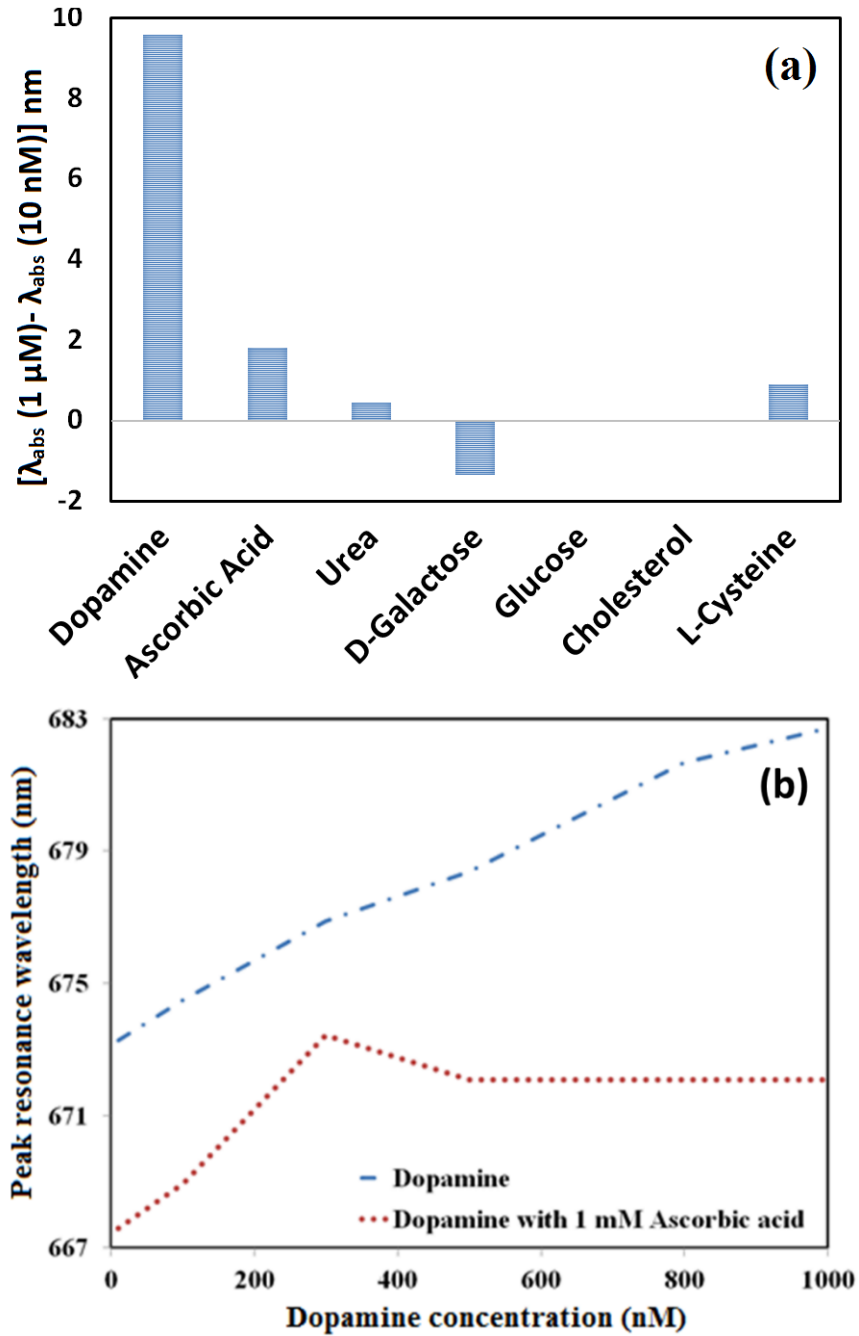


Figure 3.7: Selectivity test for dopamine sensor (a) test 1 (in presence of other analytes), and (b) test 2 (in presence of ascorbic acid coexist with dopamine) [131] © 2019 IEEE.

response is observed, and results are presented in Fig. 3.7. For this, difference between peak resonance wavelength of 10 nM and 1  $\mu$ M concentration of DA was calculated. The difference between peak resonance wavelengths is observed as 0.0 nm, 0.9 nm, 0.0 nm,  $-1.349$  nm, 0.45 nm, 1.799 nm, and 9.586 nm for the Cho, L-Cys, Glucose, D-Galactose, Urea, AA, and DA samples, respectively. This shows the highest specificity of proposed sensor towards DA samples. Further, the reusability and reproducibility tests of proposed DA sensor are presented in Fig. 3.8. To confirm the reproducibility, performance of proposed sensor is checked at 10  $\mu$ M concentration of DA with three different probes, indicated in Fig. 3.8(a). Further, repeatability of

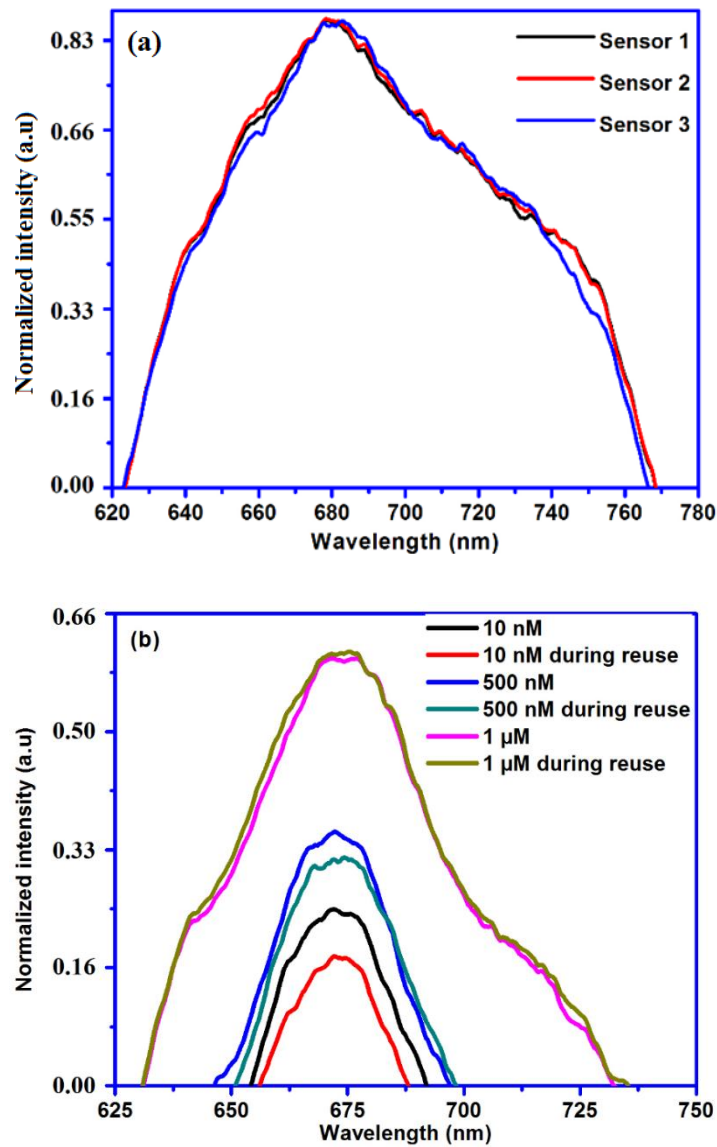


Figure 3.8: (a) Reproducibility and (b) reusability test of dopamine sensor [131] © 2019 IEEE.

the proposed sensor is checked at 1  $\mu\text{M}$ , 500 nM, and 10 nM concentration of DA, indicated in Fig. 3.8(b).

### 3.5 Summary

The performance of proposed AgNPs-PEG functionalized tapered LSPR phenomenon-based DA sensor is demonstrated in this chapter. The use of polyether compound (i.e. PEG) in functionalization of proposed DA sensor probe mainly helps to reduce protein absorption and protects the lipoplexes from interaction with blood components. In this study, RI sensitivity is characterized by wavelength shift. This characterization technique is highly effective; as smallest possible wavelength shifts that occur due to biomolecular binding are easily detectable with greater accuracy [137]. The mean diameter of AgNPs is reported as  $7.5 \pm 0.5$  nm used for immobilization process. A fine coating of lower size AgNPs provides improved sensitivity of probe. The characterization instruments namely SEM, HR-TEM, EDS, and UV-Vis-spectrophotometer are used for the characterization of synthesized AgNPs and nanocoated probes. The comparative study of the DA sensors is indicated in Table 3.1, which reveals very good performance of reported DA probe. The study shows the improved performance of proposed LSPR phenomenon-based DA sensor in comparison with other DA sensors reported in open source. The important sensing parameter such as linear range, *LoD*, sensitivity, and CC are reported as 10 nM - 1  $\mu\text{M}$ , 0.058  $\mu\text{M}$ , 9.7 nm/  $\mu\text{M}$ , and 0.992, respectively.

# **Chapter 4**

## **Development of Ascorbic Acid Sensor using Periodically Tapered Optical Fiber Sensor Probe**

## 4.1 Introduction

Chapter 3 explains about fabrication and experimental validation of single tapered P-OFSs for the detection of DA. This sensor shows the improved performance on various prime sensing parameters such as sensitivity, *LoD*, CC, and linearity in comparison with other DA sensors reported in open source. In present chapter, AuNPs and GO immobilized periodically tapered structure-based P-OFSs for ascorbic acid (AA) detection have been proposed. The targeted element i.e., AA is a vital organic constituent in the serum of human body system. It acts as an antioxidant that helps to fight bacterial infections [138]. Further, AA contributes to various processes in human body system such as formation of collagen, bones, teeth, skin, capillaries, and connective tissue. The typical range of AA is 100  $\mu\text{M}$  to 500  $\mu\text{M}$  present in serum [139], and an abnormal concentration of AA leads to Alzheimer's disease, cancer, scurvy, and other chronic diseases. The different optical fiber-based configurations in biosensing approach for the detection of analytes include, i) FBG, ii) LPG, iii) refractometers, iv) photonic crystal fiber, and v) other optical configurations have been reported in past [140]. The proposed multi-taper configuration-based P-OFSs comes under optical method-based sensing and is one of the simplest fabrication methods of OFSs. The tapering section provides access to EWs to interact with surrounding medium [141]. In basic principle of tapering, several tapers are directly related to the measurement sensitivity. To study the effect of tapering, four tapers, five tapers, and eight tapers-based optical fiber structures are also investigated. Further, highly biocompatible NMs like AuNPs and GO are deposited onto a multi-tapered probe. Due to high specific surface area, higher biocompatibility, and solubility GO-modified P-OFSs attract great attention from researchers [142]. The P-OFSs are one of the most attractive biosensors, with many benefits like low pressure, remote sensing capabilities, less cost, and resistance to electromagnetic interference [141]. The different steps or processes involved in the development of newly developed AA sensors are: bare probe fabrication, synthesis of AuNPs and GO colloidal, NMs immobilization process, enzyme functionalization process, and characterization of GO, and AuNPs. Further, performance of prepared sensor probe is checked with AA test samples, selectivity test of probe is also conducted. All these steps involved in the development AA sensor and measurement results are discussed in the following sections.

## 4.2 Experimental Methodology

In this section, experimental methodology involving design considerations, various processes related to the fabrication of AA probes, such as synthesis of NMs, immobilization process, test sample preparation, and measurement setup are described systematically.

### 4.2.1 Sensor Fabrication and Design Consideration

The P-OFSs with four-, five-, and eight-section periodically placed tapers have been designed and analyzed here. The optical fiber, such as SMF (9/125  $\mu\text{m}$ ), and MMF (62.5/125  $\mu\text{m}$ ) are used to design the proposed configurations. The fusion splicer is used to design proposed multi-tapered configurations. The schematic view of the multi-tapered bare fiber structure and its different configurations are presented in Fig. 4.1. The proposed sensing probes are designed with following specifications: i) tapered section of length 1000  $\mu\text{m}$ , ii) embedding periodically tapered region of length  $\sim$  1 mm, and iii) tapered section of diameter of 40  $\mu\text{m}$ . The proposed AA sensor was realized with diameter of 40  $\mu\text{m}$  by considering the different aspects as briefly discussed in chapter 3 (section 3.2.1). The fusion arc technique is adopted during the fabrication of all the proposed configurations.

### 4.2.2 Synthesis of Nanomaterials

The NMs used in nanocoating process such as AuNPs and GO are prepared using Turkevich method [143] and modified Hummer's method [144], respectively. Reagents such as gold (III) Chloride trihydrate (Hydrogentetrachloroaurate), tri-sodium citrate,  $\text{H}_2\text{SO}_4$ , potassium permanganate ( $\text{KMnO}_4$ ), sodium nitrate, hydro-chloric acid ( $\text{HCl}$ ), and graphite powder are used during the synthesis of mentioned NMs.

The above-mentioned Turkevich methods were adopted to control the size and shape of AuNPs. Initially, 100 mM -  $\text{HAuCl}_4$  solution (150  $\mu\text{l}$ ) is added to the DI water (14.85 ml- boiling at 100  $^\circ\text{C}$ ). Further, 38.8 mM tri-sodium citrate (1.8 ml) is added and stirred till resultant solution turns red-wine in color.

In next step, GO flakes are prepared using modified Hummer's method. For this  $\text{NaNO}_3$  (0.25 g), and graphite powder (0.5 g) are added to the stirred concentrated  $\text{H}_2\text{SO}_4$  solution (11.5

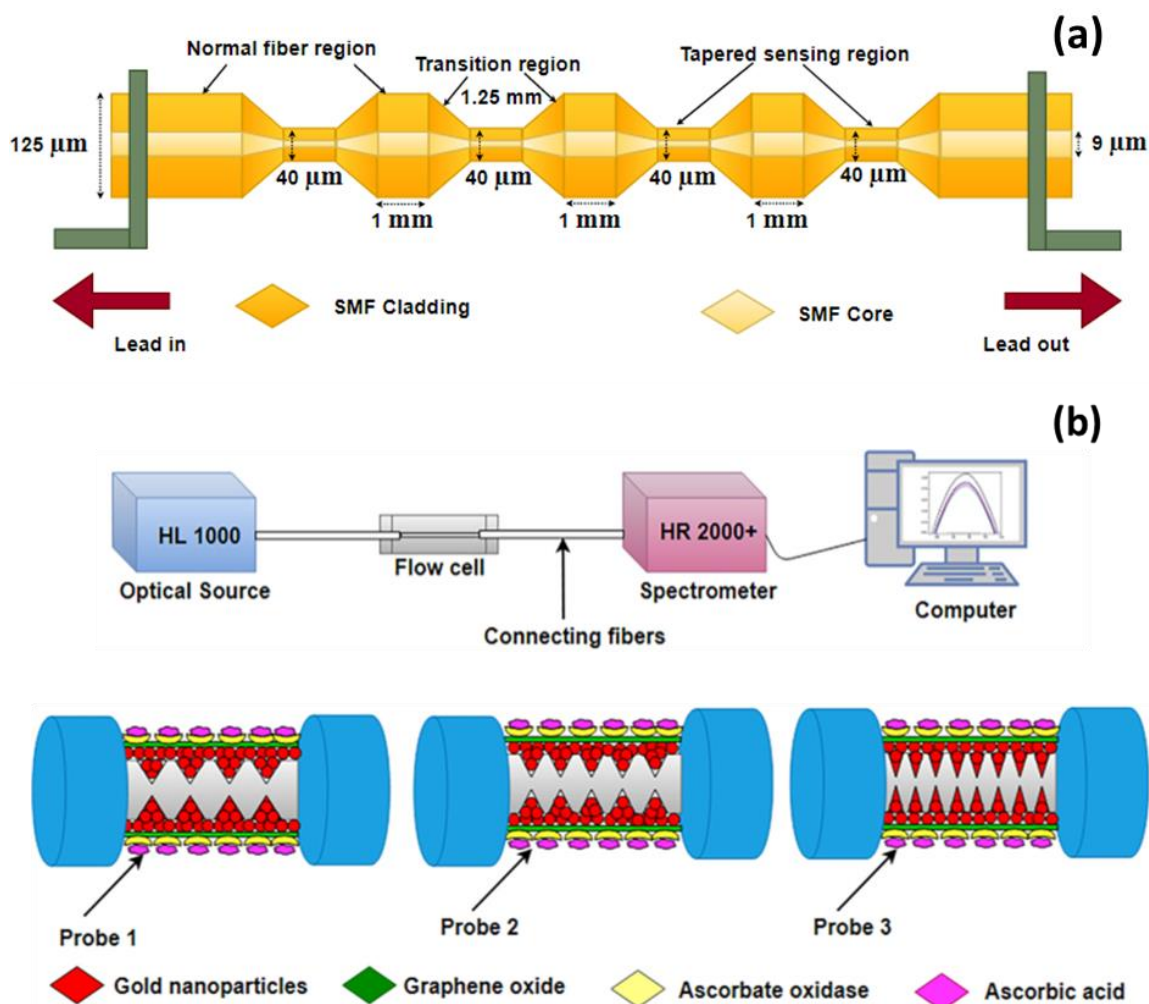


Figure 4.1: Schematic of (a) four tapered structure, and (b) experimental setup and different configurations of AA sensor (Probe-1: four-tapered/GO/AuNPs/P-OFSs probe; Probe: five-tapered/GO/AuNPs/P-OFSs probe; Probe-3: eight-tapered/GO/AuNPs/P-OFSs probe) [145] © 2020, Elsevier.

ml). In next stage, resultant solution is kept at 20 °C temperature after adding 1.5 g  $\text{KMnO}_4$ . Further, the prepared solution is diluted with DI water (250 ml) and  $\text{H}_2\text{O}_2$  (2.5 ml) is added and its temperature is raised to 98 °C. After this, HCl (5%) and water mixture is used to filter and wash the final solution. In last stage of GO flakes preparation, solidification, and grinding of the resultant concentrated solution are carried out.

The color of synthesized AuNPs and GO solution turns red-wine and yellowish, respectively indicating the formation of NMs, which is further confirmed using UV-spectrophotometer by observing the absorbance spectrum. The morphology of the prepared NMs is studied using HR-TEM.

### 4.2.3 Nanocoating and Enzyme Functionalization

The proposed optical fiber bare probe is immobilized and functionalized with AuNPs, GO, and ascorbate oxidase (AOx). The AuNPs have higher biocompatibility [146], whereas GO has good chemical stability, wide-surface area, excellent mechanical behavior, and higher electrical conductivity [147]. Reagents such as AOx (1000 - 3000 unit/mg protein), ethyl (dimethyl aminopropyl) carbodiimide (EDC), MUA, and N-Hydroxysuccinimide (NHS) are used during the nanocoating process. The nanocoating and functionalization process is carried out as shown in Fig. 4.2. Initially, the proposed multi-tapered probes are dipped in acetone and Piranha solution for 20 min and 30 min, respectively. The reagents such as H<sub>2</sub>O<sub>2</sub> and H<sub>2</sub>SO<sub>4</sub> are added in a ratio of 3:7 to prepare the Piranha solution. This process primarily cleans the sensors and exposes the hydroxide radicals. Secondly, an adhesive layer is formed using MPTMS coupling agent. Now, the already prepared AuNPs were deposited over the cleaned and silanized multi-tapered probe. Bare probes are dipped for 48 hrs for a fine and effective coating. Most of the time metal NPs, such as AuNPs, are prepared using wet reduction method. After the coating, it leaves some toxic residues on sensor surface which affects the sensor performance. For this, we have further coated the probe using another synthesized NMs i.e., GO. The deposition of GO was done by dipping and drying (in oven at 70°C) technique. For the uniformity in GO nanocoating, this process was repeated thrice. The sonication method is adopted to prepare the GO solution from GO flakes. Initially, this nanocoated probe is functionalized with MUA (0.5 mM), EDC (200 mM), and NHS (50 mM) to produce and activate the carboxyl groups [145] then is further functionalized with AOx enzyme (1,000- 3,000 units'/mg protein).

### 4.3 Characterization and Measurement

The characterization of synthesized NMs such as AuNPs and GO, and NMs immobilized probes are discussed extensively in this section. The structural analysis of four, five, and eight multi-tapered bare fiber probes (i.e., fiber length vs. waist diameter) and SEM image are presented in Fig. 4.3. The variation of the diameter along the length of the fiber of the proposed probes was recorded using combiner manufacturing systems (CMS, 3SAE) machine during fabrication of

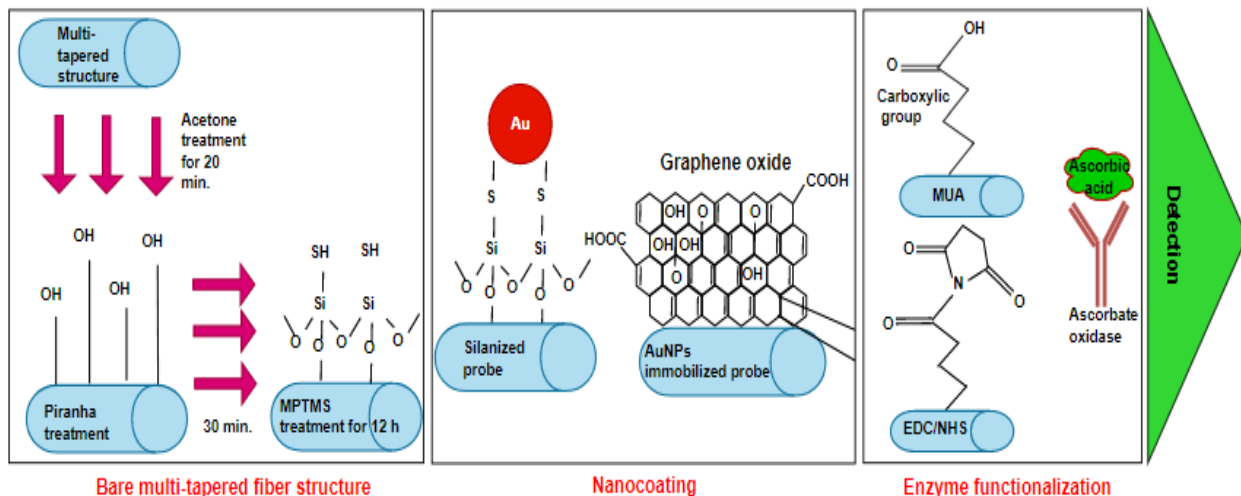


Figure 4.2: Schematic of nanocoating, and functionalization process [145] © 2020, Elsevier.

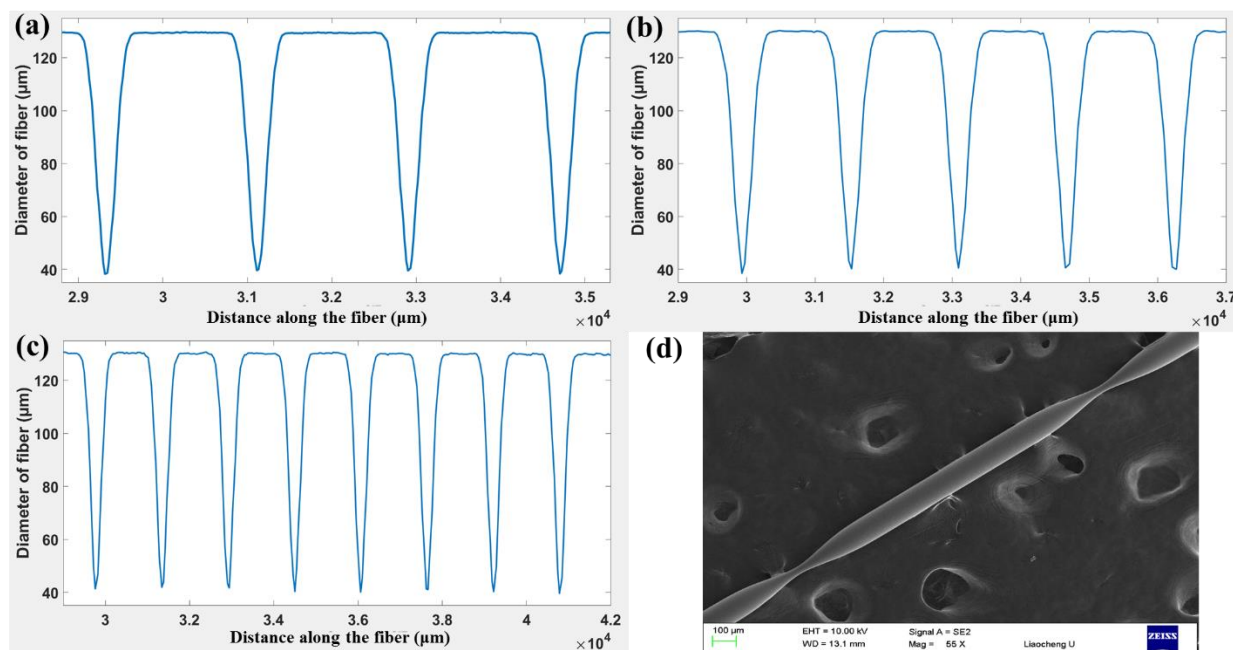


Figure 4.3: The variation of the diameter along the length of the fiber of (a) Probe-1, (b) Probe-2, and (c) Probe-3; and (d) SEM image of the multi-tapered probe [145] © 2020, Elsevier.

probes and plotted using MATLAB. SEM image was included to represent the correlation between bare fiber probe and fabricated sensor probe. Further, characterization results of AuNPs and GO are presented in Fig. 4.4. Briefly, the absorbance of GO and AuNPs (to check the formation of synthesized NMs), HR-TEM image of GO and AuNPs (to check the morphology of

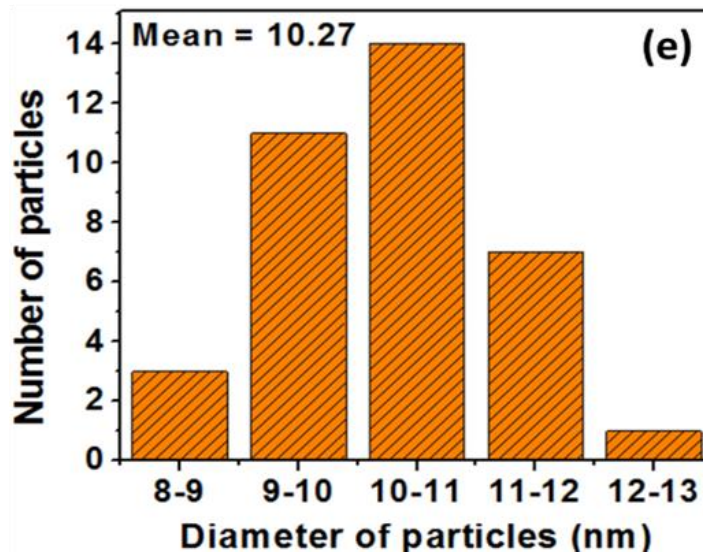
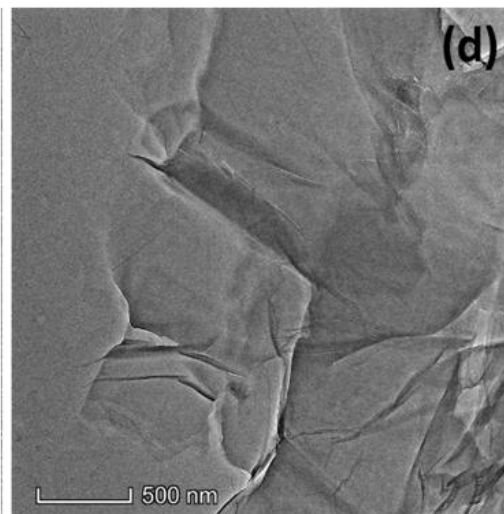
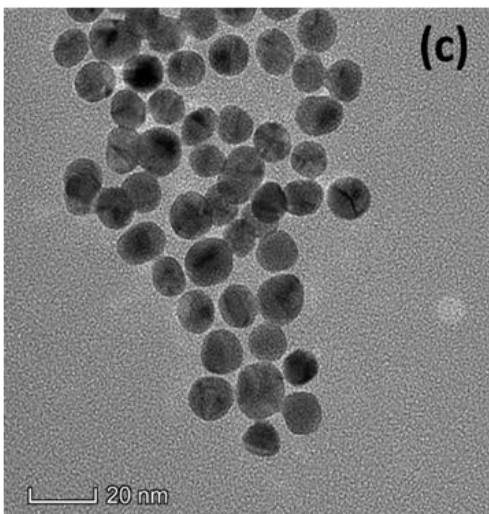
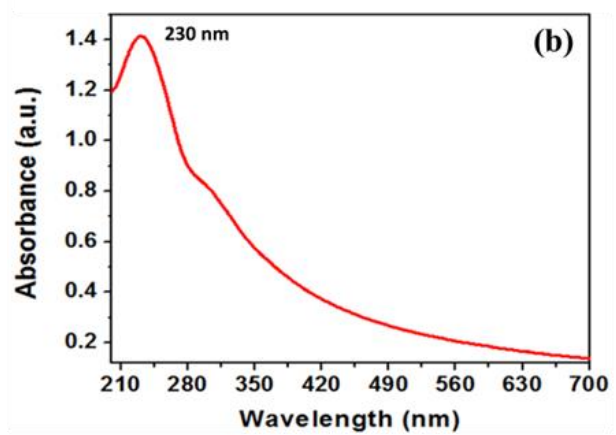
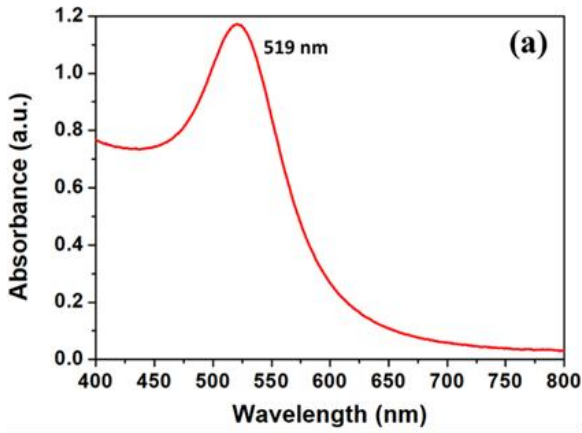


Figure 4.4: Absorbance spectrum of (a) AuNPs, and (b) GO; HR-TEM image of (c) AuNPs, and (d) GO; and (e) histogram of AuNPs [145] © 2020, Elsevier.

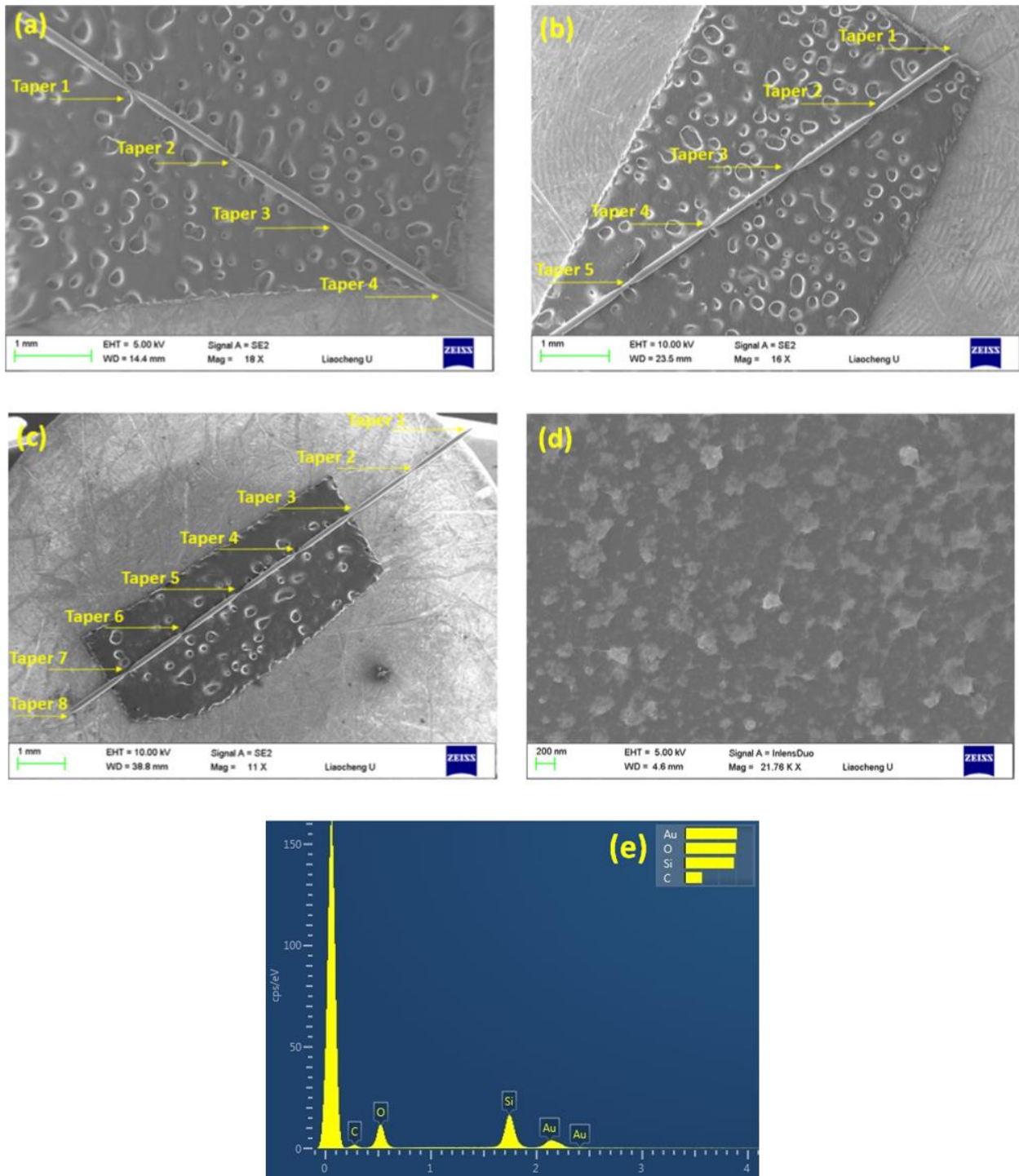


Figure 4.5: SEM image of (a) Probe-1, (b) Probe-2, and (c) Probe-3 at lower magnification; (d) SEM image at higher magnification, and (e) EDS image [145] © 2020, Elsevier.

NMs), and AuNPs analysis with histogram are presented. Moreover, physical characterization results of four-, five-, and eight-section tapered probes at lower magnification are indicated in Fig.

4.5 (a-c), respectively, whereas morphology of nanocoated probes at higher magnification and EDS analysis are revealed in Fig. 4.5 (d-e), respectively.

## 4.4 Results and Discussion

### 4.4.1 Performance of Ascorbic Acid Sensor Probe

Initially, a comparative study over single and multi-tapered SMF/ MMF probes is presented in this section. For this, i) single tapered SMF, ii) single tapered MMF, iii) eight tapered SMF, and iv) eight tapered MMF probes are fabricated. During measurement, lowest transmission intensity is recorded in case of eight tapered SMF probes illustrated in Fig. 4.6. From these results, we can infer that multi-tapered SMF structure is well-suited for LSPR phenomena-based OFSs (observed the lowest transmission intensity at output). In this study, high radiation loss in the eight-tapered sensor probe limits its use for sensing applications. In proposed GO/AuNPs/AOx/multi-tapered probe, optical signal activity of testing response is measured at minimum of three cycles. Related LSPR plot and linearity plot is plotted with an average of those three sets of readings, presented in Fig. 4.7. The four, five, and eight periodically tapered structure-based AA sensors are proposed in this study. An optimal number of five-tapered AA sensors is very effective for AA measurement and shows the highest specificity towards AA. The superior performance has been observed in case of proposed five tapered sensor probes (Probe-2). We have also observed the enhanced performance parameters such as  $LoD$  (51.94  $\mu$ M),  $CC$  (0.9724), and sensitivity (8.3 nm/mM). The use of smaller size AuNPs ( $\sim 10$  nm) is mainly contributing to enhanced sensitivity of AA sensors.

**Probe-1:** Figure 4.7 (a-b) shows the LSPR and linearity plot of four-tapered/GO/AuNPs/P-OFSs probe. The linearity curve equation, sensitivity and  $CC$  are revealed as,

$$\lambda = 0.0011 C + 611.91 \quad (4.1)$$

1.1 nm/mM and 0.9624, respectively. In this equation,  $C$  denotes the AA concentration.

**Probe-2:** Figure 4.7 (c-d) shows the LSPR spectra and linearity plot of five-tapered/GO/AuNPs/P-OFSs probe. The linearity curve equation, and  $CC$  are revealed as,

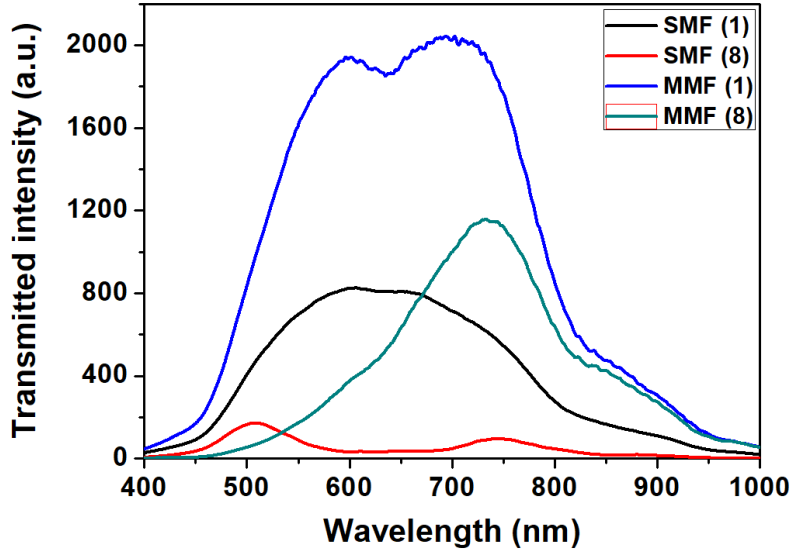


Figure 4.6: Analysis of tapered MMF vs. tapered SMF optical fiber probe [145] © 2020, Elsevier.

$$\lambda = 0.0083 C + 580 \quad (4.2)$$

and 0.9724, respectively. The sensitivity of proposed probe is 8.3 nm/mM, shows the enhanced performance in comparison with Probe-1.

**Probe-3:** Figure 4.7(e-f) shows the LSPR spectra and linearity plot of the eight-tapered/GO/AuNPs/P-OFSs probe. The linearity curve equation and correlation correlator are revealed as,

$$\lambda = - 0.0005 C + 577.85 \quad (4.3)$$

and 0.8747, respectively. The performance of this probe is degraded in comparison with Probe-1, and probe-2, as maximum radiation is coming out in this respect, which is also indicated in enlarge view of Fig. 4.7(f).

#### 4.4.2 Selectivity Test

Selectivity is a very essential feature of P-OFSs in biosensing applications. This is used to check the ability to detect particular analytes in presence of other interfering elements of the body fluids. Here, elements like Glu, urea, UA, D-Gal, Cho, and DA are used to check the specificity of the

proposed AA sensor. For this wavelength shift is measured for 1 mM and 10  $\mu\text{M}$  concentration of each analyte. The wavelength shift (difference between higher and lower peak

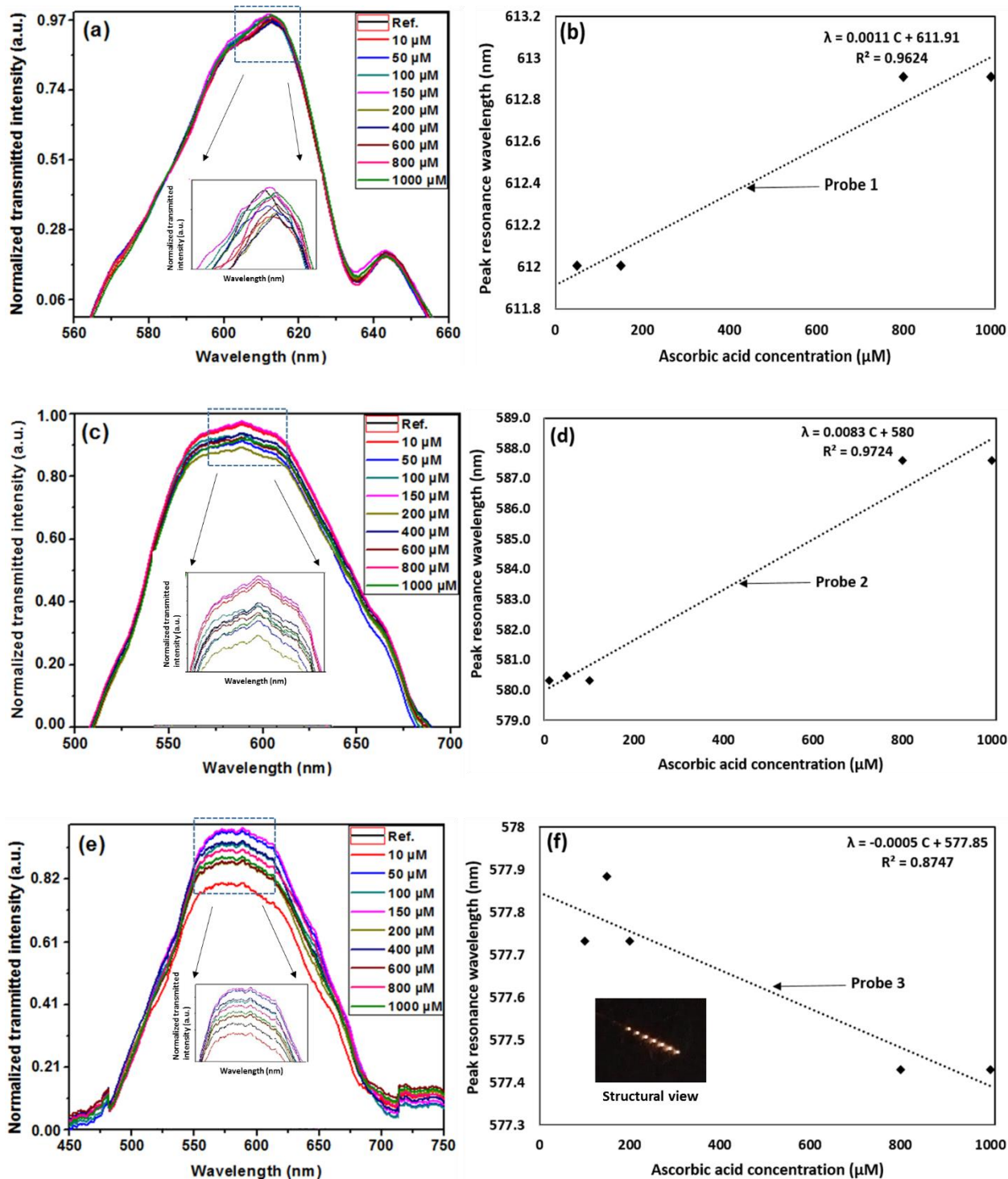


Figure 4.7: (a) LSPR spectra, and (b) linearity plot of Probe-1; (c) LSPR spectra, and (d) linearity plot of Probe-2; (e) LSPR spectra, and (f) linearity plot of Probe-3 [145] © 2020, Elsevier.

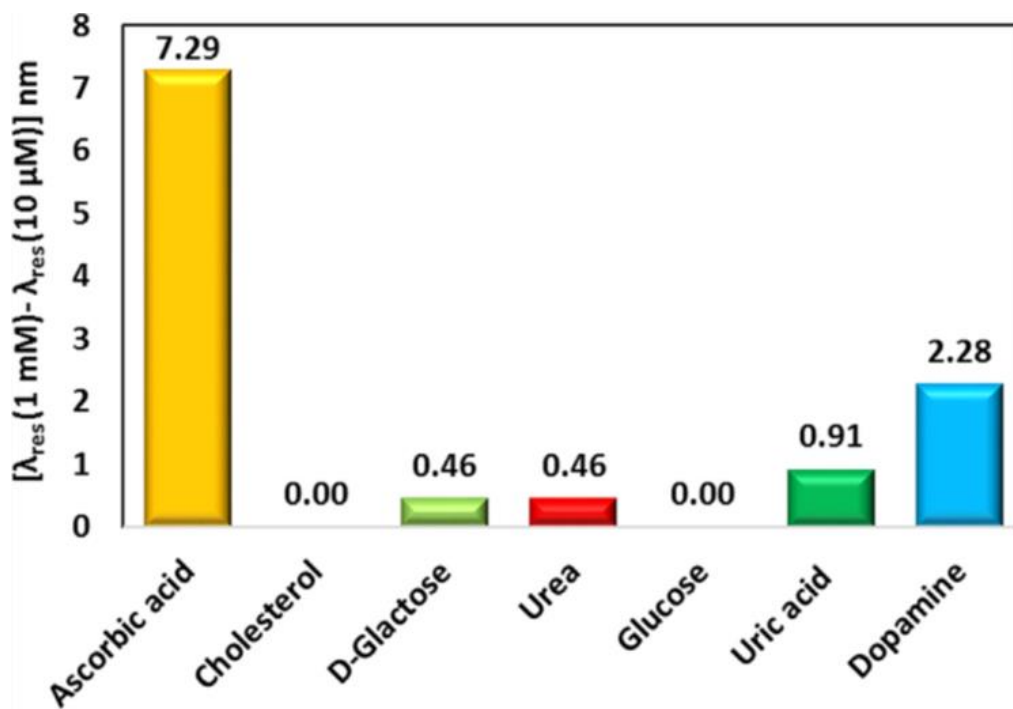


Figure 4.8: Selectivity test of the ascorbic acid sensor [145] © 2020, Elsevier.

Table 4.1  
Comparative study over ascorbic acid sensor [145], © 2020, Elsevier

Material	Method	Linearity	LoD	Sensitivity	
H2L <sup>a</sup>	Fluorescent method	0 to 60 $\mu\text{M}$	34 nM	n.r <sup>b</sup>	[148]
ClO <sup>-</sup> /TMB <sup>c</sup>	Colorimetric method	1 to 70 $\mu\text{M}$	0.58 $\mu\text{M}$	n.r <sup>b</sup>	[149]
TiO <sub>2</sub> (RGO–TiO <sub>2</sub> ) nanocomposite.	Amperometric method	1 to 1500 $\mu\text{M}$	0.512 $\mu\text{M}$	n.r <sup>b</sup>	[150]
Cadmium sulphide quantum	Fluorometry method	60 to 300 nM	2 nM	n.r <sup>b</sup>	[151]
C-dots	Colorimetric method	0.2 to 70 $\mu\text{M}$	9.3 nM	n.r <sup>b</sup>	[152]
Four tapered AA Sensor - Probe-1	LSPR technique	0.05 to 1 mM	n.r <sup>a</sup>	1.1 nm/mM	Present work
Five tapered AA Sensor- Probe-2 (Proposed sensor)		0.01 to 1 mM	51.94 $\mu\text{M}$	8.3 nm/mM	
Eight tapered AA Sensor - Probe-3		0.1 to 1 mM	n.r <sup>b</sup>	0.5 nm/mM	

<sup>a</sup>4,4' (1H pyrazole 1,3 diyl) dibenzoic acid; <sup>b</sup> not\_reported; ClO<sup>-</sup>/TMB <sup>c</sup> hypochlorite (ClO<sup>-</sup>)/tetramethylbenzidine (TMB)

wavelength) for Glu, UA, urea, D-Gal, Cho, DA, and AA samples have been observed as 0.00, 0.91, 0.46, 0.46, 0.00, 2.28, and 7.29, respectively. This indicates the maximum wavelength shift value for AA over different analytes. The resultant plot for selectivity test is indicated in Fig. 4.8.

## 4.5 Summary

In this study, four, five, and eight tapered-based AA sensors are investigated. The measurement depends on two factors, total loss in the system and the amount of EWs mode energy that is released. If number of tapered sections are more, then the loss of optical signal increases though its EWs performance is better. On the other side, if the number of sections are less then loss of optical signal is less but EWs performance also not good. In this study, five tapered probe is found to be optimum considering both the factors. The synthesis of NMs, coating process, setup, configuration, and experimental data for the proposed AA sensors are presented. Promising NSs such as GO and AuNPs were employed during the development of AA biosensors. These NSs show the well-suited merits for the biosensing applications including higher electrical conductivity, antibacterial inorganic materials, biocompatibility, and large surface area. The different structural design-based comparative study is proposed in this work. For this GO, and AuNPs immobilized four, five, and eight optical fiber tapered-based configurations for AA detection were characterized and analysed. Among the proposed three different configurations, optimal five tapered probes (GO-AuNPs-Five-Tapered-AA-P-OFSs) (Probe-2) shows the enhanced performance. The results such as *LoD*, sensitivity, and CC for proposed Probe-2 are recorded as 51.94  $\mu\text{M}$ , 8.3 nm/mM, and 0.9724, respectively. The comparative studies over a linear range, *LoD*, and sensitivity for proposed AA sensors (Probe-1, -2, and -3) and other previously reported AA sensors available in open literature are presented in Table 4.1. In conclusion, proposed AA sensor probe exhibits tremendous potential in bio-nanotechnology applications.

# **Chapter 5**

## **Development of L-Cysteine Sensor using Tapered SMS Structure-based Optical Fiber Sensor Probe**

## 5.1 Introduction

In previous chapter, LSPR phenomenon-based AA sensor is demonstrated. The multi-tapered optical fiber structures are employed for the development of AA sensors. This chapter deals with design, development, and characterization of L-Cysteine (L-Cys) sensor probe. This probe can efficiently detect and measure L-Cys concentration presented with urine in human body system. A typical range of L-Cys in urine is 240  $\mu\text{M}$  to 360  $\mu\text{M}$  [153]. It comes under one of the most essential biomolecules available with body fluids along with homocysteine, and glutathione. This biomolecule is widely related to the human physiological process, and important to sustain or improve lung, brain function, and liver detoxification. It also contributes to, i) improvement of the immunity of HIV patients, ii) recovery from surgery, iii) improvement of the men's semen quality, iv) enhanced white-blood-cell related activities, and v) regulated blood sugar levels [154]. The abnormal L-Cys concentration can lead to neuropsychiatric illness, hematopoiesis, liver damage, skin lesion, loss of muscle retarded growth, thrombosis, and hair depigmentation [153]. The plasmonic sensors for detection of L-Cys and related graphical abstract are indicated in Fig. 5.1. In graphical abstract, HR-TEM images of AgNPs and GO are present over the SEM image of sensor probe. The cutting view of proposed L-Cys sensor is also shown there. Different structural modifications such as fiber bending, hetero-core, tapering, core mismatch, and addition of external dielectric layer were proposed in past to improve the LSPR phenomenon in P-OFSs [155]. The combination of hetero-core and tapered structure-based bare fiber probe i.e., Tapered SMF-MMF-SMF (SMS) P-OFSs is proposed for L-Cys detection. These structural features (i.e., hetero-core and tapered structure) are well combined to realize the proposed sensor design. The tapered MMF section generates the higher-order modes and in turn increases the possibility of angle of incidence getting smaller than the critical angle, providing a good opportunity to signal to leak. In next step of sensor fabrication, NMs namely GO, and AgNPs are deposited on the sensing section of bare sensor probe. It is observed that the shape, composition, nature of NMs, roughness, and antibacterial behavior of NMs have greatly affected the sensitivity of LSPR sensors [156]. The deposited NMs show the features such as higher biocompatibility, thermal conductivity, intrinsic mobility, excellent additive in nature, and large surface area. In past, methods such as chromogenic, fluorescence, colorimetric, and optical are reported for the practical realization of L-Cys sensors. The LSPR sensor comes under the optical method

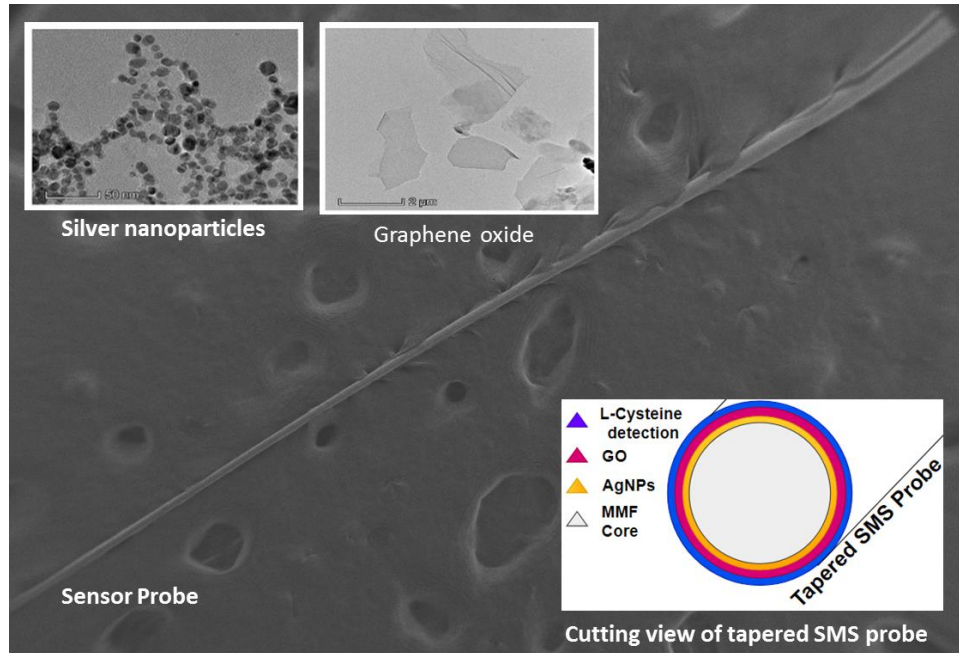


Figure 5.1: Graphical abstract of plasmonic sensors for detection of L-Cysteine [157] © 2020 *IEEE*.

categories and has the potential to develop biosensors to detect the range of biomolecules. The proposed LSPR phenomenon-based L-Cys sensor has great potential and a range of advantages which includes i) higher biocompatibility, ii) high electromagnetic immunity, iii) portability, iv) real-time monitoring, v) smaller detection time, vi) label-free detection, and vii) ease of fabrication [157]. The details of L-Cys sensor probe fabrication (i.e., bare probe design, synthesis of AgNPs, and GO, immobilization/ functionalization process, and characterization of NMs and nanocoated probe), measurement, and analysis of results are discussed in length in the following sections.

## 5.2 Experimental Methodology

The various steps and processes in designing of L-Cys sensor probe, i.e., i) fabrication of bare probe, ii) synthesis of NMs, and iii) nanocoating process are explained in following sub-sections.

### 5.2.1 Sensor Fabrications and Design Considerations

In present study, AgNPs and GO immobilized tapered SMS structure-based L-Cys sensors are realized using LSPR phenomenon. For this MMF (62.5/125  $\mu\text{m}$ ), and SMF (8.2/125  $\mu\text{m}$ ) fibers

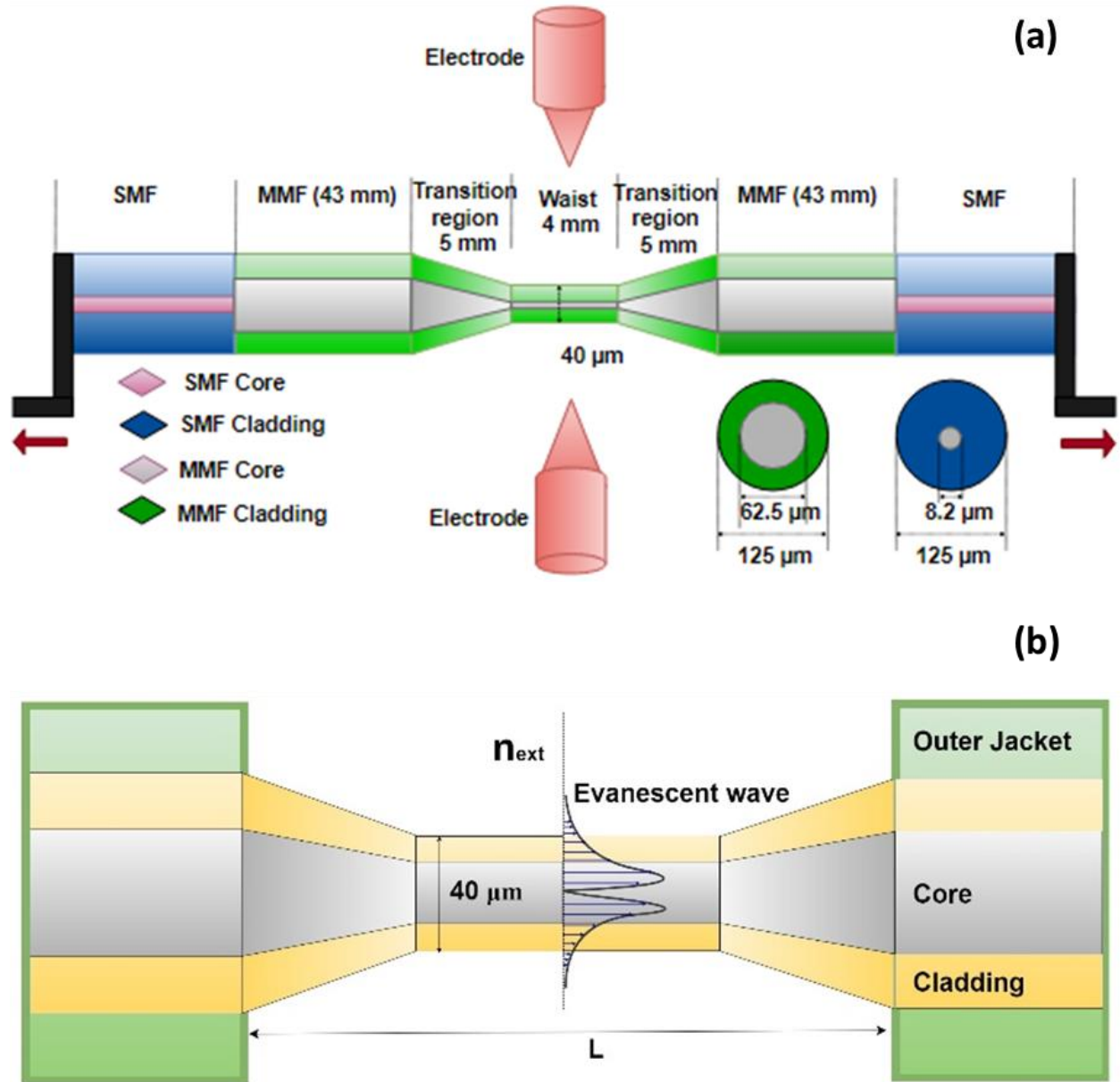


Figure 5.2: (a) Schematic view of bare fiber probe, and (b) wave propagation through sensor probe [157] © 2020 IEEE.

were employed in designing of sensor probe. The fusion splicer (Fujikura- FSM 100P+) is used to sandwich MMF section in between two SMF sections. For the tapering of spliced structure CMS (3SAE) machine is used. The fusion arc method is applied for the designing of proposed tapered structure. The schematic view of Tapered SMS sensing probe and wave propagation via probe is presented in Fig. 5.2. The design parameters of proposed sensor probe specifically waist diameter, MMF section length, transition region, and tapered section length are reported as 40 μm, 10 cm, 5

mm, and 4 mm, respectively. The proposed L-Cys P-OFSs were realized with diameter of 40  $\mu\text{m}$  by considering the different aspects as briefly discussed in chapter-3 (section 3.2.1).

## 5.2.2 Nanomaterial Synthesis and Immobilization Process

An electrochemical process [157] and modified Hummer's method [144] are applied to prepare the colloidal of AgNPs and GO, respectively. Reagents like  $\text{NaBH}_4$  (1 mM) and  $\text{AgNO}_3$  (1 mM) are used during the synthesis of AgNPs. Similarly, reagents including  $\text{KMnO}_4$ ,  $\text{H}_2\text{SO}_4$ ,  $\text{KMnO}_4$ ,  $\text{H}_2\text{O}_2$ , and  $\text{HCl}$  are used during the synthesis of GO. The synthesis process of AgNPs and GO is briefly explained in Chapter-3, and -4, respectively. The color of synthesized AgNPs and GO solution turns greenish-yellow and yellowish, respectively indicating the formation of NMs. Moreover, formation of synthesized AgNPs and GO are also confirmed with UV-Vis-spectrophotometer (observing the absorbance spectrum) and HR-TEM (observing the morphology). The nanocoating procedure is already enlightened in Chapter-3 and -4, and a schematic of nanocoating process is presented in Fig. 5.3. The deposited NMs reveal various benefits such as higher intrinsic mobility, optical transmittance, large surface area, biocompatibility, and additive nature [145].

## 5.3 Characterization and Measurement

The characterization results of NMs and immobilized probes are presented in Fig. 5.4, and Fig. 5.5, respectively. The following important observations are recorded during the characterization of NMs and nanocoated probes: i) AgNPs absorbance spectrum is recorded at 395 nm (using UV-spectrophotometer) (Fig. 5.4 (a)), ii) AgNPs are spherical with a mean size of  $7.5 \pm 0.5$  nm (Fig. 5.4 (b)), iii) GO absorbance spectrum is recorded at 233 nm (Fig. 5.4 (c)), iv) fine coating of AgNPs and GO NMs over the surface of OFSs is observed (SEM image- Fig. 5.5 (a)), and v) the present nanocoated materials are Ag (silver), and carbon (GO) over sensor surface (EDS image- Fig. 5.5 (b)).

Further, the schematic of an experimental setup for L-Cys detection is revealed in Fig. 5.6. The optical source and optical spectrometer are employed in the experiment at the input, and the output end, respectively. Centered on normal concentration of L-Cys available with urine (i.e., 240

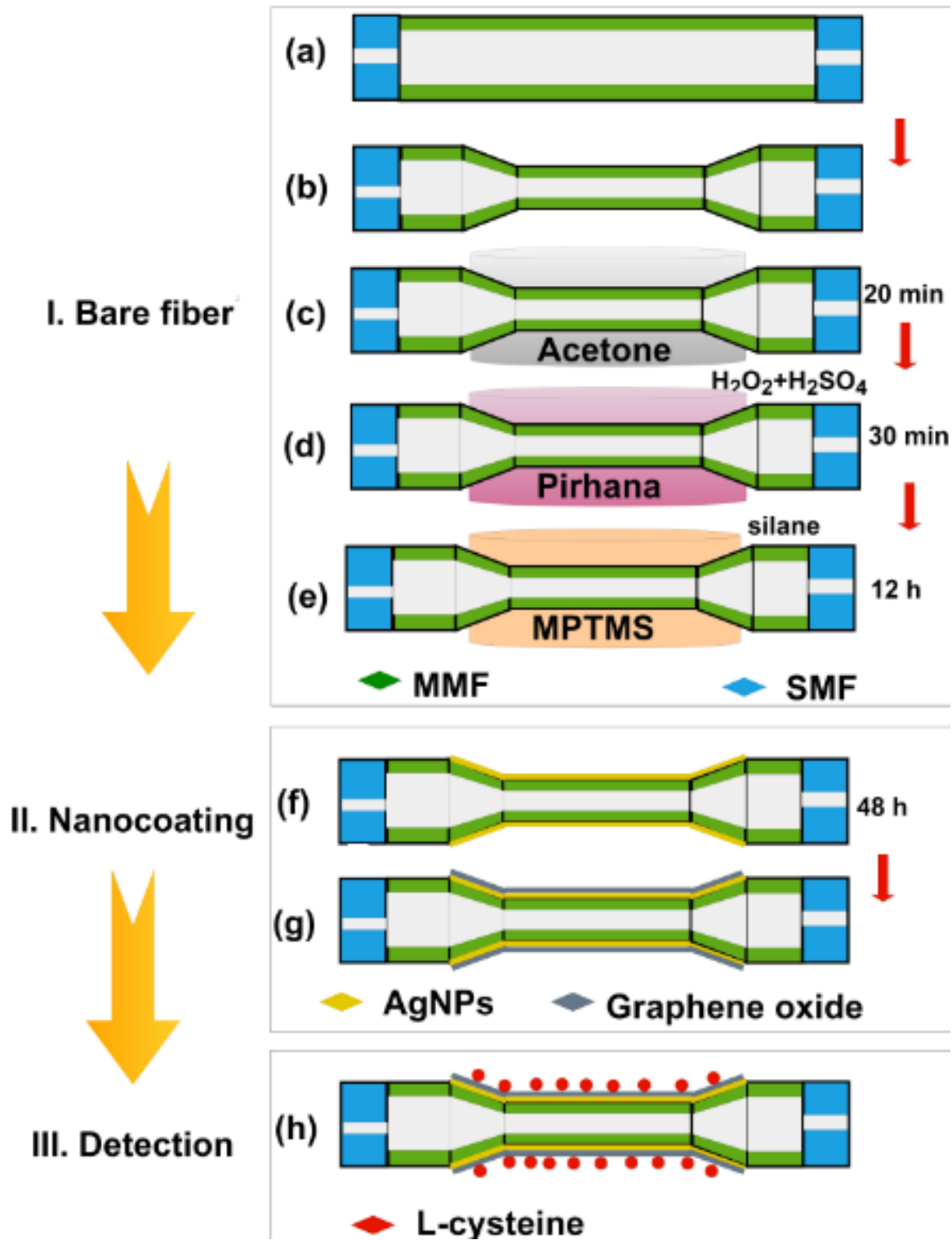


Figure 5.3: Schematic view of a nanocoating process [157] © 2020 *IEEE*.

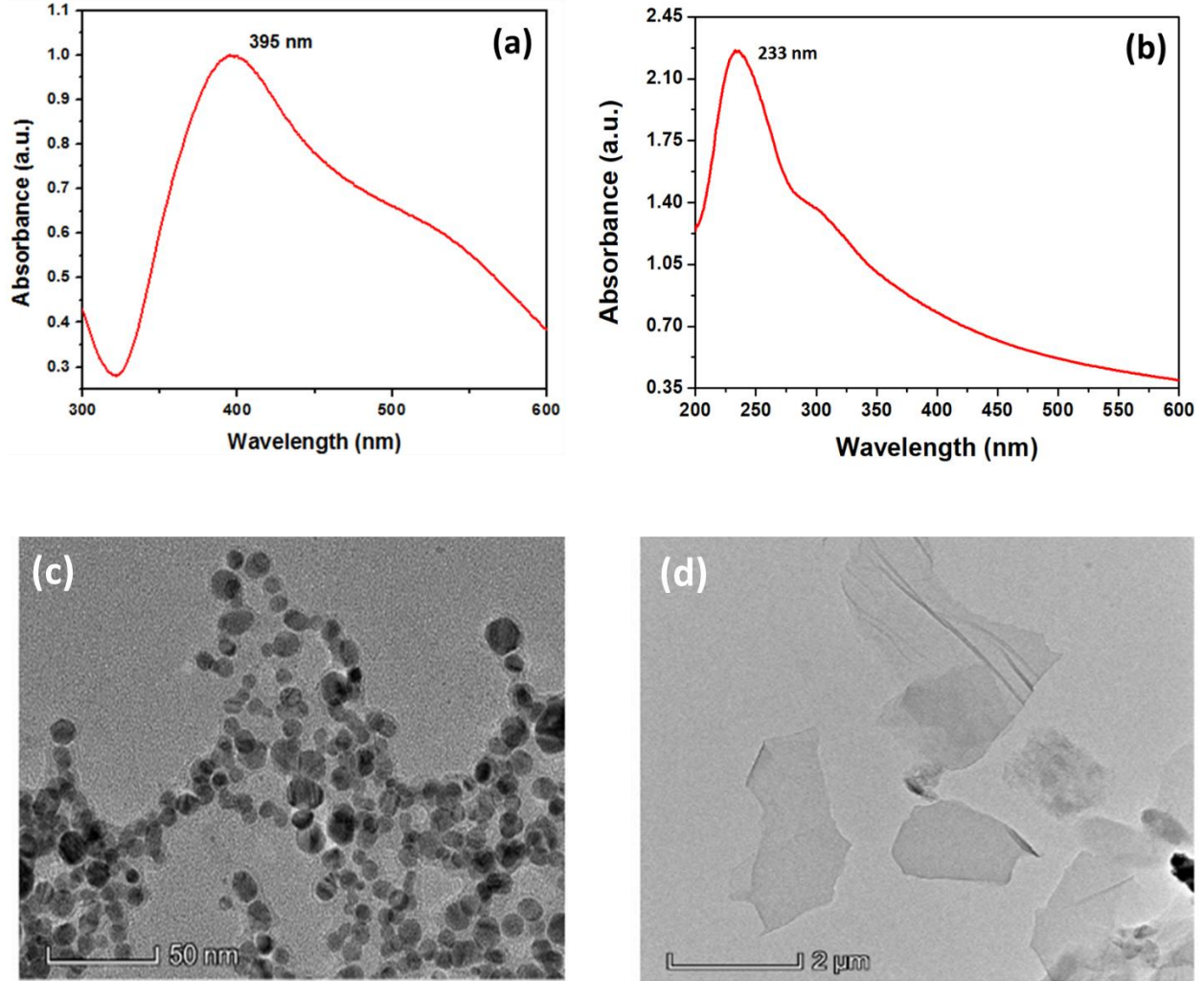


Figure 5.4: Absorbance spectrum of (a) silver NPs and (b) graphene oxide (GO); HR-TEM image of (c) silver NPs, and (d) graphene oxide [157] © 2020 IEEE.

$\mu\text{M}$  to  $360 \mu\text{M}$ ), test samples are prepared in  $10 \text{ nM}$ -  $10 \text{ mM}$  range. The L-Cys test samples are introduced in flow-cell and stabilized LSPR spectrum is noted. The base treatment is done before injecting the new L-Cys test sample.

## 5.4 Results and Discussion

The performance of the newly developed L-Cys sensor is examined based on prime indicators such as sensitivity, CC, linearity range,  $LoD$ , reusability, and reproducibility. In proposed tapered SMS structure, core-mismatch and tapering-based design provide the maximum EWs and larger

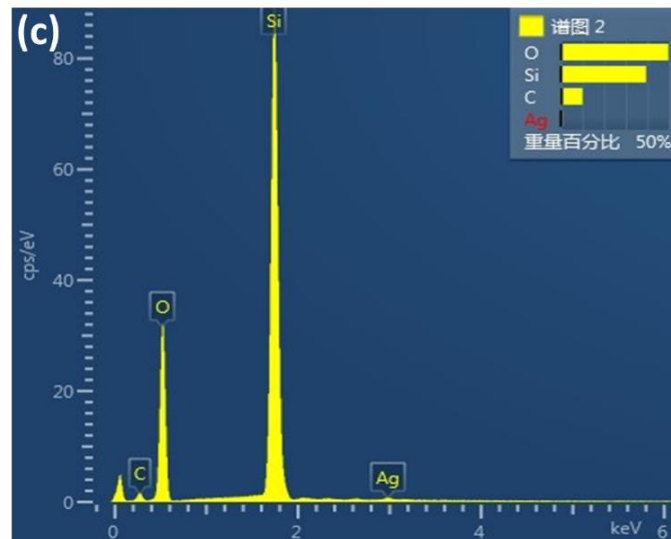
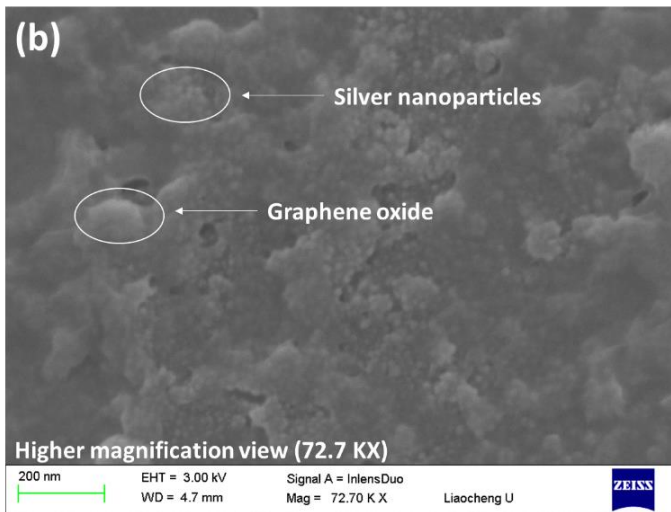
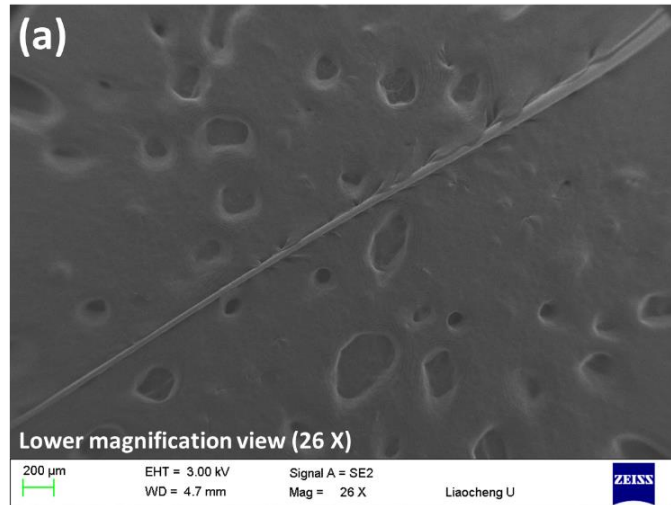


Figure 5.5: SEM image of Probe-2 recorded at (a) lower magnification, and (b) higher magnification; and (c) EDS image of Probe-2 [157] © 2020 IEEE.

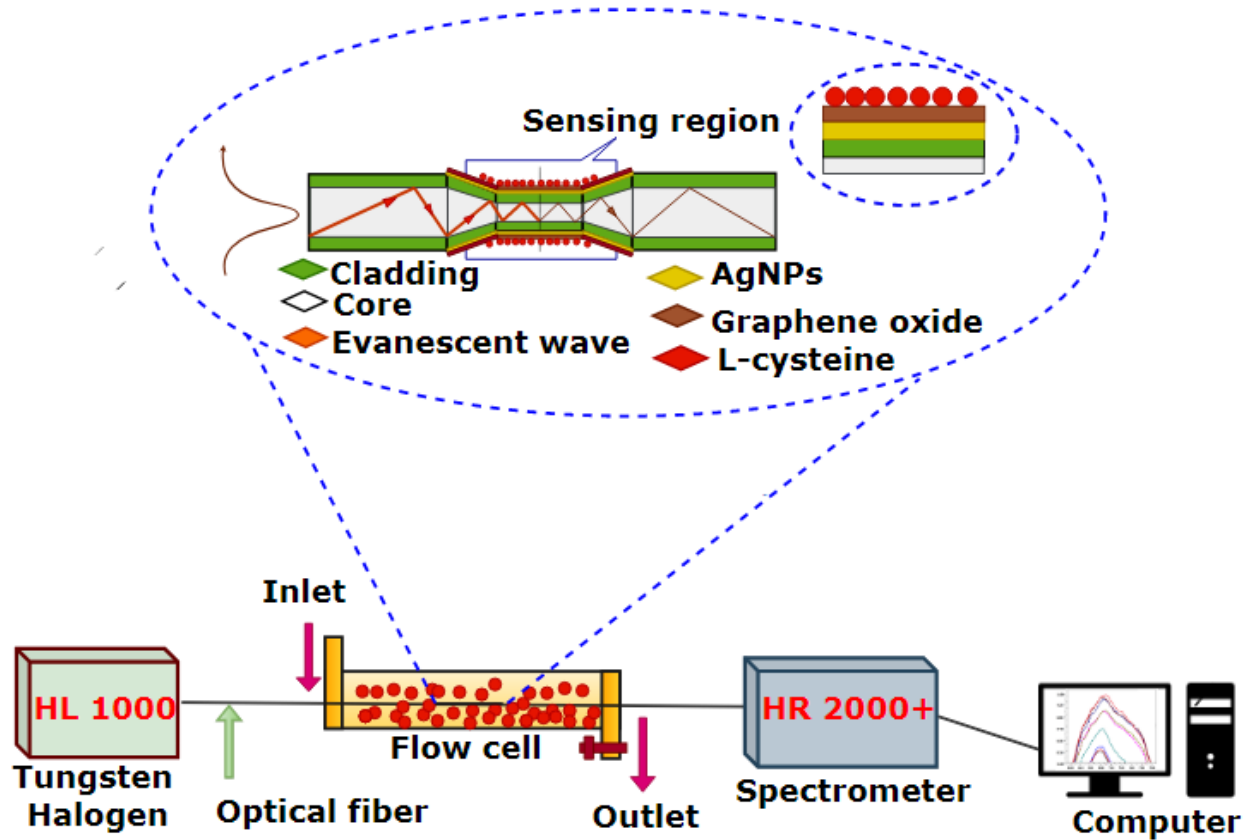


Figure 5.6: Schematic of an experimental setup for measurement of L-Cysteine [157] © 2020 IEEE.

wavelength shift. The use of lower size AgNPs ( $7.5 \pm 0.5$  nm) provides improved sensitivity of sensor probes. Further, AgNPs immobilized probe is nanocoated with GO, which can act as a stealth material, and provides a fine coating on the sensor probe. The LSPR spectra and linearity curve for the proposed L-Cys sensor are presented in Fig. 5.7 and Fig. 5.8, respectively.

**Probe-1:** Figure 5.7 (a) and Fig. 5.8 shows the LSPR spectra and linearity plot of Probe-1. The linearity curve equation, sensitivity and CC are revealed as,

$$\lambda = 0.0049 C + 669.99 \quad (5.1)$$

4.9 nm/mM and 0.8728, respectively. In this equation, C denotes the L-Cys concentration. The linearity of Probe-1 exists between  $100 \mu\text{M}$ -  $800 \mu\text{M}$  as revealed from linearity plot.

**Probe-2:** Figure 5.7 (b) and Fig. 5.8 indicates the LSPR spectra and linearity plot of Probe-2. The linearity curve equation, sensitivity and CC are revealed as,

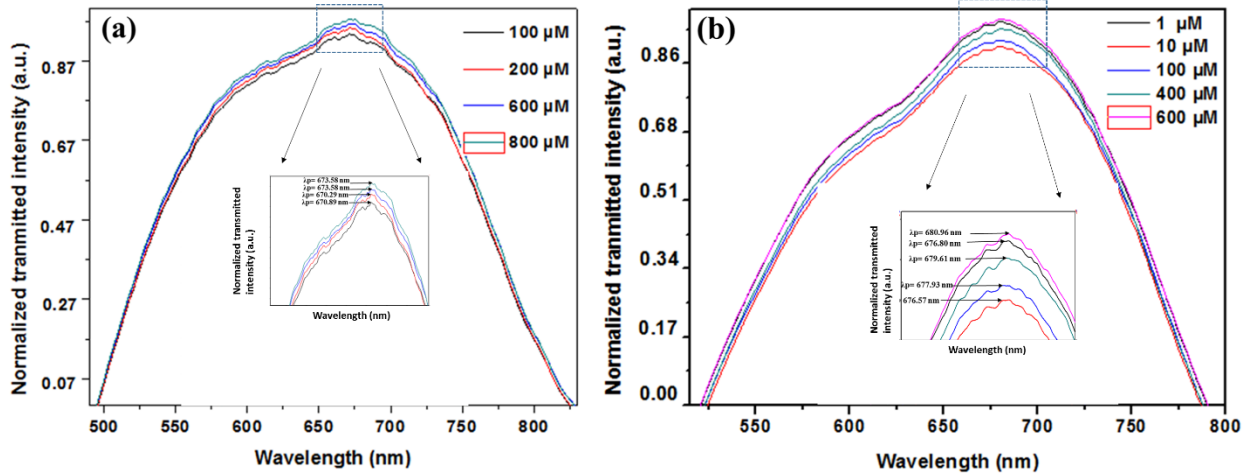


Figure 5.7: LSPR spectra of (a) Probe-1, (b) Probe-2 [157] © 2020 IEEE.

$$\lambda = 0.007 C + 676.56 \tag{5.2}$$

7.0 nm/mM and 0.9904, respectively. The linearity of Probe-2 exists between 10 nM- 1 mM as revealed from linearity plot.

In next step, to calculate the *LoD* of proposed L-Cys sensor, the standard equation is used as indicated below:

$$LoD = (3 \times SD) / \text{Sensitivity} \tag{5.3}$$

To calculate the value of SD, ten reference samples (peak resonance wavelength) are taken into consideration. To calculate the SD, the standard equation is used as indicated below:

$$\sigma = \sqrt{\frac{\sum(x_i - \mu)^2}{N}} \tag{5.4}$$

whereas, N is the size of reference samples,  $\mu$  is a mean of peak resonance wavelength of reference samples, and  $x_i$  is the peak resonance wavelength of reference sample. Here *LoD* indicates the ability to measure lowest concentration of analyte (L-Cys). The *LoD* for Probe-1 and Probe-2 are calculated as 142.84, and 63.25  $\mu\text{M}$ , respectively. Based on a comparative study of the proposed L-Cys sensor against previously reported L-Cys sensors, as shown in Table 5.1, indicates that different sensing parameters, like, sensitivity, linearity range, CC, and *LoD* have increased significantly. To confirm the reproducibility of L-Cys sensor, three separate tapered-SMS-GO-AgNPs-P-OFSs (Probe-2) sensing probe is tested with a 1  $\mu\text{M}$  L-Cys test sample. Further,

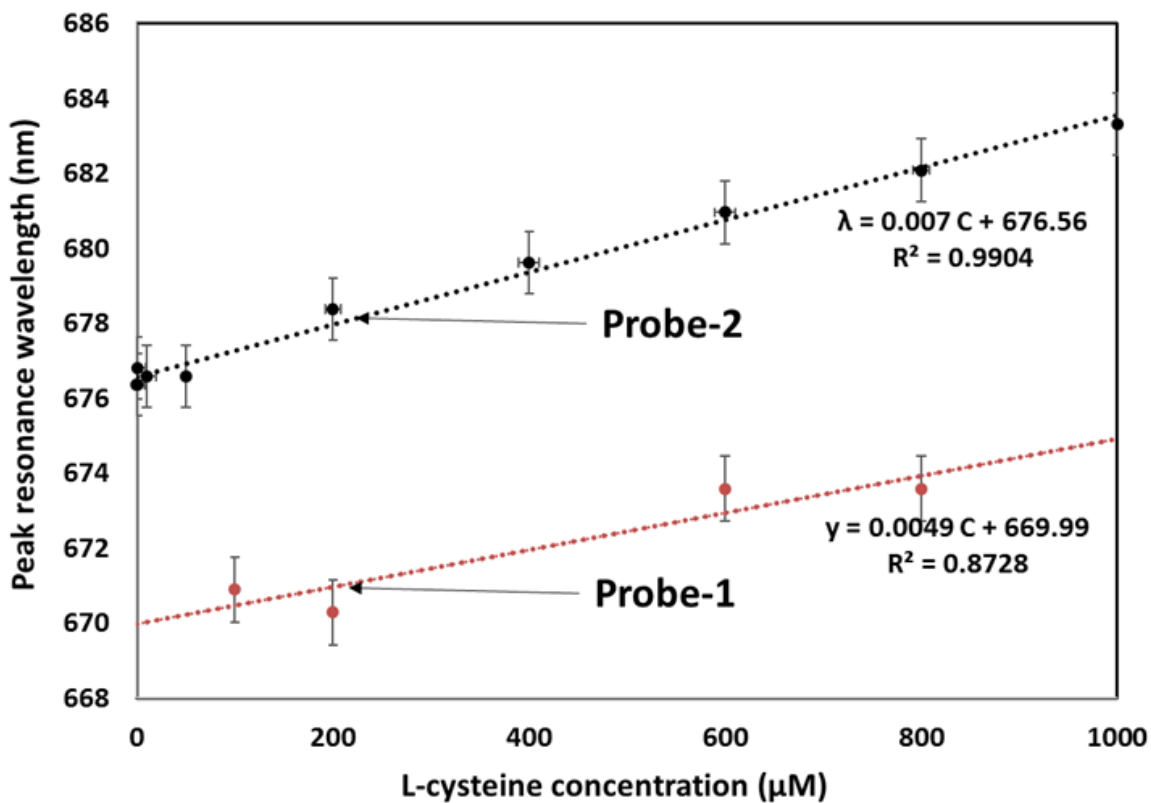


Figure 5.8: Linearity plot of L-Cysteine sensor [157] © 2020 IEEE.

Table 5.1  
Comparative study of L-Cysteine sensors [157] © 2020 IEEE

Material	Method	Linearity	Detection limit	Sensitivity	Ref.
Silver nanoparticles	Colorimetric method	1.67 to 13.36 μM	260 nM	n.r <sup>a</sup>	[158]
Gold nanoparticles	Fluorescence method	0.08 to 6.0 μM	40 nM	n.r <sup>a</sup>	[159]
Silver nanoparticles	Colorimetric method	25 to 250 μM	n.r <sup>a</sup>	n.r <sup>a</sup>	[160]
Gold nanoparticles	Chromatography	1 to 4.5 μM	800 nM	n.r <sup>a</sup>	[161]
GO and AgNPs (Probe-1)	LSPR technique	100 to 800 μM	142.84 μM	4.9 nm/mM	This Work
GO and AgNPs (Probe-2)	LSPR technique (Proposed sensor)	10 nM to 1 mM	63.25 μM	7.0 nm/mM	

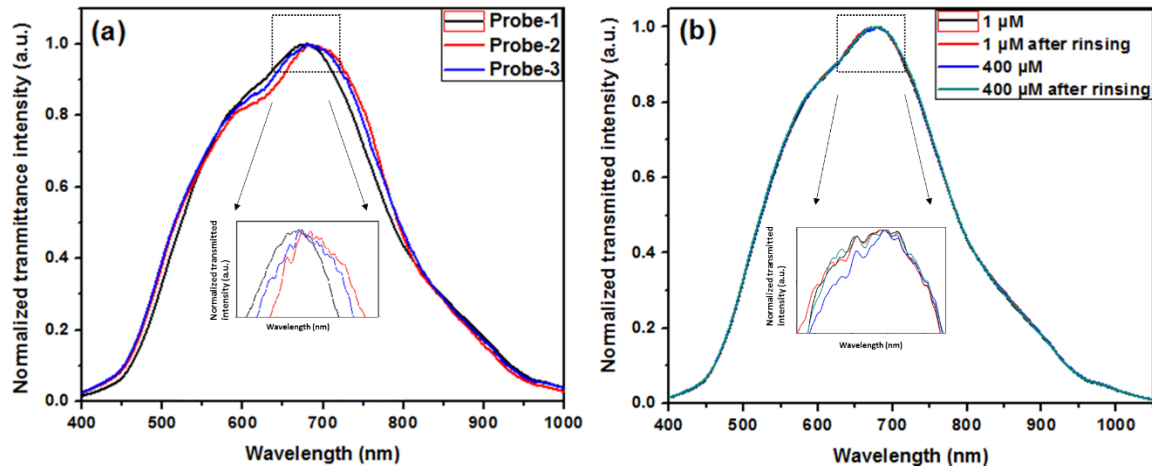


Figure 5.9: (a) Reproducibility, and (b) reusability test for Probe-2 [157] © 2020 IEEE.

reusability test of proposed probe is tested with 1  $\mu\text{M}$  and 400  $\mu\text{M}$  L-Cys test samples. The reproducibility test and reusability test plot are shown in Fig. 5.9(a)-(b), respectively. Other parameters like repeatability and reusability also reveal great performance, indicates the potential use of proposed sensor probe for effective detection of L-Cys.

## 5.5 Summary

In present study, practical realization of proposed tapered-SMS-GO-AgNPs-P-OFSs is stated for effective detection of L-Cys urinary protein. Due to the combined features of two different structural modifications (i.e., tapered and hetero-core), results like linearity range, CC, sensitivity, and  $LoD$  are significantly increased and recorded as 10 nM- 1 mM, 99.04%, 7.0 nm/mM, and 63.25  $\mu\text{M}$ , respectively. The improved performance of proposed sensor shows a potential application for L-Cys detection. In conclusion, proposed L-Cys P-OFSs is economical, compact, and can be used for remote sensing application. The proposed L-Cys sensor probe is analyzed and indicates the potential use of sensing probes for effective and accurate L-Cys detection in biological fluids.

# **Chapter 6**

## **Development of Cholesterol Sensor using Core Mismatch MPM/SPS Structure-based Optical Fiber Sensor Probe**

## 6.1 Introduction

The previous chapter of the thesis dealt with development and experimental validation of tapered SMS structure-based P-OFSs for L-Cys detection. The development of yet another LSPR phenomenon-based OFSs for detection of Cholesterol (Cho), an important component of bio-fluid, is discussed in this chapter. This sensor uses a hetero-core MMF-PSF-MMF (MPM)/ SMF-PSF-SMF (SPS) structure. In a hetero-core-based LSPR sensor, a small length of fiber with different core diameters is inserted between low transmission-loss normal SMFs. This chapter explains about fabrication of proposed hetero-core design-based SPS and MPM sensor probe and their design considerations for the detection of Cho present with human body fluid, synthesis of NPs, nanocoating, and functionalization process, characterization of NPs, and nanocoated probe. The performance of proposed Cho sensor is also checked over the different prime sensing parameters. In addition, results of selectivity, reproducibility, and reusability test are presented below sections. The operational mechanism of these sensors is discussed in terms of leaks occurring at the hetero-core interfaces [162]. This phenomenon combines the features of hetero-core structure-based OFSs and EWs sensors. In this sensor, a single-mode beam partly leaks into cladding at the boundary interface between hetero-core section and transmission fiber. Since a large core diameter at the hetero-core part could be sufficient to sustain single-mode propagation, the maximum power can be transmitted over proposed structure with a comparatively low loss [163]. Hetero-core design-based P-OFSs have higher sensitivity due to the mode-coupling at the spliced part. Since there is a substantial variation in diameter of cores, optical signals can leak into the cladding region after the splice [43]. All the information and rationale behind the selection of PSF and MMF in proposed structure, along with the advantages of using a hetero-core design-based sensor for the bio-sensing application is presented in this study. Also, the brief information on the binding of AuNPs and ZnO-NPs, and specific application in biosensing field are discussed in this chapter. The LSPR spectra are recorded at different Cho test samples in the range of 0.1- 10 mM. The Cho is one of the essential biological supplies (sterols) like steroid hormones, Vitamin-D, and bile acids of the human body system [164]. In present study, three different configurations are designed, developed, and tested using the applied selection of SMF/ MMF/ 10nm\_Au+ZnO-NPs/ 30nm\_Au+ZnO-NPs, hereinafter named as Probe-1 (MPM/ZnO-NPs/AuNPs(10nm)/P-OFSs), Probe-2 (MPM/ZnO-NPs/AuNPs(30nm)/P-OFSs), and Probe-3 (SPS/ZnO-NPs/AuNPs(10nm)/ P-OFSs).

## 6.2. Experimental Methodology

The plasmonic phenomenon-based OFSs is proposed to detect the Cho concentration available with serum in human body. The different steps in development of proposed Cho sensors, like sensor fabrication and design consideration, synthesis, and immobilization of NMs are described below.

### 6.2.1. Sensor Fabrication and Design Consideration

The optical fibers such as SMF, MMF, and PSF are used in the development of MPM/SPS-based design of Cho sensor. Three different configurations are designed and studied. The schematic of MPM/ SPS bare fiber probe and three configurations of proposed sensor probes are displayed in Fig. 6.1, and Fig. 6.2, respectively. These structures offer several benefits, such as i) lower insertion loss, ii) less attenuation, iii) low birefringence due to higher difference in core/ cladding index iv) cladding mode suppression, iv) RI of PSF core is greater than of conventional fiber v) enhanced sensitivity, v) can withstand at a higher temperature (sustained up to 300°C for long term duration and up to 400°C for short term duration) due to polyimide coating, vi) excellent resistance to micro and macro bend losses due to higher NA, vii) 5 times more Ge-doping, etc., of using PSF in comparison with conventional SMF. As the attenuation in PSF is small, it permits the use of long-distance communication and reduces the insertion loss in designing fiber optic components [165], and as such PSF based sensor is widely used in bio-sensing applications [166]. Further, the use of PSF in projected MPM and SPS configurations, enhances various sensor performance parameters which include, i) sensitivity, ii) *LoD*, iii) selectivity and iv) CC. Here, core-mismatch design and etched PSF segment play an essential role in light leakage through sensing region which excites the desired LSPR phenomenon into outside media.

### 6.2.2 Nanomaterial Realization, Nanocoating, and Functionalization Process

Reagents such as H<sub>2</sub>SO<sub>4</sub>, H<sub>2</sub>O<sub>2</sub>, ChOx enzyme ( $\geq 20$  unit/mg protein), NHS, EDC, MUA, Cho (C8667, Sigma-Aldrich) MPTMS, ZnO-NPs ( $\leq 40$  nm), tri-sodium citrate, HAuCl<sub>4</sub>, hydrofluoric acid (HF), 5% Triton X-100, DI, PBS, glucose, AA, D-Gal, UA, and urea are used during synthesis, immobilization, and functionalization process of proposed Cho sensor. AuNPs (sizes:

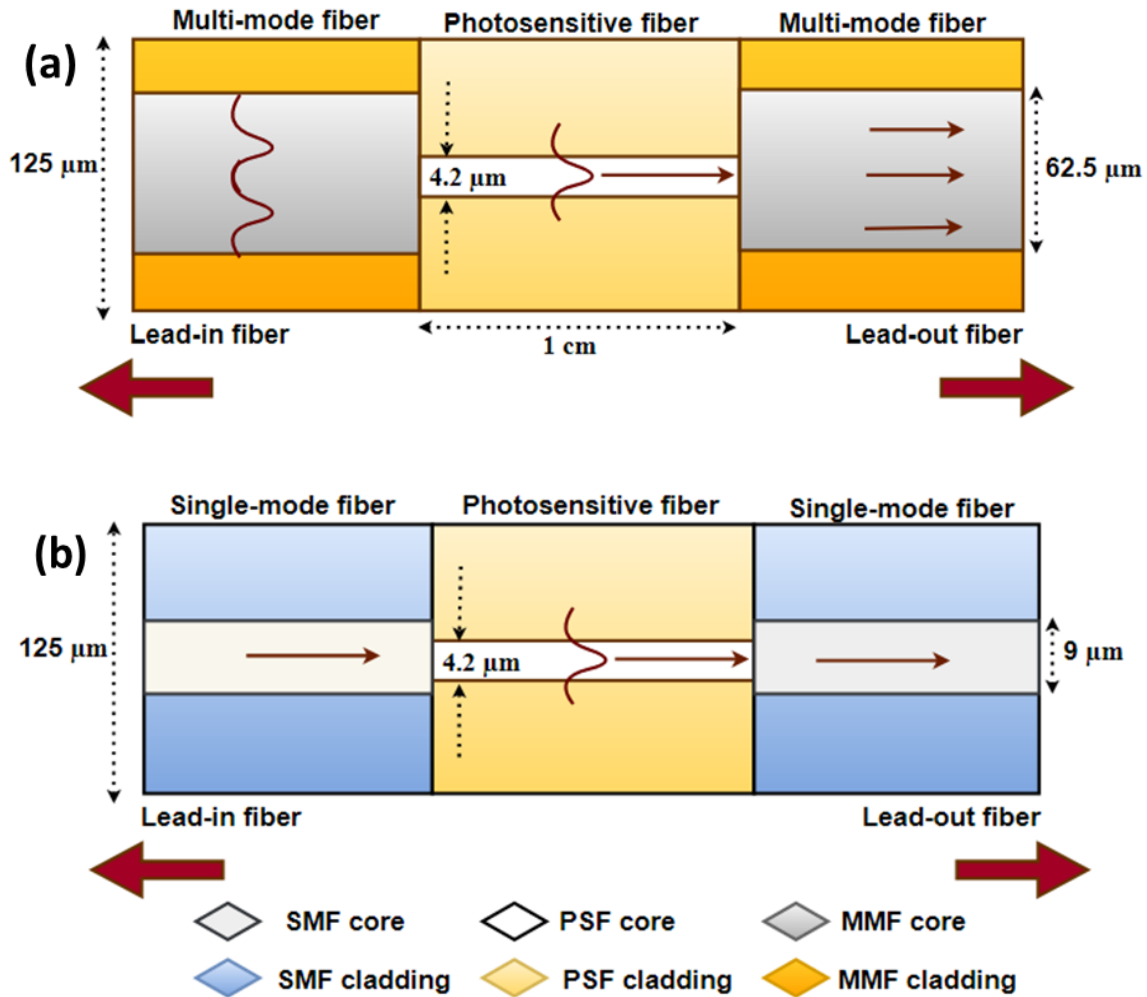


Figure 6.1: Schematic of different configurations and design considerations of proposed P-OFSs (a) MPM, and (b) SPS [43] © 2020 *IEEE*.

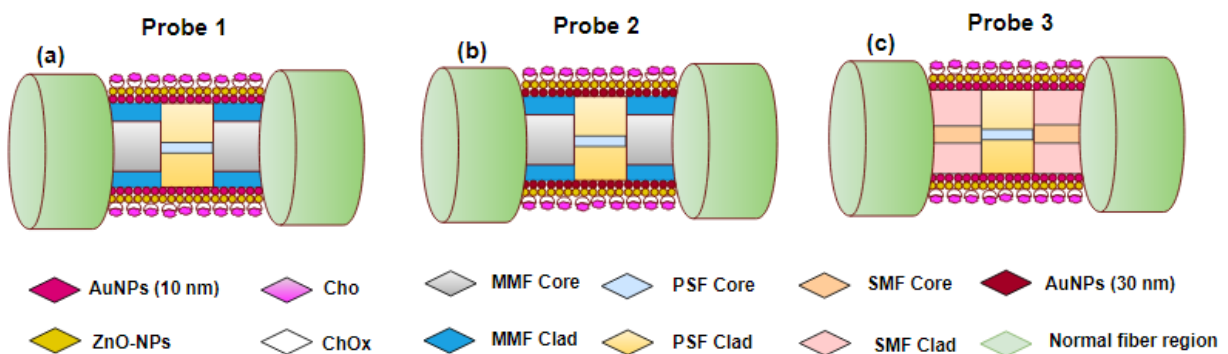


Figure 6.2: Different configurations of cholesterol sensor, (a) Probe-1, (b) Probe-2, and (c) Probe-3 [43] © 2020 *IEEE*.

30 and 10 nm) are synthesized using Turkevich method. The AuNPs synthesis process is briefly described in the experimental methodology section of Chapter 4. A wide range of solution-based approaches is reported to control size [167], shape [168], and surface functionality [169] of the AuNPs. The color of synthesized 10nm\_AuNPs and 30nm\_AuNPs solutions turns to reddish and dark reddish, respectively indicating the formation of proposed NMs. The absorbance, size, and shape of resultant AuNPs are confirmed with HR-TEM and UV-spectrophotometer. In next step, an aqueous solution of ZnO-NPs is prepared by titration method [169]. The proposed SPS/ MPM bare fiber structure is nanocoated with 10nm\_AuNPs/ 30nm\_AuNPs followed by ZnO-NPs. The schematic of nanocoating procedure is presented in Fig. 6.3. The AuNPs immobilization process is carried out as described in experimental methodology section of Chapter 4. The AuNPs immobilized probe is further nanocoated by ZnO-NPs. For this, a probe is rinsed with ethanol and then dipped into ZnO-NPs aqueous solution for 10 min. Then, it is annealed at 150°C in the oven for 20 min. The above process was repeated thrice for uniform coating of ZnO-NPs [170].

In next step, the nanocoated probe is functionalized with MUA (0.5 mM), EDC (200 mM), and NHS (50 mM) to produce and activate the carboxyl groups. Then it is further functionalized with cholesterol oxidase (ChOx) ( $\geq 20$  unit/mg protein). For this ChOx (0.32 mg) is added to 1 X PBS (0.5 ml) and probe is dipped for 12 hrs. The mechanism used for the functionalization of an enzyme (ChOx) is revealed in Fig. 6.4.

### 6.3 Characterization and Measurement

The characterization results of AuNPs and ZnO-NPs are shown in Fig. 6.5 and the results of the immobilized probes are shown in Fig. 6.6. Various sophisticated instruments, e.g., HR-TEM, EDS, UV-spectrophotometer, SEM, and AFM are used to characterize the NMs and nanocoated sensor probes. The following important observations are recorded during the characterization of NMs and immobilized sensor probes:

- i. absorbance spectrum of ZnO-NPs, 10nm\_AuNPs, and 30nm\_AuNPs are recorded at 370, 519, and 527 nm, respectively,
- ii. spherical shape with uniform size of the prepared 10nm\_AuNPs and 30nm\_AuNPs are confirmed with HR-TEM,

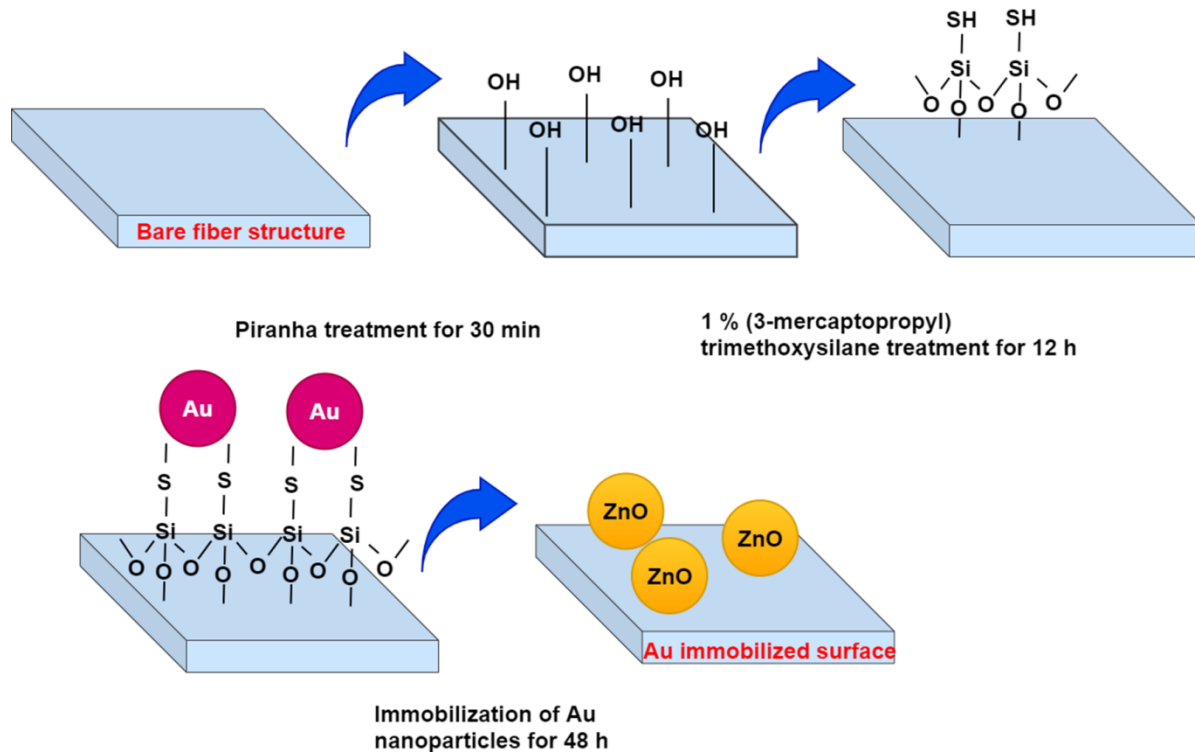


Figure 6.3: Schematic of nanocoating process [43] © 2020 IEEE.

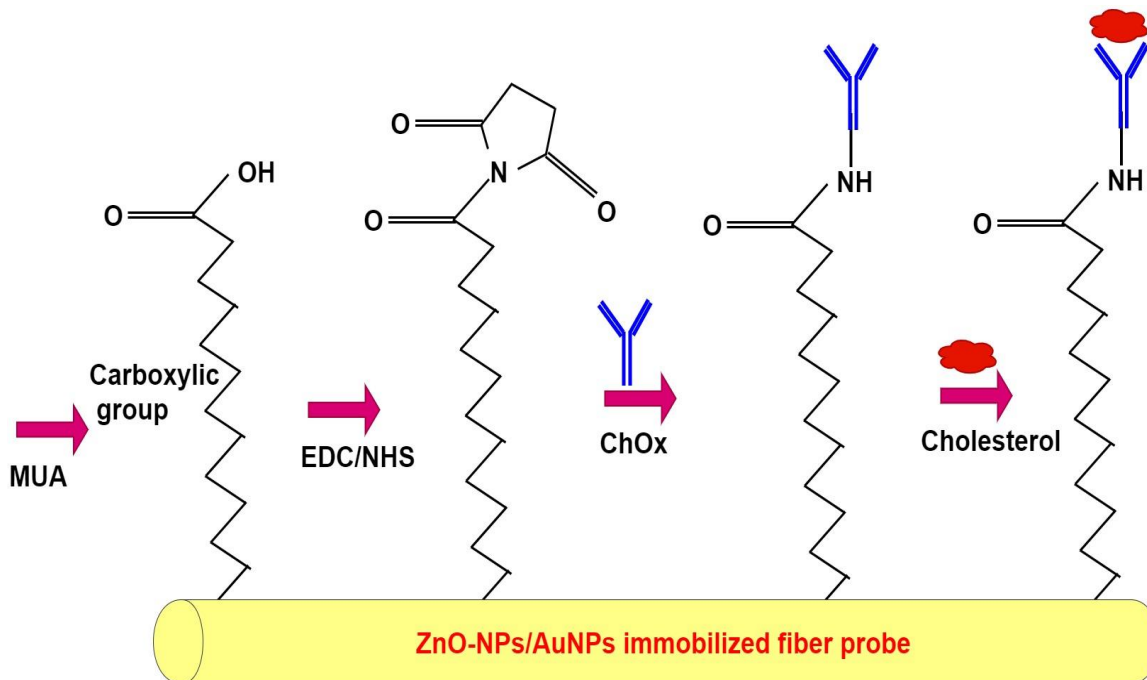
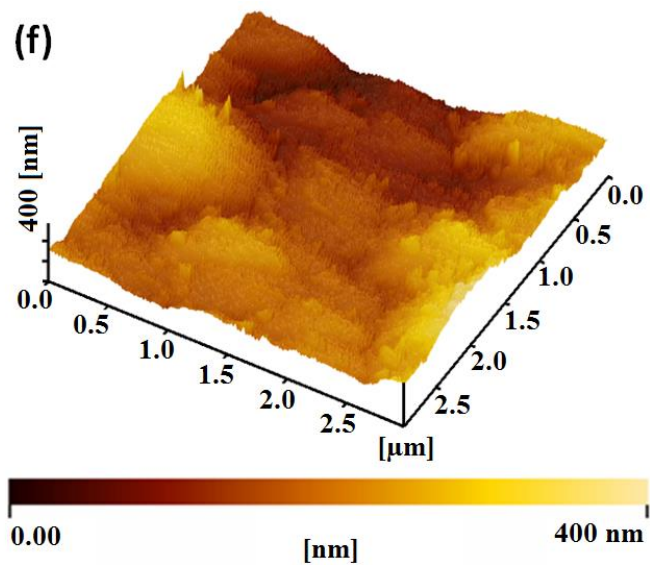
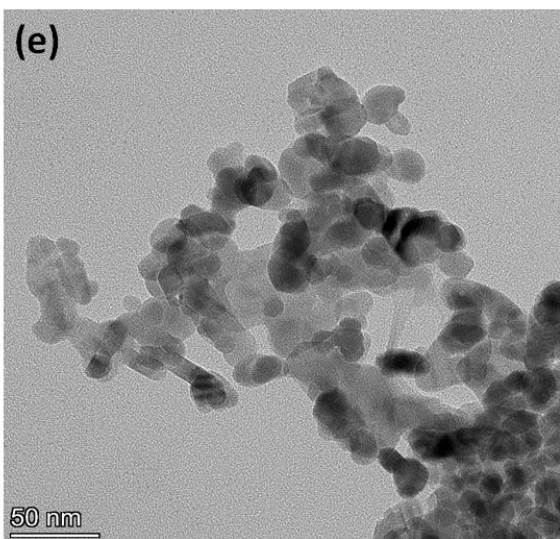
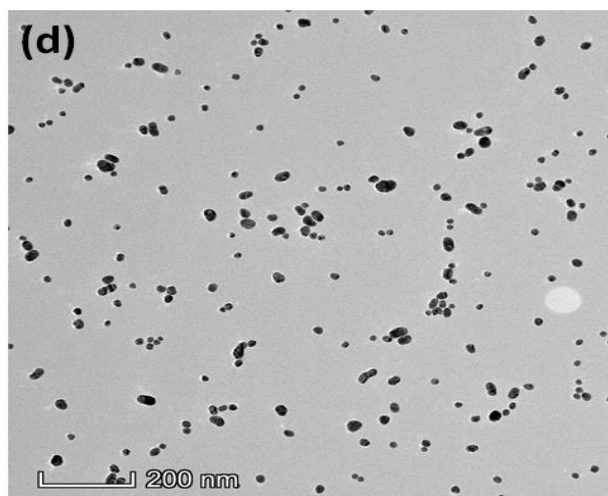
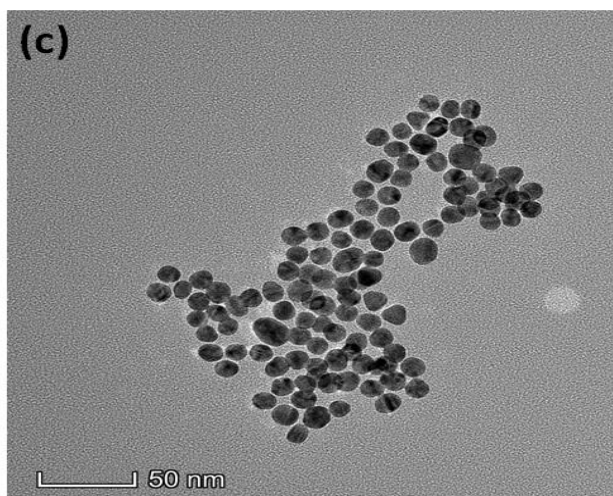
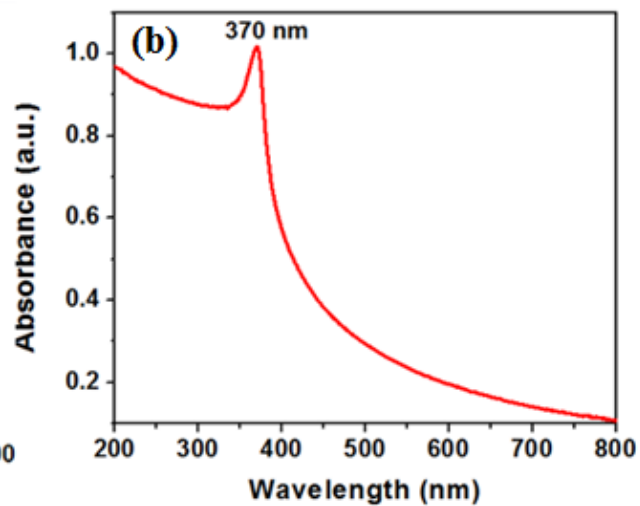
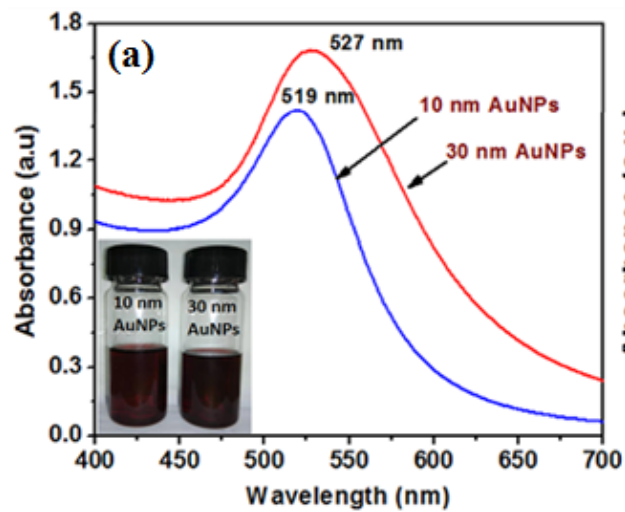


Figure 6.4: Schematic of enzyme functionalization process [43] © 2020 IEEE.



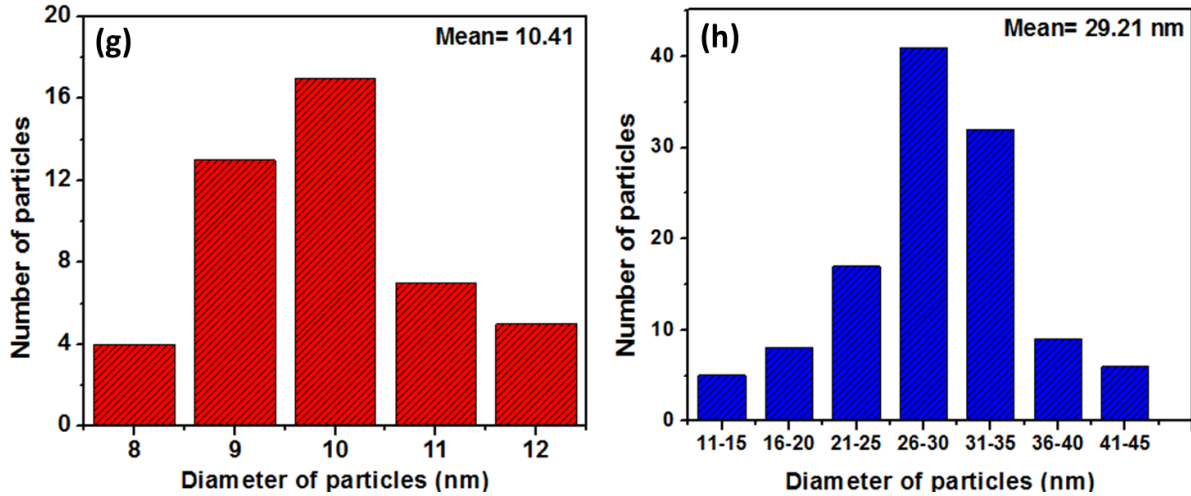


Figure 6.5: Absorbance spectrum of (a) 10nm and 30nm\_AuNPs, and (b) ZnO-NPs; HR-TEM image of (c) 10nm\_AuNPs, (d) 30nm\_AuNPs, and (e) ZnO-NPs; (f) AFM of ZnO-NPs, histogram analysis of (g) 10nm\_AuNPs, and (h) 30nm\_AuNPs [43] © 2020 IEEE.

- iii. mean particle size of 30nm\_AuNPs and 10nm\_AuNPs are observed at 29.21, and 10.41 nm, respectively, (revealed from histogram analysis using Image J-10 software)
- iv. extremely fine nanocoating over sensor surface is observed in case of 10nm\_AuNPs in comparison with 30nm\_AuNPs.

The experimental setup for Cho measurement is presented in Fig. 6.7. The wide-range Cho test samples, in the range of 100  $\mu$ M – 10 mM are prepared to check the performance of proposed Cho sensors. This stock solution is prepared using 5% Triton X-100, and Cho (C8667). To generate the optical signal, and record the LSPR spectra, instruments such as optical source and optical spectrometer are used. The performance of Cho sensor is analyzed thoroughly, and the spectral signal was recorded after stabilization. It was observed that normalized transmitted intensity of LSPR spectrum changes with different Cho concentrations. The wavelength shift is because of Cho-ChOx reaction, where the enzyme(ChOx) oxidizes the detection element (Cho) in presence of oxygen into cholestenone and H<sub>2</sub>O<sub>2</sub>. The volume of H<sub>2</sub>O<sub>2</sub> varies with Cho concentration, which changes the RI of an analyte and corresponds to the shift in LSPR spectra.

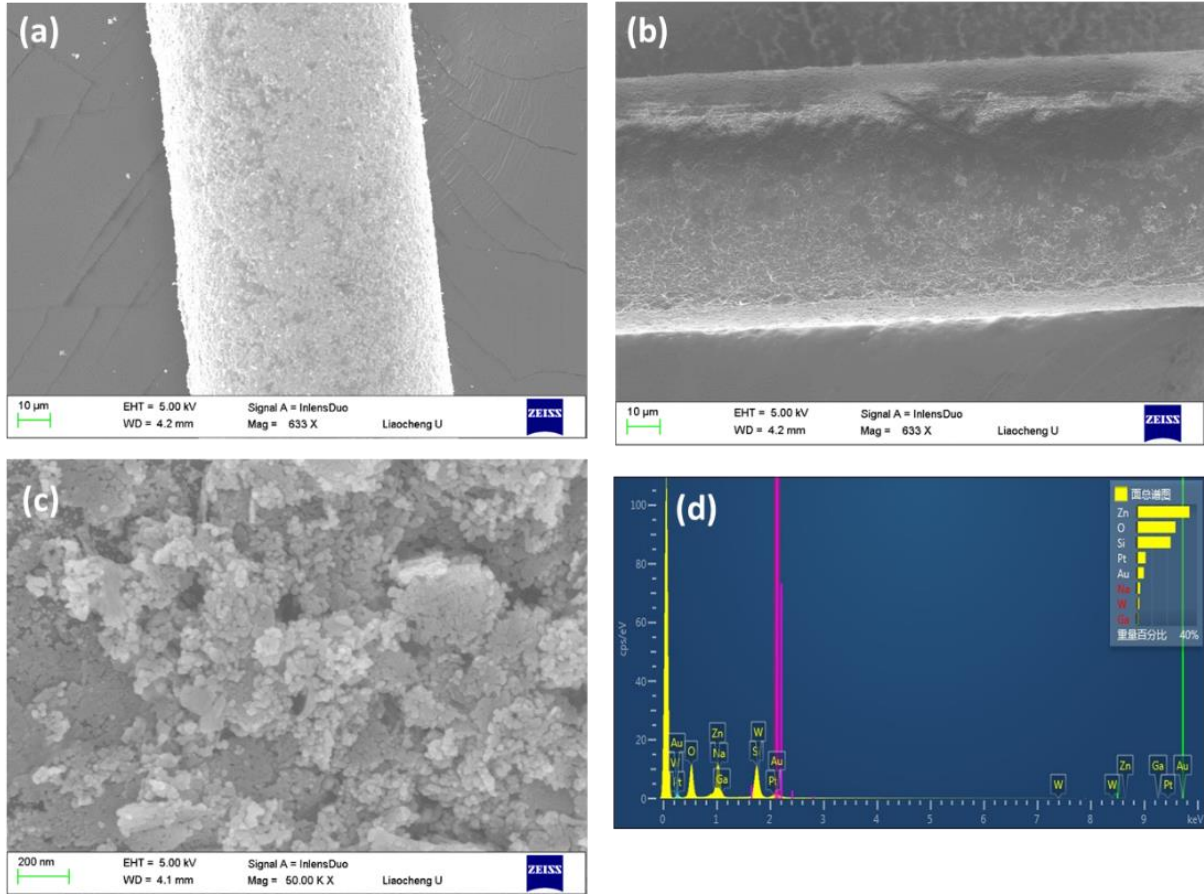


Figure 6.6: SEM image of (a) ZnO-NPs, and 10nm\_AuNPs nanocoated probe, (b) ZnO-NPs, and 30nm\_AuNPs nanocoated probe, and (c) sensor probe at higher magnification, and (d) EDS image [43] © 2020 *IEEE*.

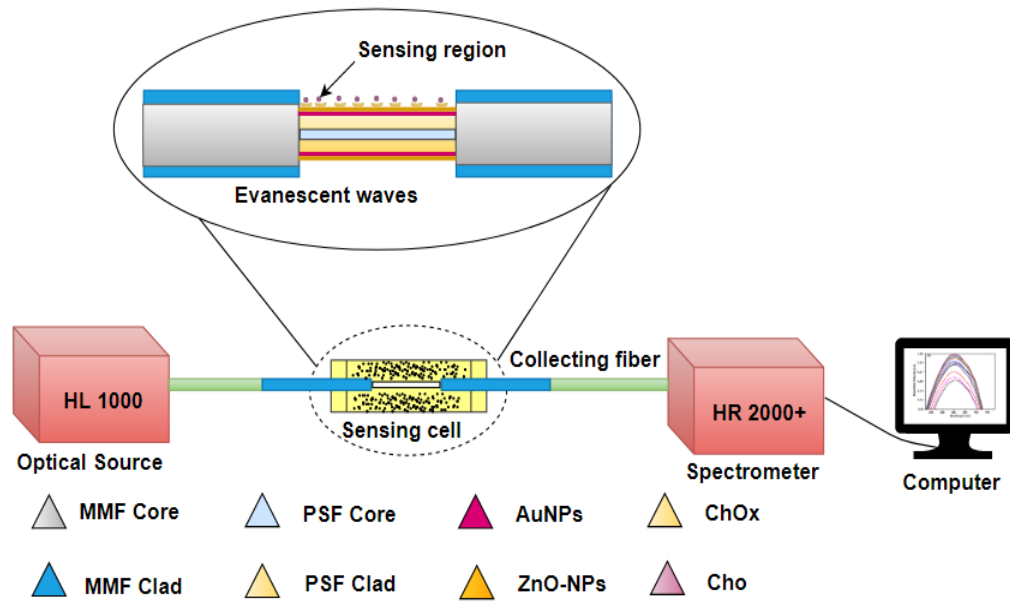


Figure 6.7: Schematic of an experimental setup for the measurement of cholesterol [43] © 2020 *IEEE*.

## 6.4 Results and Discussion

### 6.4.1 Performance of Cholesterol Sensor

Various optimization results, such as i) MPM Vs. MSM structure analysis, ii) calibration curve of PSF length vs. normalized intensity, iii) calibration plot to analyze an etching time of probe, and iv) etching time vs. waist diameter calibration plots are presented in Fig. 6.8. The

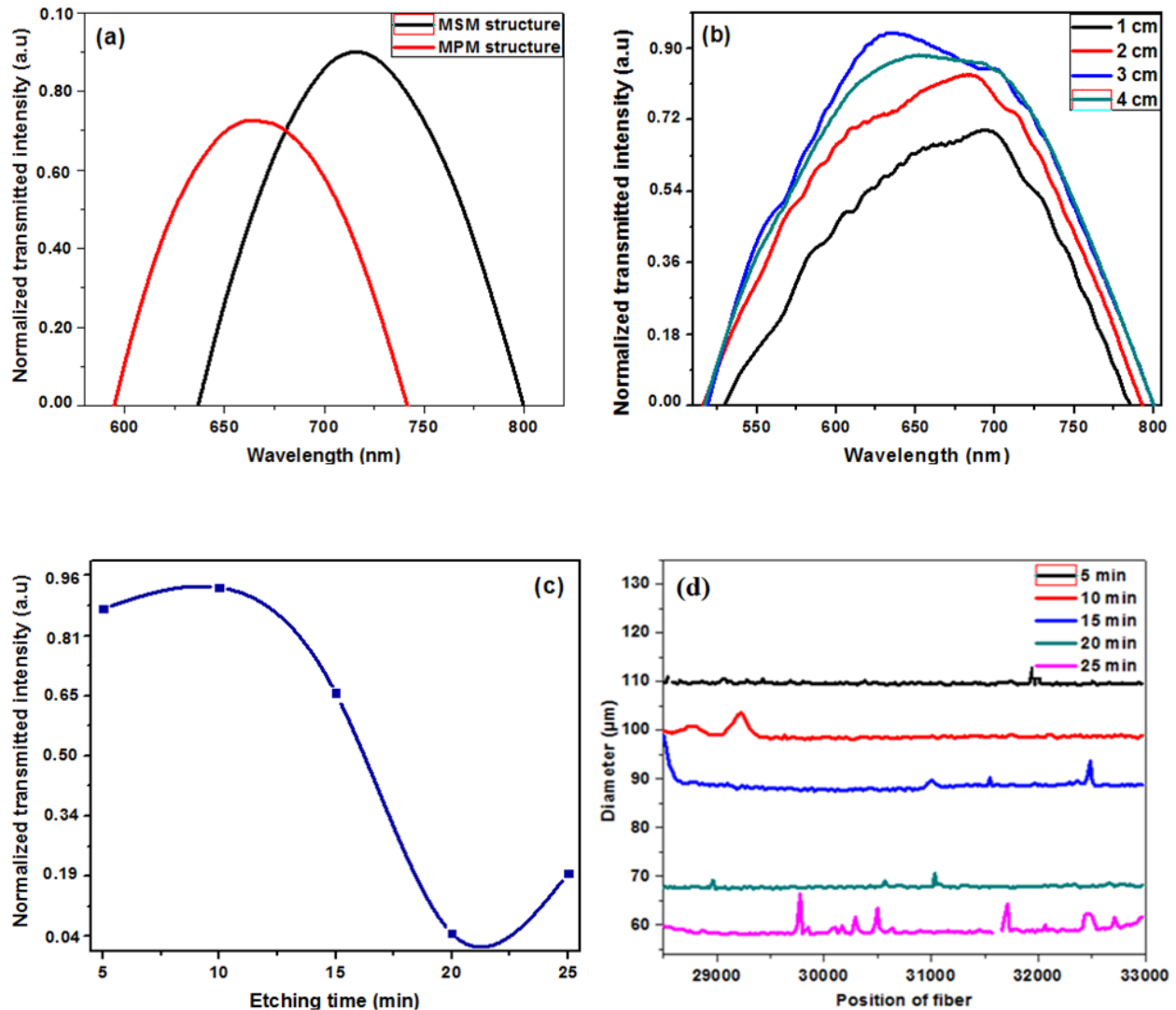


Figure 6.8: Structural optimization of (a) MPM Vs. MSM structure, (b) calibration curve of PSF length used is proposed SPS/ MPM structure, (c) calibration plot to analyze the etching time of probe and (d) etching time Vs. waist diameter calibration plot [43] © 2020 IEEE.

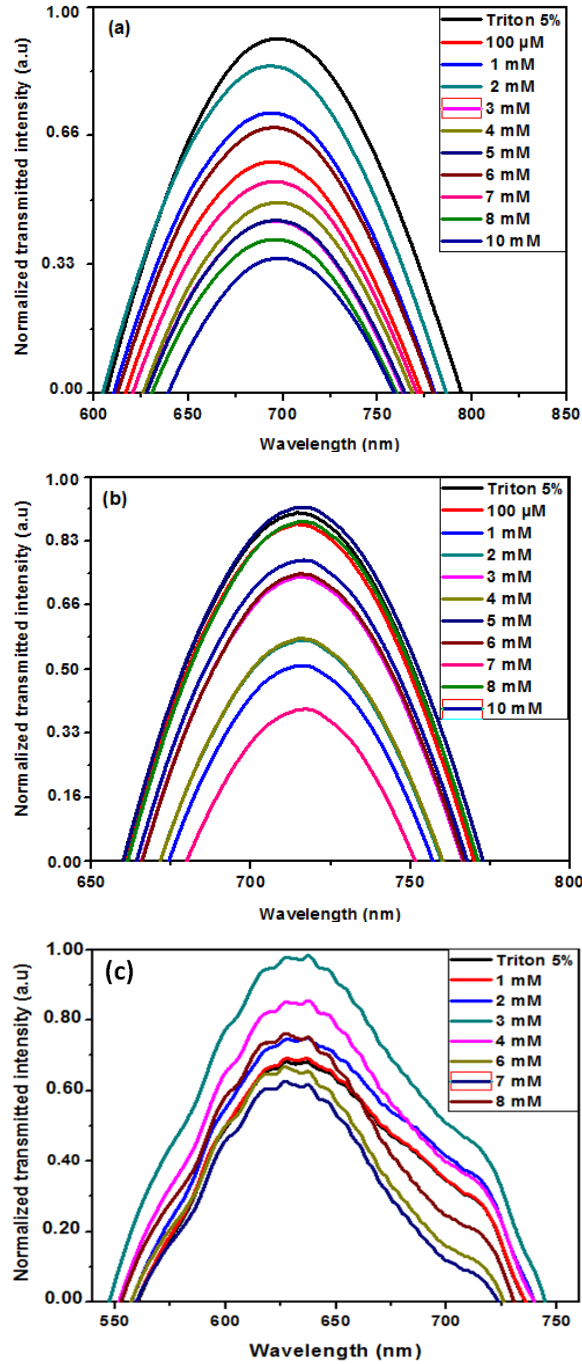


Figure 6.9: LSPR spectra for (a) Probe-1, (b) Probe-2, and (c) Probe-3 [43] © 2020 *IEEE*.

measurement results form of LSPR spectra and linearity plot are revealed in Fig. 6.9, and Fig. 6.10, respectively. On average, three independent measurements are observed to plot the LSPR spectra and linearity plots.

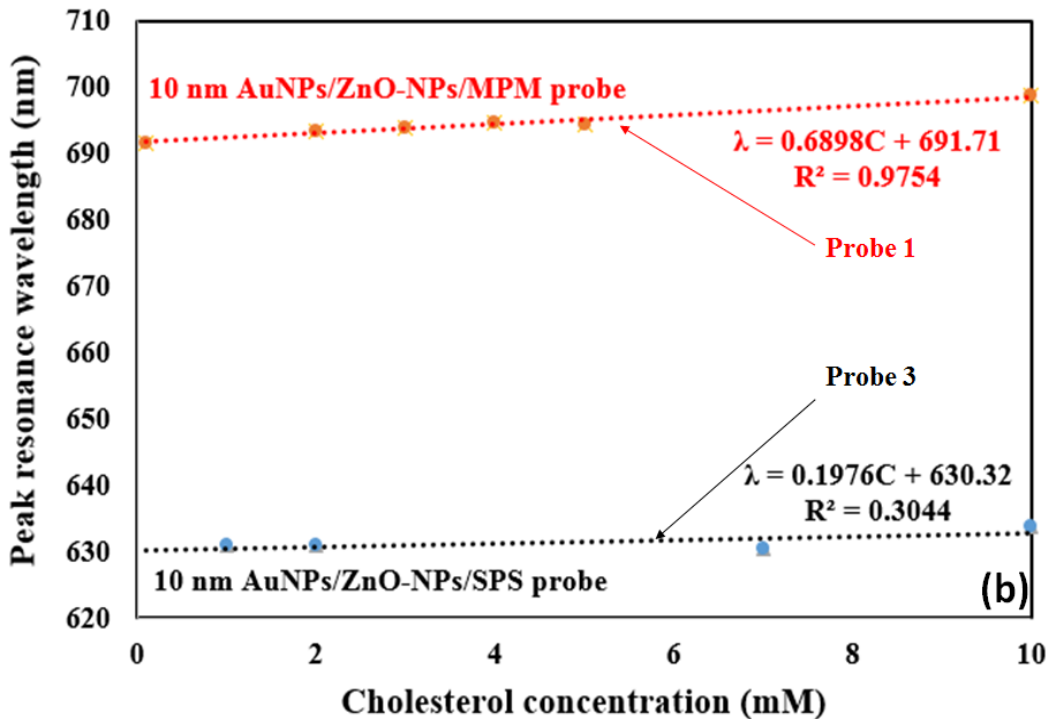
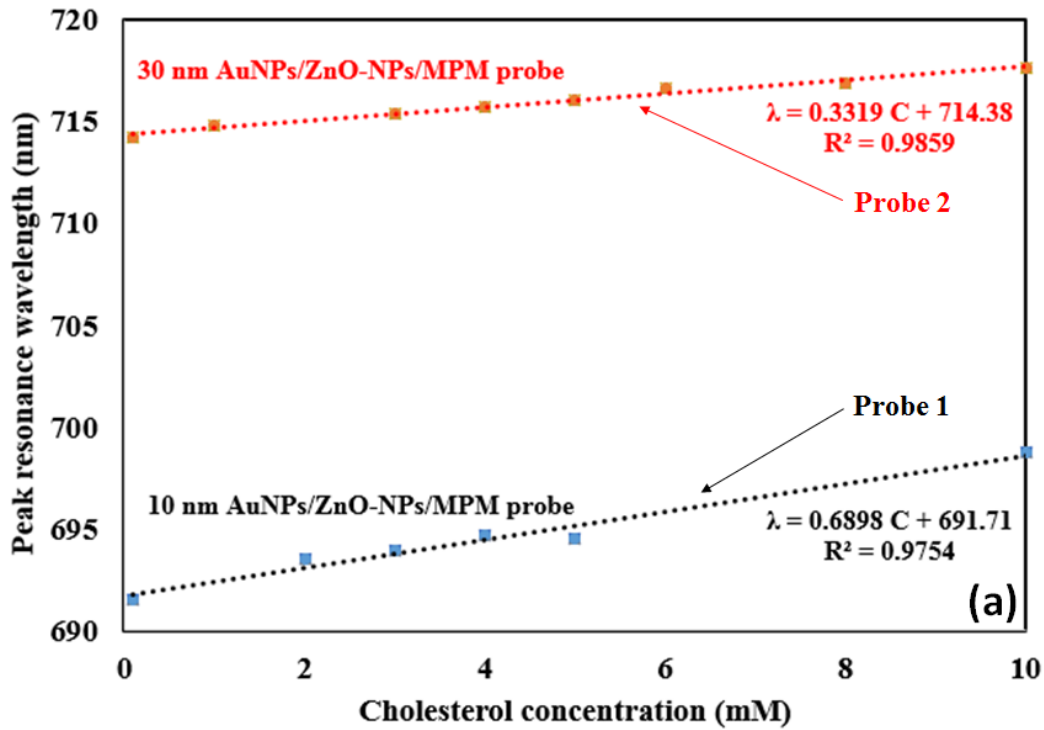


Figure 6.10: (a) Linearity plot of Probe-1 and -2, and (b) linearity plot of Probe-1 and -3 [43] © 2020 *IEEE*.

**Probe-1** (MPM/ZnO-NPs/10nm\_AuNPs/ P-OFSs): The results such as LSPR spectra and linearity plot of Probe-1 are revealed in Fig. 6.9(a), and Fig. 6.10(a), respectively. The measured sensing

parameters of Cho sensor like *LoD*, CC, and sensitivity for Probe-1 are recorded as 0.6161 mM, 0.9754, and 0.6898 nm/mM, respectively.

**Probe-2** (MPM/ZnO-NPs/30nm\_AuNPs/P-OFSs): The results such as LSPR spectra and linearity plot of Probe-2 are displayed in Fig. 6.9(b), and Fig. 6.10(b), respectively. The measured sensing parameters, such as *LoD*, CC, and sensitivity for Probe-2 are observed as 1.2777 mM, 0.9859, and 0.3319 nm/mM, respectively.

**Probe-3** (SPS/ZnO-NPs/10nm\_AuNPs/P-OFSs): The results such as LSPR spectra and linearity plot of Probe-3 are displayed in Fig. 6.9(c), and Fig. 6.10(b), respectively. Here, Probe-3 is comprised as a reference for structural evaluation.

The linearity of the proposed sensor (Probe-1) is 0.1 to 10 mM, which is well-suited for detection of Cho in serum as normal concentration of Cho is  $\sim 5.17$  mM. The comparative study over proposed Probe-1, -2, and -3 is indicated in Table 6.1.

#### 6.4.2 Reusability, Reproducibility, and Selectivity test

The test results of proposed Cho sensor probes such as reusability and reproducibility test, and selectivity test are shown in Fig. 6.11, and Fig. 6.12, respectively. These tests are very crucial for

Table 6.1  
Performance of proposed cholesterol sensors [43] © 2020 IEEE

Material used	Sensor structure	Mechanism	Linear range	Limit of detection	Sensitivity	Proposed Sensor
Zinc and gold (10 nm) nanoparticles	MPM structure	LSPR	1 - 10 mM	0.6161 mM	0.6898 nm/mM	Probe-1 (Proposed sensor)
Zinc and gold (30 nm) nanoparticles	MPM structure	LSPR	0.1 - 10 mM	1.2777 mM	0.3319 nm/mM	Probe-2
Zinc and gold (10 nm) nanoparticles	SPS structure	LSPR	0.1 - 10 mM	2.1748 mM	0.1976 nm/mM	Probe-3

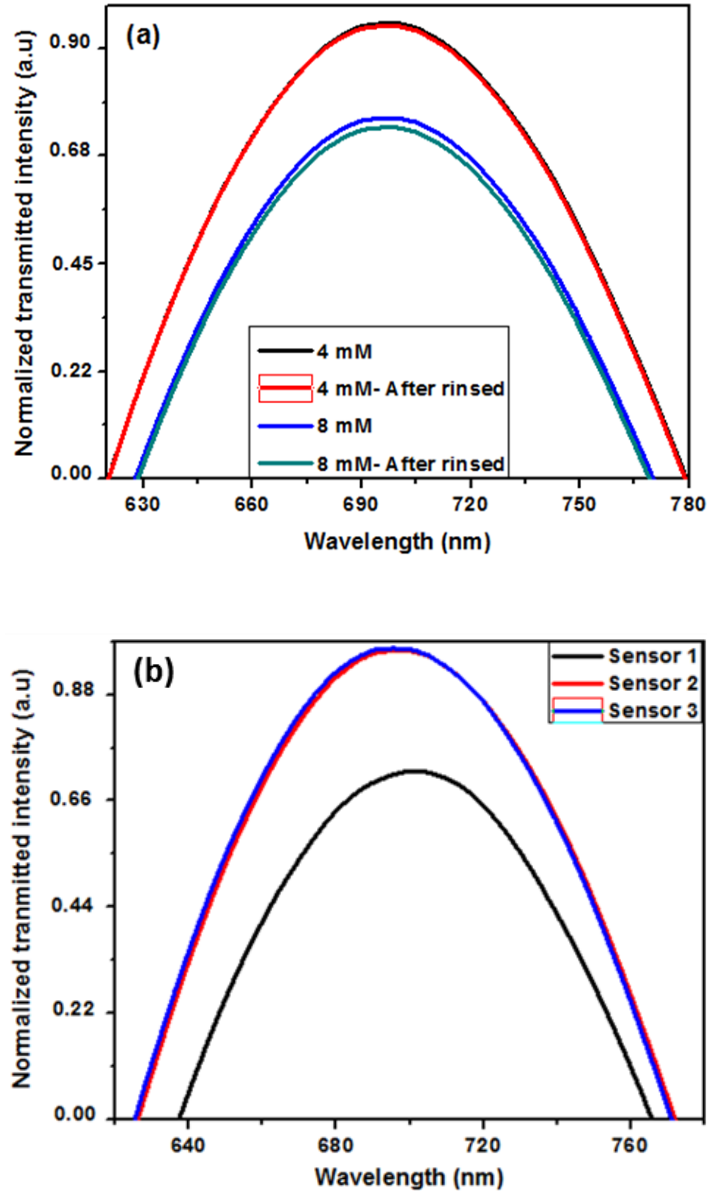


Figure 6.11: (a) Reusability, and (b) reproducibility test for Probe-1 [43] © 2020 IEEE.

the LSPR phenomenon-based biosensing device. Among the proposed probes (Probe-1, 2, and 3) it is found that Probe-1 has shown superior performance in terms of sensitivity,  $LoD$ , and  $CC$  parameters, compared to the other two probes (Probe-2 and -3). Due to this reusability, and reproducibility results are investigated with Probe-1 only. The reusability test for Probe-1 has been measured over 8 mM and 4 mM Cho samples. Similarly, reproducibility test of Probe-1 is tested over the Cho samples of 7 mM. After each experiment, sensor probe is cleaned with buffer solution (PBS) to eliminate the suspension of previous Cho sample. A combination of reagents such as UA,

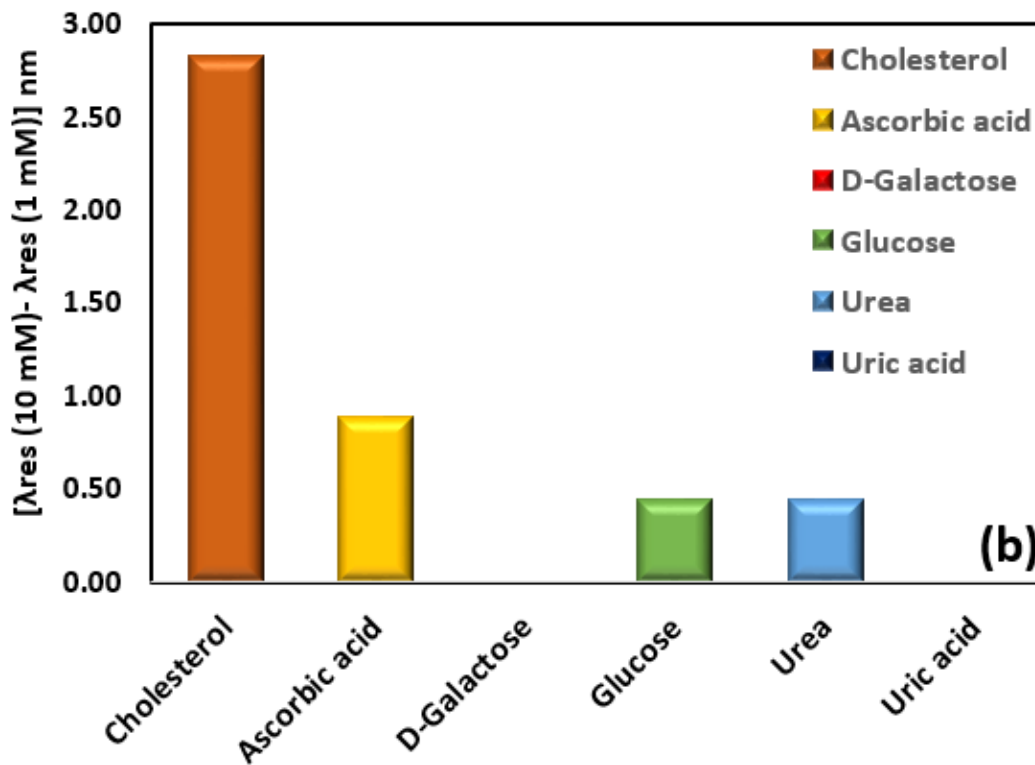
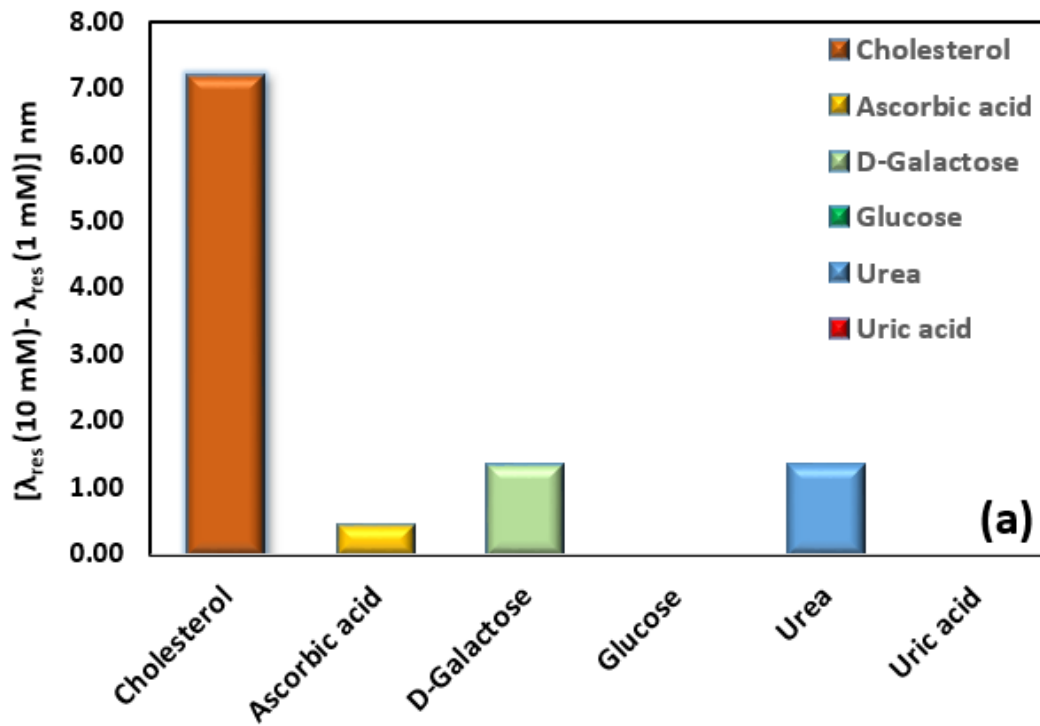


Figure 6.12: Selectivity test for (a) Probe-1, and (b) Probe-2 [43] © 2020 *IEEE*.

Table 6.2  
Comparative study of cholesterol sensors [43] © 2020 *IEEE*

Material	Method	Linearity	LoD	Sensitivity	Ref.
AgNPs	Hydrogen Peroxide Sensing	0 to 50 $\mu\text{M}$	5.50 $\mu\text{M}$	n.r <sup>a</sup>	[171]
Au/BDT <sup>b</sup> /Ag	SERS method <sup>c</sup>	0 to 100 $\mu\text{M}$	5.50 $\mu\text{M}$	n.r <sup>a</sup>	[172]
Al-doped zinc oxide (AZO)	CBD method <sup>d</sup>	1.3 mM to 13 mM	n.r <sup>a</sup>	93.82 $\mu\text{A}/\text{mM}$ $\text{cm}^2$	[173]
ChOx/TPU nano-fibre <sup>s</sup>	Colorimetric method	2 mM to 10 mM	2.0 mM	n.r <sup>a</sup>	[174]
AuNPs	LSPR	10 nM to 1 $\mu\text{M}$	25.5 nM	16.149 nm/ $\mu\text{M}$	[92]
AuNPs	LSPR	10 nM to 1 $\mu\text{M}$	53.1 nM	0.125%/mM	[156]
AuNPs/ ZnO-NPs (Probe-1: proposed sensor)	LSPR	0.1 mM to 10 mM	0.6161 mM	0.6898 nm/mM	This work
AuNPs/ ZnO-NPs (Probe-2)		0.1 mM to 10 mM	1.2777 mM	0.3319 nm/mM	
AuNPs/ ZnO-NPs (Probe-3)		1 mM to 10 mM	2.1748 mM	0.1976 nm/mM	

<sup>a</sup>not reported; <sup>b</sup>benzene dithiol; <sup>c</sup>surface enhanced Raman scattering; <sup>d</sup>chemical bath deposition; <sup>e</sup>thermoplastic polyurethane.

urea, glucose, D-Gal, AA, and Cho are used to check the selectivity of Probe-1 and -2. The Probe-1 shows a higher specificity towards Cho detection than that of Probe-2.

## 6.5 Summary

The practical realization and experimental validation of proposed SMS/MPM (core mismatch) structure-based OFSs are reported in this study. The comparative study of Cho sensor over previous studies is presented in Table 6.2. Nanocoating materials used in the present work such as ZnO-NPs and AuNPs are reported as highly biocompatible, and antibacterial materials [175]. In proposed sensors, the chemical etching technique has been adopted to etch out the waist and immobilized it with AuNPs and ZnO-NPs. The focus of the work presented in this chapter is on the application of different NPs in the development of a novel Cho sensor, using lightwave technology. The salient features and uniqueness of the present work are stated below:

- i. A fiber-optic-based LSPR sensor is reported for sensing Cho. It is designed by the coating with different sizes of AuNPs i.e. 10 nm and 30 nm followed by ZnO-NPs and further functionalized with a ChOx.
- ii. AuNPs are widely used in bio-nanotechnology applications due to their distinctive features like multiple surface functionalities, conductivity, and output signals falling in detectable range (properties widely employed for diagnostics). ZnO-NPs are also used in experiments due to their high performance and reliability in health products.
- iii. The use of AuNPs and ZnO-NPs has resulted in an enhancement in sensitivity. This is due to the inherent properties of AuNPs and ZnO-NPs, such as large surface area or high porosity.
- iv. Metal NPs are in great demand for use in biosensing applications because of strong absorption bands in the visible and NIR.

The superior performance of the developed Cho sensors over various sensing parameters makes it a powerful candidate for real-time medical diagnostics.

# **Chapter 7**

## **Development of Uric Acid Sensor using SMSMS-MZI Structure-based Optical Fiber Sensor Probe**

## 7.1 Introduction

Chapter 6 explains about fabrication and experimental validation of SMS/ MPM hetero-core structure-based P-OFSs for the detection of Cho. Also, brief information on the binding of NMs i.e., AuNPs and ZnO-NPs, and specific applications in biosensing field are discussed. The development of AgNPs and CuO-NPs nanocoated hetero-core SMSMS design-based P-OFSs for the detection of uric acid (UA) is discussed in this chapter. The normal range of UA in serum is reported as 100  $\mu$ M- 400  $\mu$ M, whereas in urine it is 1.5 mM- 4.4 mM [176]. Balance of UA is very important for normal functioning of the physiological system. Deficiency of UA in human body leads to range of disorders/ diseases including metastatic cancer, bone marrow disorders, indication of gout, diabetes, hypoparathyroidism, anconi syndrome, and leukemia whereas, surplus amount of UA in human body leads to the formation of kidney stones [177]. In recent times, P-OFSs are applied to a variety of applications such as strain measurement, chemical detection, gas detection, environmental monitoring, structural, vibration tests, food safety, pressure measurement, and biomolecules detection [20]. Many of the P-OFSs suffer from a narrow range of measurement. To mitigate this problem various hetero-core structure-based P-OFSs have been proposed. On the other hand, proposed SMSMS design-based P-OFSs are applied in multipurpose applications i.e., detection of UA available with human serum and urine. This structure is also known as the In-line-MZI structure. Nowadays, In-line MZI-OFSs are largely replacing the conventional MZI based sensors, and being employed in ultrafast optical signal processing applications [178]. Various methods, such as fluorescence, electrochemical, enzymatic process, optical, and chromatography techniques are reported in past for the detection of UA [179]. Among these, optical methods such as SPR and LSPR were used for the measurement of different analytes including UA. The proposed UA sensor has many attractive features which include a wide measurement range, less fabrication cost, label-free detection, remote monitoring, and ease of structural design. The details of UA sensor such as experimental methodology (sensor design, synthesis of NMs, nanocoating and functionalization process), characterization and measurement procedure, and performance of UA sensor are thoroughly presented in following sections.

## 7.2 Experimental Methodology

The experimental details in the development of UA sensor probe viz. sensor design and design considerations, synthesis of AgNPs, and CuO-NPs, Nano-coating process, and functionalization process are briefly discussed in following sub-sections.

### 7.2.1 Sensor Fabrication and Design Consideration

The UA sensors reported previously and available in open literature, suffer from a narrow range of measurement. To overcome this problem, a novel SMSMS optical fiber structure-based LSPR sensor is proposed in this study. The above optical design based on two different configurations i.e. Probe-1 (SMSMS/CuO-NPs/P-OFSs) and Probe-2 (SMSMS/CuO/AgNPs/P-OFSs) is developed and presented in this chapter. The combination of MMF (62.5/125  $\mu\text{m}$ ), and SMF (9/125  $\mu\text{m}$ ) along with NMs such as CuO-NPs and AgNPs are used in the fabrication of UA sensor probes. The proposed structure contains two MMF sections and three SMF sections which are joined together as shown in Fig. 7.1. The length of embedded MMF1, SMF2, and MMF2 sections (sandwiched between SMF1 and SMF3 sections) are 12 mm, 30 mm, and 12 mm, respectively. The MMF1 and MMF2 sections used in proposed SMSMS structure act as a splitter and combiner, respectively. The schematic of optical signal propagation through proposed SMSMS optical fiber design is also shown in Fig. 7.1.

### 7.2.2 Nanomaterial Realization, Immobilization, and Functionalization Process

The CuO-NPs and AgNPs immobilized UA sensor is designed and presented in this work. For this, different reagents such as HF, H<sub>2</sub>SO<sub>4</sub>, MPTMS, H<sub>2</sub>O<sub>2</sub>, EDC, MUA, NHS, NaBH<sub>4</sub>, L-Proline, urea, glycine, Cho, uricase (U0880-250UN, Sigma-Aldrich), UA (U2625-100G, Sigma-Aldrich), Copper-(II) Oxide Nanopowder (~50 nm), AA, D-Gal, glucose, L-Alanine (L-Ala),  $\beta$ -Cyclodextrin ( $\beta$ CD), and PBS (pH7.4) are used. The electrochemical method as described in Section 3.2.2 of Chapter-3 is adopted to synthesize AgNPs used for the development of proposed UA sensor. Further, colloidal CuO-NPs are prepared and deposited over AgNPs nanocoated probe. In this process, copper oxide Nano-powder and DI water have been mixed well using a

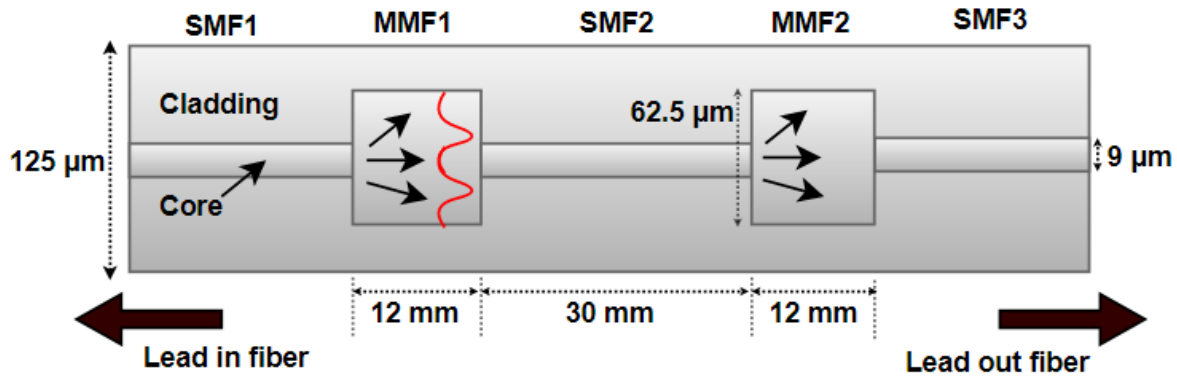


Figure 7.1: Schematic of optical signal propagation via. proposed structure [20] © 2020 IEEE.

magnetic stirrer. The high-power ultra-sonicator is used to make the suspension further homogeneous.

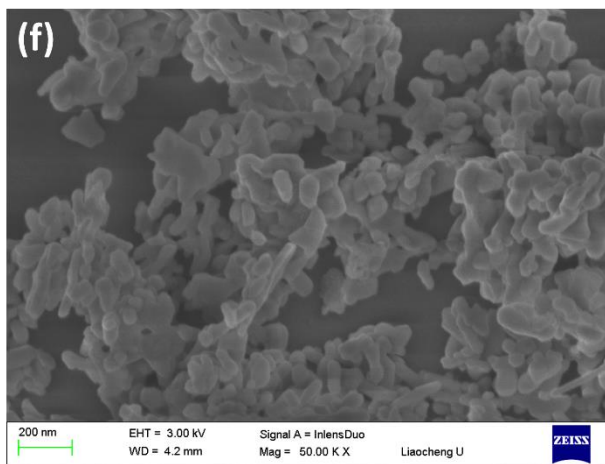
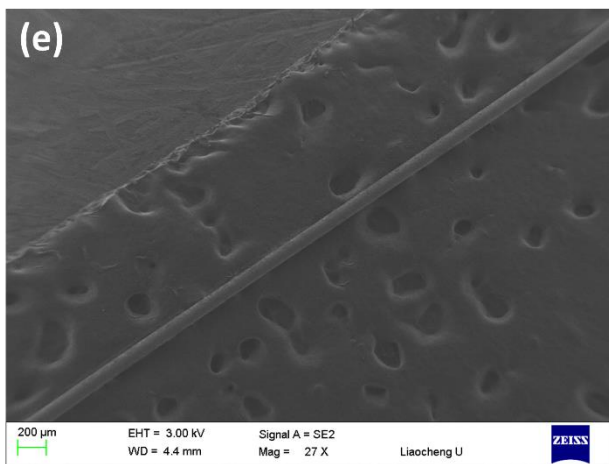
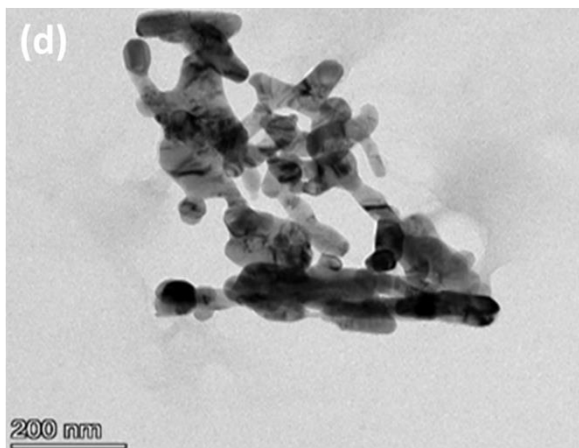
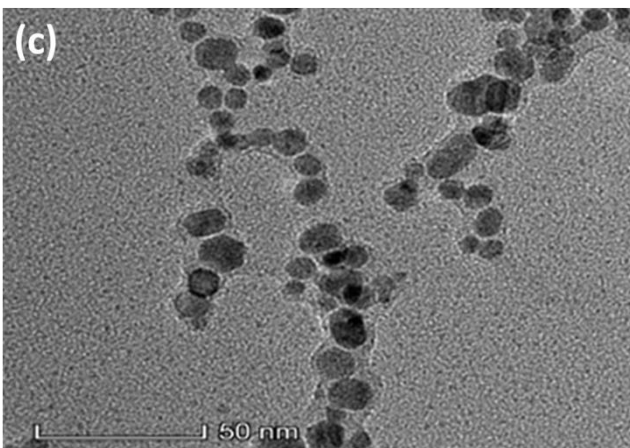
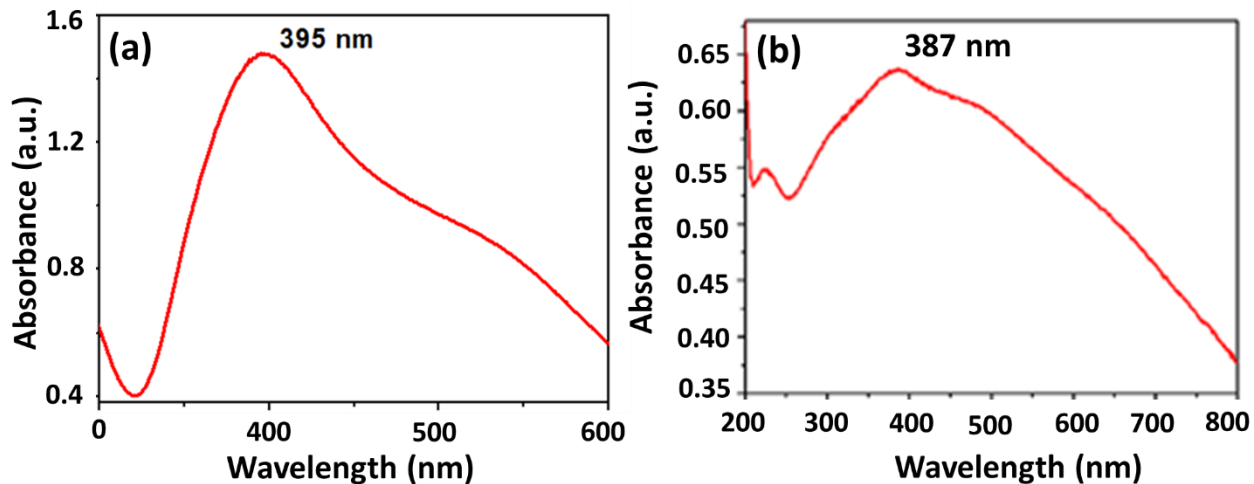
In nanocoating process, a bare probe is immobilized with AgNPs initially as described in Section 3.2.3 of Chapter-3. After the completion of AgNPs nanocoating, some residual toxic elements might have been left over the surface of sensor probe during the AgNPs synthesis using wet chemical method. This can affect the measurement of analytes and sensitivity. To mitigate this issue, AgNPs immobilized sensor probe is further nanocoated with CuO-NPs. For this, AgNPs immobilized probe is dipped (30 min) in prepared CuO-NPs solution and dried (6 min) at a temperature of 70°C. This is repeated thrice to ensure uniform and fine coating of CuO-NPs above the AgNPs nanocoated probe.

In next step, AgNPs and CuO-NPs immobilized probe is functionalized with uricase. For this, pre-enzyme functionalization process i.e., deposition of MUA (0.5 mM), NHS (50 mM), and EDC (200 mM) (to produces and activate the carboxylic group) are performed as reported in the ‘Experimental Methodology’ section (4.2.3) of Chapter 6. Later, this pre-functionalized probe is functionalized with uricase (0.137 mg/ml) [20].

### 7.3 Characterization and Measurement

The characterization results of AgNPs, CuO-NPs, and nanocoated probes are shown in Fig. 7.2. The characterization process is broadly distributed into two parts: i) characterization of NMs and ii) characterization of immobilized probe. In first part, absorbance spectra and morphology of

AgNPs and CuO-NPs are recorded using UV-Vis-spectroscopy, and HR-TEM respectively. The absorbance spectra of AgNPs and CuO-NPs are reported at 395 nm and 387 nm wavelength,



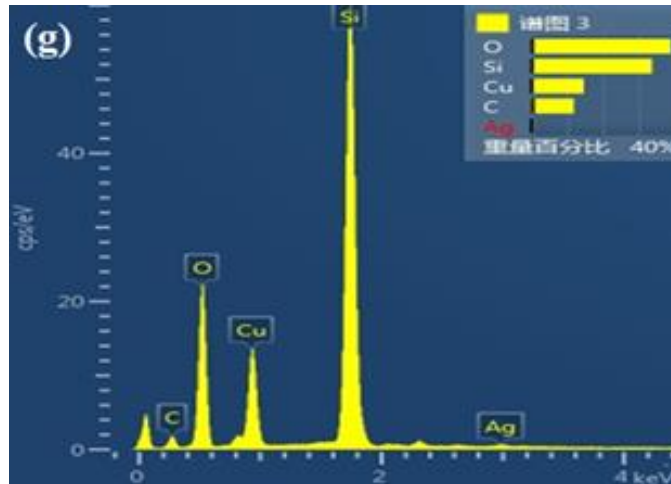


Figure 7.2: Absorbance spectrum of (a) AgNPs, and (b) CuO-NPs; HR-TEM image of (c) AgNPs, and (d) CuO-NPs; SEM image at (e) lower magnification, and (f) higher magnification; (g) EDS image [20] © 2020 IEEE.

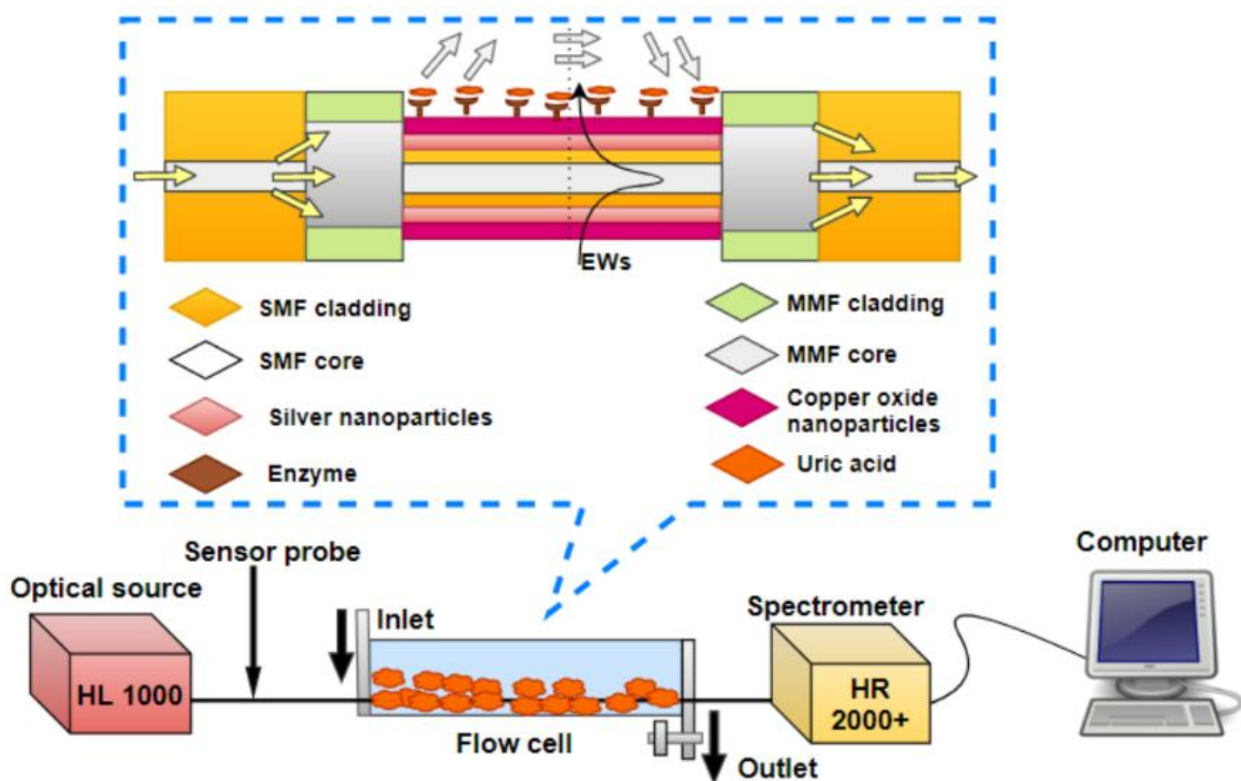


Figure 7.3: Schematic of a measurement setup for the detection of uric acid and enlarge view of sensor [20] © 2020 IEEE.

respectively. The mean approximate size of the spherical AgNPs is found to be  $7.5 \pm 0.5$  nm. In next part, NMs immobilized probes are characterized using SEM, and EDS. SEM images are obtained at lower magnification to check shape of the proposed sensor probes. Higher magnified

SEM image of nanocoated probe confirms the presence of uniform coating of the CuO-NPs, and AgNPs. Further, the characteristics of the nanocoating materials on sensor surface are confirmed using EDS analysis. The UA detection measurement setup is shown in Fig. 7.3. Wide-range of UA test samples are prepared in 10 nM - 10 mM range to check the performance of proposed UA sensors. This range of samples can well cover the normal range of UA available in both mentioned body fluids i.e., serum and urine. An optical source (300- 1800 nm) has been employed to generate the light signal and LSPR spectra are observed using an optical spectrometer.

## 7.4 Results and Discussion

### 7.4.1 Performance of Uric Acid Sensor

The measured performances of Probe-1 and -2 are presented here. The LSPR spectra and linearity plots are displayed in Fig. 7.4, and Fig. 7.5, respectively. To ensure the reliability of UA sensor, optical signal activity of testing response is measured at minimum of three cycles to plot the LSPR spectra and linearity plot. Following are the important observations with the two probes:

**Probe-1 (CuO-NPs/SMSMS/P-OFSs):** The results such as LSPR spectra and linearity plot of Probe-1 are presented in Fig. 7.4 (a), and Fig. 7.5 (a-b), respectively.

**For the serum sample:** linearity curve equation, sensitivity, *LoD* and correlation correlator are revealed as,

$$\lambda = 4.0303 C + 661.22 \quad (7.1)$$

4.0303 nm/ mM, 162.17  $\mu$ M, and 0.9539, respectively. In this equation C denotes the UA concentration.

**For the urine sample:** linearity curve equation, sensitivity, *LoD* and correlation correlator are revealed as,

$$\lambda = 0.6691 C + 662.35 \quad (7.2)$$

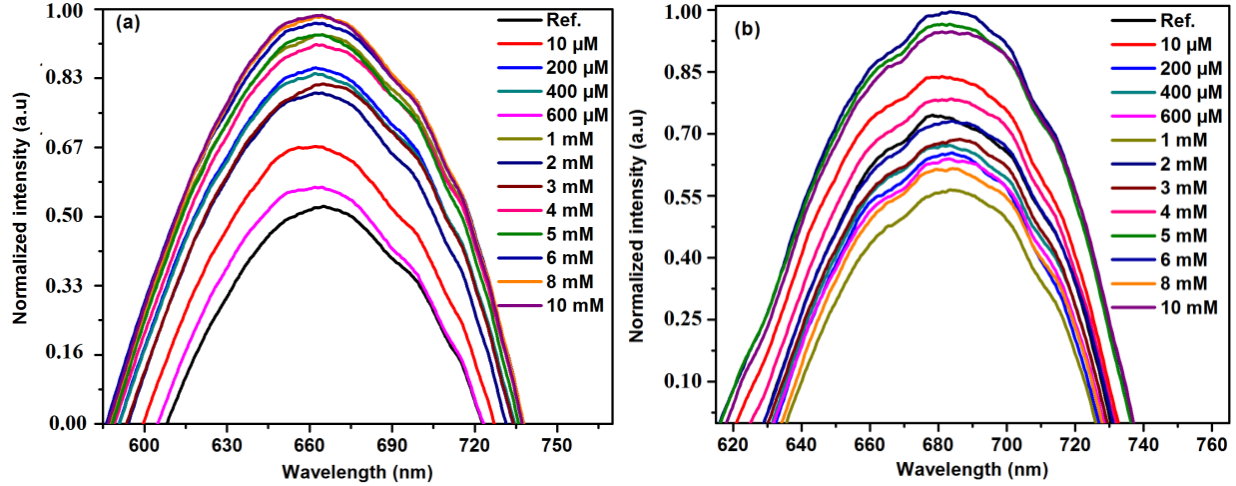


Figure 7.4: LSPR spectra for (a) Probe-1, and (b) Probe-2 [20] © 2020 IEEE.

0.6691 nm/ mM, 0.98 mM, and 0.9845, respectively.

**Probe-2 (CuO-NPs/AgNPs/SMSMS/P-OFSs):** The results such as LSPR spectra and linearity plot of Probe-2 are presented in Fig. 7.4 (b), and Fig. 7.5 (a-b), respectively.

**For the serum sample:** linearity curve equation, sensitivity, *LoD* and correlation correlator are revealed as,

$$\lambda = 6.1525 C + 675.67 \quad (7.3)$$

6.1525 nm/ mM, 69.26 μM, and 0.9439, respectively.

**For the urine sample:** linearity curve equation, sensitivity, *LoD* and correlation correlator are revealed as,

$$\lambda = 1.2322 C + 676.41 \quad (7.4)$$

1.2322 nm/mM, 0.35 mM, and 0.9695, respectively. Table 7.1 provides a comprehensive summary of Probe-1 and -2 results.

## 7.4.2 Reproducibility, Reusability, and Selectivity Test

The reproducibility and reusability, test results of projected UA probe are shown in Fig. 7.6. The reproducibility test is measured over 1 mM UA sample using three sensors each for both types of probes (Probe-1 and -2). Similarly, reusability test for Probe-1 is measured over 400 μM and 4

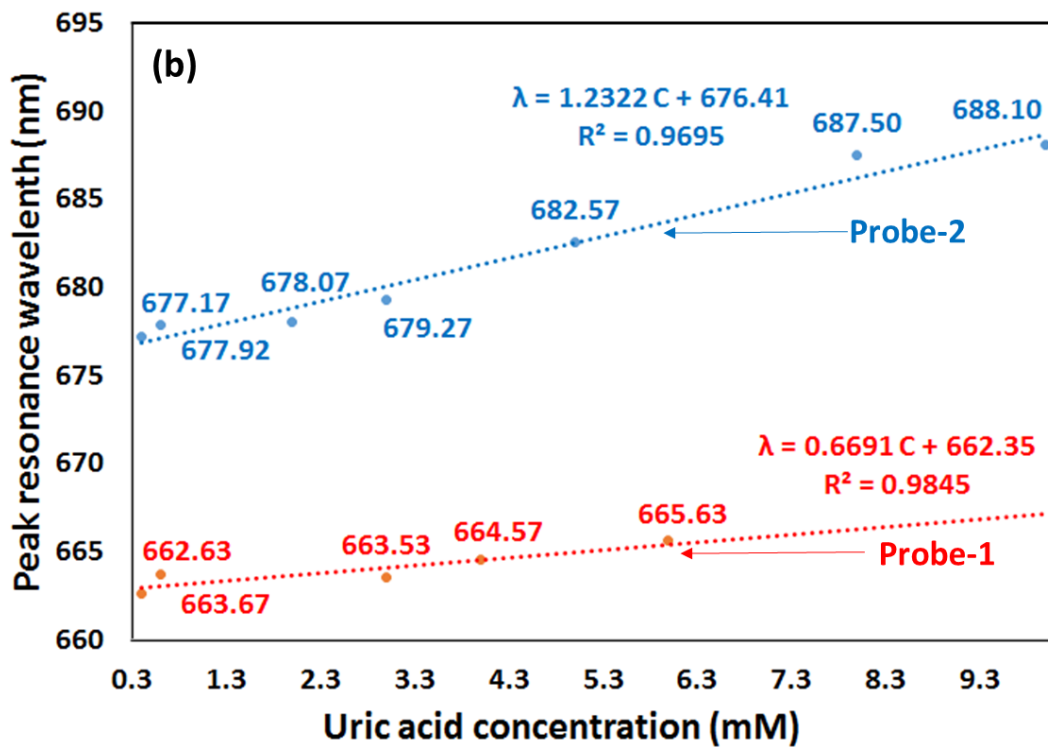
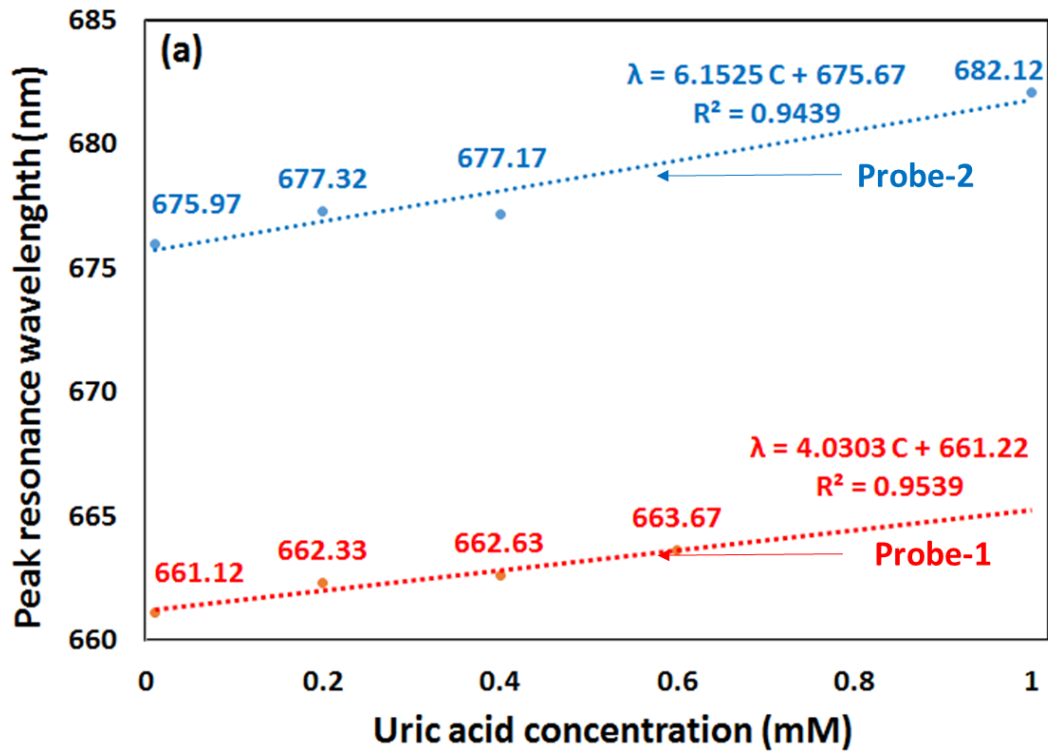


Figure 7.5: Linearity plot of uric acid sensor for (a) serum sample, and (b) urine sample [20] © 2020 IEEE.

Table 7.1  
Performance of proposed uric acid sensor [20] © 2020 *IEEE*

Parameters	Testing Sample	Probe-1	Probe-2
Linearity	Over the serum range	10 $\mu\text{M}$ to 600 $\mu\text{M}$	10 $\mu\text{M}$ to 1 mM
Correlation coefficient		0.9539	0.9439
<i>LoD</i>		162.17 $\mu\text{M}$	69.26 $\mu\text{M}$
Sensitivity		4.03 nm/mM	6.15 nm/mM
Linearity	Over the urine range	0.4 mM to 6 mM	0.4 mM to 10 mM
Correlation coefficient		0.9695	0.9845
<i>LoD</i>		0.98 mM	0.35 mM
Sensitivity		0.67 nm/mM	1.23 nm/mM

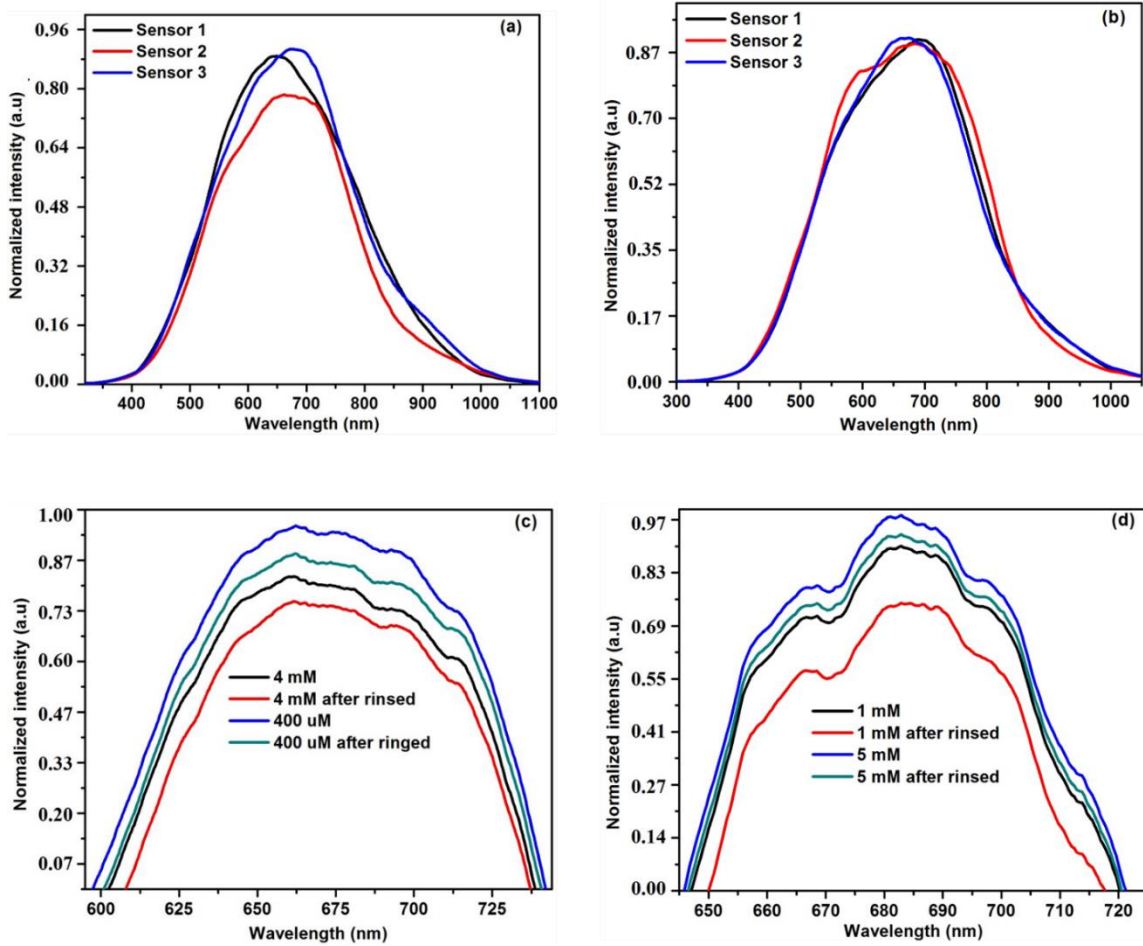


Figure 7.6: Reproducibility test for (a) Probe-1, (b) Probe-2; and reusability test for (c) Probe-1 (d) Probe-2 [20] © 2020 *IEEE*.

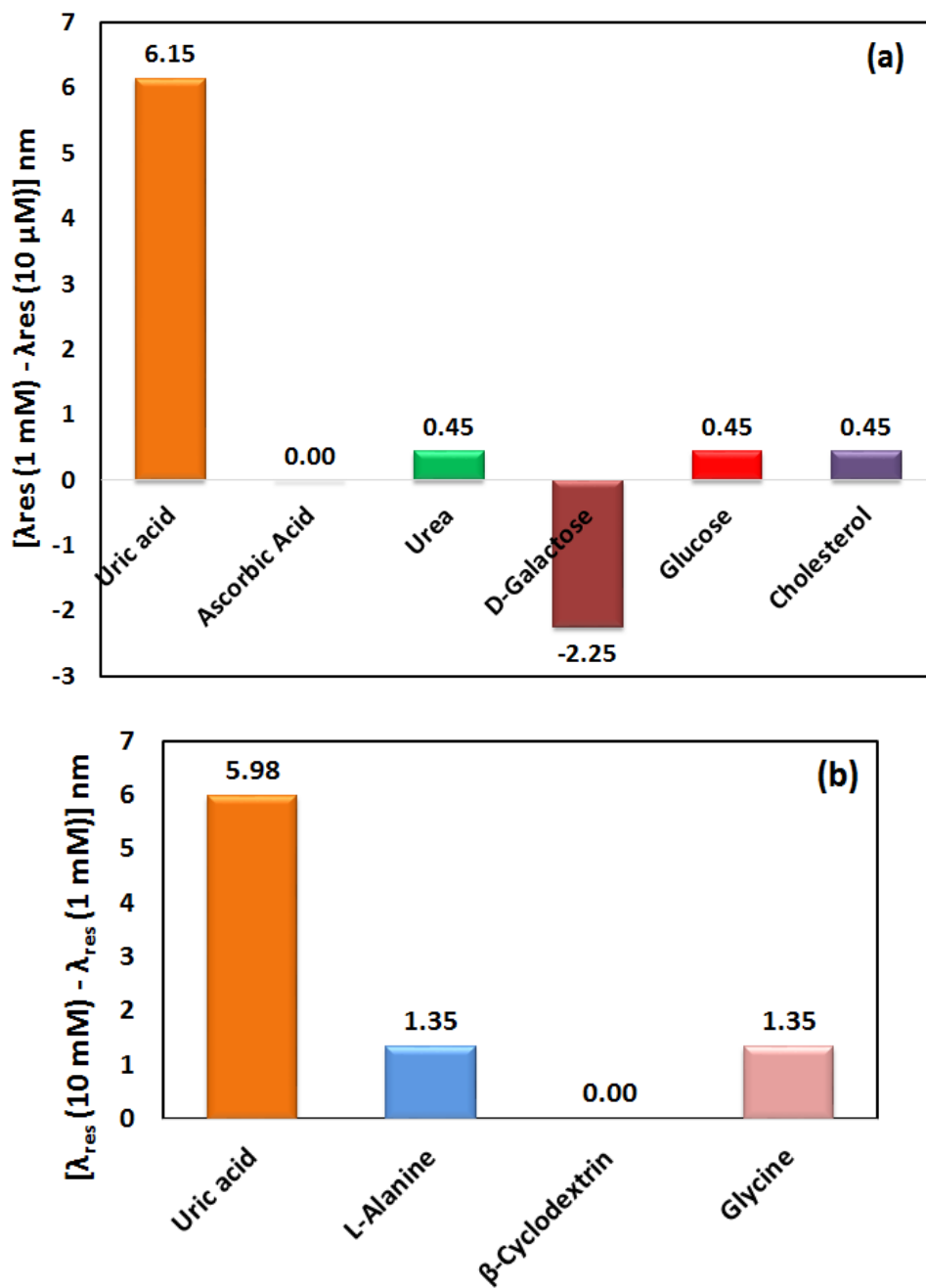


Figure 7.7: Selectivity test of probe-2 with (a) serum biomolecules, and (b) urine biomolecules [20] © 2020 IEEE.

mM UA samples, whereas in case of Probe-2 reusability is tested over 1 mM and 5 mM UA samples. After each experiment, UA probe is ringed with buffer solution and dried to eliminate the suspension of previous UA sample. The selectivity result of proposed sensor is revealed in Fig. 7.7. The selectivity test indicates the capability of the probe to detect the targeted biomolecule among the other available or interfering biomolecules in human body fluids. Here, biomolecules

including AA, D-Galactose, Urea, Glucose, Cho, and UA (different analytes presents in serum) are used to check the specificity of UA sensor. For this, wavelength shift is measured in case of 1 mM and 10  $\mu$ M concentration of each analyte. The difference between higher and lower peak wavelength for AA, Urea, D-Galactose, Glucose, Cho, and UA samples, have been observed as 0.00, 0.45, -2.25, 0.45, 0.45, and 6.15, respectively. This indicates the maximum value of shift for UA over different analytes presents in serum as shown in Fig. 7.7 (a). Similarly, biomolecules including Glycine,  $\beta$ -Cyclodextrin, L-Alanine, and UA (different analytes presents in serum) are used to check the specificity of UA sensor. The wavelength shift is measured in case of 10 mM and 1 mM concentration of each analyte. As in the previous case, here also the difference between higher and lower peak wavelength is calculated for Glycine,  $\beta$ -

Table 7.2  
Comparative study of uric acid sensors [20] © 2020 IEEE

Material	Method	Test sample	Linearity	LoD	Sensitivity	Ref.
Polyvinyl pyrrolidone-Ag	LSPR	Serum	0 to 50 $\mu$ M	5.00 $\mu$ M	n.r <sup>a</sup>	[180]
ZnO/Ag <sub>2</sub> O/Co <sub>3</sub> O <sub>4</sub>	Wet-chemical method	n.r <sup>a</sup>	0.1 nM to 10 $\mu$ M	n.r <sup>a</sup>	82.33 $\mu$ A $\mu$ M <sup>-1</sup> cm <sup>-2</sup>	[181]
Platform based on porous g-C <sub>3</sub> N <sub>4</sub> / multi-walled carbon nanotubes	Electrochemical method	Serum	0.2 $\mu$ M to 20 $\mu$ M	0.139 $\mu$ M	n.r <sup>a</sup>	[182]
Terbium (III)	Fluorescent method	n.r <sup>a</sup>	n.r <sup>a</sup>	0.028 $\mu$ M	n.r <sup>a</sup>	[183]
Cadmium	Fluorescent method	n.r <sup>a</sup>	125 $\mu$ M to 1000 $\mu$ M	125 $\mu$ M	n.r <sup>a</sup>	[184]
Poly (hydroxyethyl methacrylate methacryloyl)-Fe <sup>3+</sup>	SPR	n.r <sup>a</sup>	n.r <sup>a</sup>	0.247 mg/L	n.r <sup>a</sup>	[185]
Probe-1 (CuO-NPs/SMSMS/P-OFSs)	LSPR technique	Urine	0.4 mM to 6 mM	0.98 mM	0.67 nm/mM	This work
		Serum	10 $\mu$ M to 600 $\mu$ M	162.17 $\mu$ M	4.03 nm/mM	
Probe-2 (CuO-NPs/AgNPs/SMSMS/P-OFSs)		Urine	0.4 mM to 10 mM	0.35 mM	1.23 nm/mM	
		Serum	10 $\mu$ M to 1 mM	69.26 $\mu$ M	6.15 nm/mM	

<sup>a</sup>not reported.

Cyclodextrin, L-Alanine, and UA samples and have been observed as 1.35, 0.00, 1.35, and 5.98, respectively as shown in Fig. 7.7 (b). This also clearly indicates the maximum wavelength shift value for UA over different analytes present in urine.

## 7.5 Summary

This study reports the practical implementation of a newly designed optical fiber-based SMSMS probe for the measurement of UA concentration available with urine and serum of human body fluid. In reported sensors, chemical etching method is used to etch out the sensing part and immobilized it with CuO-NPs, and AgNPs. The mean diameter of AgNPs is reported as  $7.5 \pm 0.5$  nm used for immobilization process, a fine coating of lower size AgNPs provides improved sensitivity of probe. In addition, CuO-NPs are also immobilized over AgNPs nanocoated probe, which provides advantages viz. specific surface area, high biocompatibility, and low toxicity. The characterization instruments, namely SEM, HR-TEM, EDS, and UV-spectrophotometer are used for the characterization of AgNPs, CuO-NPs, and nanocoated probes. The immobilized probe is further functionalized with uricase enzyme. The results of proposed Probe-2 for the measurement of UA concentration available with serum such as *LoD*, sensitivity, and correlation correlator are observed as 69.26  $\mu\text{M}$ , 6.15 nm/mM, and 0.9439, respectively. Whereas results for the measurement of UA concentration available with urine such as *LoD*, sensitivity, and correlation correlator are observed as 0.35 mM, 1.23 nm/mM, and 0.9695, respectively. The above results show the improved performance of Probe-2 in comparison with Probe-1. The comparative studies for proposed UA sensors and other previously reported UA sensors available in open literature are presented in Table 7.2. In conclusion, proposed UA sensor probe exhibits great potential in biotechnology applications.

# **Chapter 8**

## **Conclusion and Future Scope**

## 8.1 Conclusion

In this thesis design, development, practical realization, and systematic characterization of new genre of LSPR phenomenon-based novel and efficient OFSs with great potential of detection of different analytes present in human body are presented. This chapter summarizes plasmonic phenomenon-based *in-vitro* sensing strategies and their perspectives for the future. In-depth study, experimental realization, and systematic characterization of the newly developed LSPR sensors for the detection/diagnosis of an array of important biomolecules available with bio-fluids in human body, such as Cho, DA, AA, UA, and L-Cys are successfully exhibited. Due to the enhancement in localized electromagnetic fields and exposure towards the surrounding medium, LSPR sensors are significantly attracted to bio-sensing applications [186]. Several new structures have been introduced to enhance the LSPR phenomenon. Advanced models and alterations, such as tapering, chemical etching, core mismatch, and hetero-core structure, have been particularly employed in development of the probes. Also, highly biocompatible NMs, such as AuNPs, AgNPs, ZnO-NPs, CuO-NPs, and GO are used. The superior performance of the projected sensors on various parameters, namely, linearity range, *LoD*, sensitivity, selectivity, CC, and reproducibility, make them powerful candidates for real-time biological monitoring. Different important observations and features of the realized sensor probes, distributed over five important chapters, as indicated below have been recorded in this thesis:

- i. The use of primary nanocoating NMs, such as AuNPs and AgNPs in plasmonic sensors has attracted remarkable attention, because of their exclusive chemical and physical properties. The features, like stability, low sintering temperatures, large surface area, biocompatibility, high field enhancements, high electrical conductivity, strong light absorbance, and scattering are of great significance in improving the biosensing phenomenon of proposed P-OFSs.
- ii. In the development of the DA sensor, AgNPs immobilized probe is further functionalized with polyether compound i.e., PEG. This polyether compound has a range of applications from medicine to industrial manufacturing. The PEG mainly helps to reduce protein absorption. It also protects the lipoplexes from interaction with blood components.

- iii. Further, in the development of proposed AA and L-Cys sensor, AgNPs/AuNPs nanocoated probes are coated with stealth material, like GO, synthesized using modified Hummer's method. The GO carries unique optical properties, such as excellent biocompatibility, high carrier mobility, and solubility. It also has a very high extraction capacity of biomolecules per unit area.
- iv. Similarly, in the development of Cho and UA sensors, AgNPs/AuNPs nanocoated probe was immobilized with ZnO-NPs/CuO-NPs. These materials are used due to their very low toxicity and offer various advantages, such as harmonic surface immobilization, robustness, higher biocompatibility, thermal resistance, long shelf life, and chemical stability.
- v. In all these cases AuNPs/AgNPs nanocoated probe is further immobilized/ functionalized with secondary material i.e., GO/ZnO-NPs/CuO-NPs/PEG. The use of primary NMs i.e. AuNPs/AgNPs is highly biocompatible. But these NMs are synthesized using conventional wet-reduction methods that may leave some toxic chemical species probe surface that may affect the sensitivity of sensor probes. Due to this in most cases, secondary material is immobilized/functionalized over the AuNPs/AgNPs nanocoated probe.
- vi. Different sizes of AuNPs were investigated and used in the development of Cho sensor. It can be observed that small size of AuNPs (10 nm) enhances the sensitivity and detection range.
- vii. The use of special fiber such as (Ge)-doped PSF in the development of Cho sensor, enhanced the sensing performance significantly. The PSF reveals distinct properties such as withstanding up to 300 - 400°C (applicable in a harsh environment), less attenuation (allows to be used in longer lengths), and a larger difference in core/cladding index. Due to these exceptional features, it is well suited for hydrophones, temperature sensing, FBG, strain sensing, geophones, biomedical sensing applications.
- viii. The proposed hetero-core-based optical fiber sensor designs such as SPS, MPM, and SMSMS structure enhance the LSPR phenomenon of sensor. In this technique propagating light waves might leak into the cladding layer and will suit for LSPR phenomenon.

There are various plasmonic phenomenon-based sensing techniques available and explored in past. In recent times, P-OFSs are found to be useful for biomedical diagnoses, drug discovery, and therapies, material analysis, and shaping, (bio) chemical sensing, and environmental monitoring applications. This study was aimed to address some of the most promising opportunities for LSPR phenomenon-based sensors in biosensing applications. These days, attention is paid to the formation of plasmon-enhanced NSs that produce potential applications in biosensing field. Increased sensitivity of plasmonic NSs changes their local dielectric environment leading to the introduction of new sensing strategies and systems. It is demonstrated that by regulating the size and shape of NMs in an immobilized surface, it is possible to enhance plasmonic phenomenon-based sensing. The emphasis is also placed on use of metallic and other novels NMs, which have been used to plasmonic enhancement of EMF, correlated with research methods. The innovations in the realization of plasmon NMs, immobilization of NMs, and expansion of extremely sensitive optical characterization tools are propelled mainly by advances in nanoscience, nanotechnology, and biotechnology. The different methods to Nano-structuring metals led to remarkable optical properties and functionality via management of the plasmon modes. In the field of bio-diagnostics, selectivity is an important parameter, and it is enhanced through functionalization layer. This layer is made up of a range of molecules that attract the specific protein.

## **8.2 Future Scope**

The design, development, practical realization, and characterization of an array of plasmatic sensors for biomedical applications are reported in this thesis. Thanks to the generality of the design approaches, proposed work and methodologies can be extended for designing various other important bio-sensors with improved performance for versatile applications. The packaging of newly developed sensors is also a very important area, which has a large potential for commercial applications like those of cholesterol sensor or pregnancy tester. Proposed work can also be extended into following futuristic research work and directions:

- The investigation and development of rapid, highly sensitive P-OFSs reported in the thesis can be further optimized for performance enhancement and validated for commercial applications.

- The current work can be extended for the synthesis of metallic NSs of various other shapes such as cubic, tripod, dendrites, hollow, etc.
- Investigation of the different NPs, nanoclusters, and nanosheets to enhance the performance of sensors can be explored.
- The prepared NSs and based sensors could be subjected to *in-vivo* sensing applications.
- In near future, research can be extended to the detection of pathogenic microorganisms and point-of-care applications.

Optimum configuration and modification of the proposed sensors to explore their possibility of working in hazardous and complex environments can be investigated.

## REFERENCES

- [1] P. Mehrotra, "Biosensors and their applications - A review," *Journal of oral biology and craniofacial research*, vol. 6, no. 2, pp. 153-159, May-Aug, 2016.
- [2] A. Hasan, M. Nurunnabi, M. Morshed, A. Paul, A. Polini, T. Kuila, M. Al Hariri, Y.-k. Lee, and A. A. Jaffa, "Recent Advances in Application of Biosensors in Tissue Engineering," *BioMed Research International*, vol. 2014, pp. 307519, 2014/08/06, 2014.
- [3] Y. Esfahani Monfared, "Overview of Recent Advances in the Design of Plasmonic Fiber-Optic Biosensors," *Biosensors*, vol. 10, no. 7, 2020.
- [4] R. Peltomaa, B. Glahn-Martínez, E. Benito-Peña, and M. C. Moreno-Bondi, "Optical Biosensors for Label-Free Detection of Small Molecules," *Sensors (Basel, Switzerland)*, vol. 18, no. 12, pp. 4126, 2018.
- [5] A. Kersey, and A. Dandridge, *Applications of Fiber-Optic Sensors*, 1989.
- [6] J.-F. Masson, "Portable and field-deployed surface plasmon resonance and plasmonic sensors," *Analyst*, vol. 145, no. 11, pp. 3776-3800, 2020.
- [7] S. Xing, N. Wallmeroth, K. W. Berendzen, and C. Grefen, "Techniques for the Analysis of Protein-Protein Interactions in Vivo," *Plant physiology*, vol. 171, no. 2, pp. 727-758, 2016.
- [8] A. Kussrow, C. S. Enders, and D. J. Bornhop, "Interferometric methods for label-free molecular interaction studies," *Analytical chemistry*, vol. 84, no. 2, pp. 779-792, 2012.
- [9] V. Semwal, and B. D. Gupta, "Experimental studies on the sensitivity of the propagating and localized surface plasmon resonance-based tapered fiber optic refractive index sensors," *Applied Optics*, vol. 58, no. 15, pp. 4149-4156, 2019/05/20, 2019.
- [10] X. Fan, I. M. White, S. I. Shopova, H. Zhu, J. D. Suter, and Y. Sun, "Sensitive optical biosensors for unlabeled targets: A review," *Analytica Chimica Acta*, vol. 620, no. 1, pp. 8-26, 2008/07/14/, 2008.
- [11] J. L. Hammond, N. Bhalla, S. D. Rafiee, and P. Estrela, "Localized surface plasmon resonance as a biosensing platform for developing countries," *Biosensors*, vol. 4, no. 2, pp. 172-188, 2014.
- [12] S. Ray, G. Mehta, and S. Srivastava, "Label-free detection techniques for protein microarrays: prospects, merits and challenges," *Proteomics*, vol. 10, no. 4, pp. 731-748, 2010.
- [13] B. Wang, and Q. Wang, "Sensitivity-Enhanced Optical Fiber Biosensor Based on Coupling Effect Between SPR and LSPR," *IEEE Sensors Journal*, vol. 18, no. 20, pp. 8303-8310, 2018.
- [14] M. Li, S. K. Cushing, and N. Wu, "Plasmon-enhanced optical sensors: a review," *The Analyst*, vol. 140, no. 2, pp. 386-406, 2015.

- [15] A. Sharma, R. Jha, and B. Gupta, "Fiber-Optic Sensors Based on Surface Plasmon Resonance: A Comprehensive Review," *Sensors Journal, IEEE*, vol. 7, pp. 1118-1129, 09/01, 2007.
- [16] R. M. Measures, "Fiber-Optic-Based Smart Structures," *Encyclopedia of Physical Science and Technology (Third Edition)*, R. A. Meyers, ed., pp. 769-802, New York: Academic Press, 2003.
- [17] P. Roriz, S. Silva, O. Frazão, and S. Novais, "Optical Fiber Temperature Sensors and Their Biomedical Applications," *Sensors*, vol. 20, no. 7, 2020.
- [18] N. Bhalla, P. Jolly, N. Formisano, and P. Estrela, "Introduction to biosensors," *Essays in biochemistry*, vol. 60, no. 1, pp. 1-8, 2016.
- [19] F. Jiang, Y. Jiang, H. Zhi, Y. Dong, H. Li, S. Ma, Y. Wang, Q. Dong, H. Shen, and Y. Wang, "Artificial intelligence in healthcare: past, present and future," *Stroke and Vascular Neurology*, vol. 2, no. 4, pp. 230, 2017.
- [20] N. Agrawal, C. Saha, C. Kumar, R. Singh, B. Zhang, and S. Kumar, "Development of Uric Acid Sensor Using Copper Oxide and Silver Nanoparticles Immobilized SMSMS Fiber Structure-Based Probe," *IEEE Transactions on Instrumentation and Measurement*, vol. 69, no. 11, pp. 9097-9104, 2020.
- [21] X.-d. Wang, and O. S. Wolfbeis, "Fiber-Optic Chemical Sensors and Biosensors (2015–2019)," *Analytical Chemistry*, vol. 92, no. 1, pp. 397-430, 2020/01/07, 2020.
- [22] M. E. Bosch, A. J. R. Sánchez, F. S. Rojas, and C. B. Ojeda, "Recent Development in Optical Fiber Biosensors," *Sensors (Basel, Switzerland)*, vol. 7, no. 6, pp. 797-859, 2007.
- [23] M. E. Stewart, C. R. Anderton, L. B. Thompson, J. Maria, S. K. Gray, J. A. Rogers, and R. G. Nuzzo, "Nanostructured Plasmonic Sensors," *Chemical Reviews*, vol. 108, no. 2, pp. 494-521, 2008/02/01, 2008.
- [24] C. Caucheteur, T. Guo, and J. Albert, "Review of plasmonic fiber optic biochemical sensors: Improving the limit of detection," *Analytical and bioanalytical chemistry*, vol. 407, 01/24, 2015.
- [25] L. Tong, H. Wei, S. Zhang, and H. Xu, "Recent Advances in Plasmonic Sensors," *Sensors (Basel, Switzerland)*, vol. 14, pp. 7959-73, 05/01, 2014.
- [26] S. Zeng, D. Baillargeat, H.-P. Ho, and K.-T. Yong, "Nanomaterials enhanced surface plasmon resonance for biological and chemical sensing applications," *Chemical Society Reviews*, vol. 43, pp. 3426-3452, 08/18, 2014.
- [27] T. Chung, S. Y. Lee, E. Y. Song, H. Chun, and B. Lee, "Plasmonic nanostructures for nano-scale bio-sensing," *Sensors (Basel)*, vol. 11, no. 11, pp. 10907-29, 2011.
- [28] K. Tiwari, S. C. Sharma, and N. Hozhabri, "High performance surface plasmon sensors: Simulations and measurements," *Journal of Applied Physics*, vol. 118, no. 9, pp. 093105, 2015/09/07, 2015.

- [29] M. Yang, W. Cai, Y. Wang, M. Sun, and G. Shang, "Orientation-and polarization-dependent optical properties of the single Ag nanowire/glass substrate system excited by the evanescent wave," *Scientific Reports*, vol. 6, no. 1, pp. 25633, 2016/05/09, 2016.
- [30] Y. Tang, X. Zeng, and J. Liang, "Surface Plasmon Resonance: An Introduction to a Surface Spectroscopy Technique," *J Chem Educ*, vol. 87, no. 7, pp. 742-746, Jul, 2010.
- [31] W. M. Mullett, E. P. Lai, and J. M. Yeung, "Surface plasmon resonance-based immunoassays," *Methods*, vol. 22, no. 1, pp. 77-91, Sep, 2000.
- [32] C. Li, Z. Li, S. Li, Y. Zhang, B. Sun, Y. Yu, H. Ren, S. Jiang, and W. Yue, "LSPR optical fiber biosensor based on a 3D composite structure of gold nanoparticles and multilayer graphene films," *Opt Express*, vol. 28, no. 5, pp. 6071-6083, Mar 2, 2020.
- [33] A. K. Sharma, A. K. Pandey, and B. Kaur, "A Review of advancements (2007–2017) in plasmonics-based optical fiber sensors," *Optical Fiber Technology*, vol. 43, pp. 20-34, 2018/07/01/, 2018.
- [34] J. Kiss, Á. Kukovecz, and Z. Kónya, "Beyond Nanoparticles: The Role of Sub-nanosized Metal Species in Heterogeneous Catalysis," *Catalysis Letters*, vol. 149, no. 6, pp. 1441-1454, 2019/06/01, 2019.
- [35] L. B. Sagle, L. K. Ruvuna, J. A. Ruummele, and R. P. Van Duyne, "Advances in localized surface plasmon resonance spectroscopy biosensing," *Nanomedicine (Lond)*, vol. 6, no. 8, pp. 1447-62, Oct, 2011.
- [36] Y. Chen, and H. Ming, "Review of Surface Plasmon Resonance and Localized Surface Plasmon Resonance Sensor," *Photonic Sensors*, vol. 2, 03/01, 2012.
- [37] B. Lee, J. H. Park, J. Y. Byun, J. H. Kim, and M. G. Kim, "An optical fiber-based LSPR aptasensor for simple and rapid in-situ detection of ochratoxin A," *Biosens Bioelectron*, vol. 102, pp. 504-509, Apr 15, 2018.
- [38] N. Agrawal, B. Zhang, C. Saha, C. Kumar, B. K. Kaushik, and S. Kumar, "Development of Dopamine Sensor using Silver Nanoparticles and PEG - Functionalized Tapered Optical Fiber Structure," *IEEE Transactions on Biomedical Engineering*, pp. 1-1, 2019.
- [39] J.-E. Park, J. Kim, and J.-M. Nam, "Emerging plasmonic nanostructures for controlling and enhancing photoluminescence," *Chemical Science*, vol. 8, no. 7, pp. 4696-4704, 2017.
- [40] D. Viegas, J. Goicoechea, J. Santos, F. Araújo, L. Ferreira, F. Arregui, and I. Matias, "Sensitivity Improvement of a Humidity Sensor Based on Silica Nanospheres on a Long-Period Fiber Grating," *Sensors (Basel, Switzerland)*, vol. 9, pp. 519-27, 01/16, 2009.
- [41] E. Petryayeva, and U. J. Krull, "Localized surface plasmon resonance: Nanostructures, bioassays and biosensing—A review," *Analytica Chimica Acta*, vol. 706, no. 1, pp. 8-24, 2011/11/07/, 2011.

- [42] K. A. Willets, and R. P. Van Duyne, "Localized Surface Plasmon Resonance Spectroscopy and Sensing," *Annual Review of Physical Chemistry*, vol. 58, no. 1, pp. 267-297, 2007/05/01, 2007.
- [43] N. Agrawal, B. Zhang, C. Saha, C. Kumar, X. Pu, and S. Kumar, "Ultra-Sensitive Cholesterol Sensor Using Gold and Zinc-Oxide Nanoparticles Immobilized Core Mismatch MPM/SPS Probe," *Journal of Lightwave Technology*, vol. 38, no. 8, pp. 2523-2529, 2020.
- [44] S. Kumar, R. Singh, Q. Yang, S. Cheng, B. Zhang, and B. K. Kaushik, "Highly Sensitive, Selective and Portable Sensor Probe using Germanium-Doped Photosensitive Optical Fiber for Ascorbic Acid Detection," *IEEE Sensors Journal*, pp. 1-1, 2020.
- [45] A. Borne, T. Katsura, C. Félix, B. Doppagne, P. Segonds, K. Bencheikh, J. A. Levenson, and B. Boulanger, "Anisotropy analysis of third-harmonic generation in a germanium-doped silica optical fiber," *Optics Letters*, vol. 40, no. 6, pp. 982-985, 2015/03/15, 2015.
- [46] L. Bao, X. Dong, P. P. Shum, and C. Shen, "Temperature Sensor by Using Highly Germanium-doped Fiber," *OSA Technical Digest*. p. W4L.3.
- [47] K. M. Mayer, and J. H. Hafner, "Localized Surface Plasmon Resonance Sensors," *Chemical Reviews*, vol. 111, no. 6, pp. 3828-3857, 2011/06/08, 2011.
- [48] H. Qian, S. Anwer, G. Bharath, S. Iqbal, and L. Chen, "Nanoporous Ag-Au Bimetallic Triangular Nanoprisms Synthesized by Galvanic Replacement for Plasmonic Applications," *Journal of Nanomaterials*, vol. 2018, pp. 1263942, 2018/06/27, 2018.
- [49] B. D. Gupta, and R. K. Verma, "Surface Plasmon Resonance-Based Fiber Optic Sensors: Principle, Probe Designs, and Some Applications," *Journal of Sensors*, vol. 2009, pp. 979761, 2009/08/11, 2009.
- [50] S. Mourdikoudis, R. M. Pallares, and N. T. K. Thanh, "Characterization techniques for nanoparticles: comparison and complementarity upon studying nanoparticle properties," *Nanoscale*, vol. 10, no. 27, pp. 12871-12934, 2018.
- [51] A. Kumar, and C. K. Dixit, "3 - Methods for characterization of nanoparticles," *Advances in Nanomedicine for the Delivery of Therapeutic Nucleic Acids*, S. Nimesh, R. Chandra and N. Gupta, eds., pp. 43-58: Woodhead Publishing, 2017.
- [52] D. R. Baer, M. H. Engelhard, G. E. Johnson, J. Laskin, J. Lai, K. Mueller, P. Munusamy, S. Thevuthasan, H. Wang, N. Washton, A. Elder, B. L. Baisch, A. Karakoti, S. V. N. T. Kuchibhatla, and D. Moon, "Surface characterization of nanomaterials and nanoparticles: Important needs and challenging opportunities," *Journal of vacuum science & technology. A, Vacuum, surfaces, and films : an official journal of the American Vacuum Society*, vol. 31, no. 5, pp. 50820-50820, 2013.

- [53] N. R. Mohamad, N. H. C. Marzuki, N. A. Buang, F. Huyop, and R. A. Wahab, "An overview of technologies for immobilization of enzymes and surface analysis techniques for immobilized enzymes," *Biotechnology, biotechnological equipment*, vol. 29, no. 2, pp. 205-220, 2015.
- [54] S. Ajami, and F. Teimouri, "Features and application of wearable biosensors in medical care," *Journal of research in medical sciences : the official journal of Isfahan University of Medical Sciences*, vol. 20, no. 12, pp. 1208-1215, 2015.
- [55] S. Patel, R. Nanda, S. Sahoo, and E. Mohapatra, "Biosensors in Health Care: The Milestones Achieved in Their Development towards Lab-on-Chip-Analysis," *Biochemistry research international*, vol. 2016, pp. 3130469-3130469, 2016.
- [56] A. B. Socorro-Leránóz, D. Santano, I. Del Villar, and I. R. Matias, "Trends in the design of wavelength-based optical fibre biosensors (2008–2018)," *Biosensors and Bioelectronics: X*, vol. 1, pp. 100015, 2019/06/01/, 2019.
- [57] H. H. Nguyen, S. H. Lee, U. J. Lee, C. D. Fermin, and M. Kim, "Immobilized Enzymes in Biosensor Applications," *Materials (Basel, Switzerland)*, vol. 12, no. 1, pp. 121, 2019.
- [58] N. A. Kozitsina, S. T. Svalova, N. N. Malysheva, V. A. Okhokhonin, B. M. Vidrevich, and Z. K. Brainina, "Sensors Based on Bio and Biomimetic Receptors in Medical Diagnostic, Environment, and Food Analysis," *Biosensors*, vol. 8, no. 2, 2018.
- [59] N. Verma, and G. Kaur, "Chapter 2 - Trends on Biosensing Systems for Heavy Metal Detection," *Comprehensive Analytical Chemistry*, V. Scognamiglio, G. Rea, F. Arduini and G. Palleschi, eds., pp. 33-71: Elsevier, 2016.
- [60] Y. Wang, N. S. Reddy Satyavolu, and Y. Lu, "Sequence-specific control of inorganic nanomaterials morphologies by biomolecules," *Current Opinion in Colloid & Interface Science*, vol. 38, pp. 158-169, 2018/11/01/, 2018.
- [61] V. Juvé, M. F. Cardinal, A. Lombardi, A. Crut, P. Maioli, J. Pérez-Juste, L. M. Liz-Marzán, N. Del Fatti, and F. Vallée, "Size-Dependent Surface Plasmon Resonance Broadening in Nonspherical Nanoparticles: Single Gold Nanorods," *Nano Letters*, vol. 13, no. 5, pp. 2234-2240, 2013/05/08, 2013.
- [62] M. Wan, P. Luo, J. Jin, J. Xing, Z. Wang, and S. T. C. Wong, "Fabrication of localized surface plasmon resonance fiber probes using ionic self-assembled gold nanoparticles," *Sensors (Basel, Switzerland)*, vol. 10, no. 7, pp. 6477-6487, 2010.
- [63] B. Sepúlveda, P. C. Angelomé, L. M. Lechuga, and L. M. Liz-Marzán, "LSPR-based nanobiosensors," *Nano Today*, vol. 4, no. 3, pp. 244-251, 2009/06/01/, 2009.
- [64] M. Grzelczak, J. Pérez-Juste, P. Mulvaney, and L. M. Liz-Marzán, "Shape control in gold nanoparticle synthesis," *Chemical Society Reviews*, vol. 37, no. 9, pp. 1783-1791, 2008.

- [65] E. L. Anquillare, O. D. Miller, C. W. Hsu, B. G. DeLacy, J. D. Joannopoulos, S. G. Johnson, and M. Soljačić, “Efficient, designable, and broad-bandwidth optical extinction via aspect-ratio-tailored silver nanodisks,” *Optics Express*, vol. 24, no. 10, pp. 10806-10816, 2016/05/16, 2016.
- [66] P. Colson, C. Henrist, and R. Cloots, “Nanosphere Lithography: A Powerful Method for the Controlled Manufacturing of Nanomaterials,” *Journal of Nanomaterials*, vol. 2013, 10/22, 2013.
- [67] A. N. Pisarenko, W. U. Spindel, R. T. Taylor, J. D. Brown, J. A. Cox, and G. E. Pacey, “Detection of ozone gas using gold nanoislands and surface plasmon resonance,” *Talanta*, vol. 80, no. 2, pp. 777-780, 2009/12/15/, 2009.
- [68] G. Gupta, D. Tanaka, Y. Ito, D. Shibata, M. Shimojo, K. Furuya, K. Mitsui, and K. Kajikawa, “Absorption spectroscopy of gold nanoisland films: Optical and structural characterization,” *Nanotechnology*, vol. 20, pp. 025703, 02/01, 2009.
- [69] W. Rechberger, A. Hohenau, A. Leitner, J. R. Krenn, B. Lamprecht, and F. R. Aussenegg, “Optical properties of two interacting gold nanoparticles,” *Optics Communications*, vol. 220, no. 1, pp. 137-141, 2003/05/01/, 2003.
- [70] L. Singh, G. Zhu, R. Singh, B. Zhang, W. Wang, B. K. Kaushik, and S. Kumar, “Gold Nanoparticles and Uricase Functionalized Tapered Fiber Sensor for Uric Acid Detection,” *IEEE Sensors Journal*, vol. 20, no. 1, pp. 219-226, 2020.
- [71] Y. Mustapha Kamil, M. H. Abu Bakar, M. A. Mustapa, M. H. Yaacob, N. H. Z. Abidin, A. Syahir, H. J. Lee, and M. A. Mahdi, “Label-free Dengue E protein detection using a functionalized tapered optical fiber sensor,” *Sensors and Actuators B: Chemical*, vol. 257, pp. 820-828, 2018/03/01/, 2018.
- [72] S. K. Srivastava, V. Arora, S. Sapra, and B. D. Gupta, “Localized Surface Plasmon Resonance-Based Fiber Optic U-Shaped Biosensor for the Detection of Blood Glucose,” *Plasmonics*, vol. 7, no. 2, pp. 261-268, 2012/06/01, 2012.
- [73] Q. Wang, and Y. Liu, “Review of optical fiber bending/curvature sensor,” *Measurement*, vol. 130, pp. 161-176, 2018/12/01/, 2018.
- [74] M. Zhao, L. Dai, N. Zhong, Z. Wang, M. Chen, B. Li, B. Luo, B. Tang, S. Shi, T. Song, and X. Zou, “Wet etching technique for fabrication of a high-quality plastic optical fiber sensor,” *Appl Opt*, vol. 56, no. 31, pp. 8845-8850, Nov 1, 2017.
- [75] Q. Wang, and Y. Liu, “Optical fiber curvature sensor based on MMF-SCF-MMF structure,” *Optical Fiber Technology*, vol. 43, pp. 1-5, 2018/07/01/, 2018.
- [76] R. Tabassum, and B. D. Gupta, “Influence of Oxide Overlayer on the Performance of a Fiber Optic SPR Sensor With Al/Cu Layers,” *IEEE Journal of Selected Topics in Quantum Electronics*, vol. 23, no. 2, pp. 81-88, 2017.

- [77] S. Kumar, R. Singh, G. Zhu, Q. Yang, X. Zhang, S. Cheng, B. Zhang, B. K. Kaushik, and F. Liu, "Development of Uric Acid Biosensor Using Gold Nanoparticles and Graphene Oxide Functionalized Micro-Ball Fiber Sensor Probe," *IEEE Transactions on NanoBioscience*, vol. 19, no. 2, pp. 173-182, 2020.
- [78] Y. M. Kamil, M. H. A. Bakar, M. H. Yaacob, A. Syahir, H. N. Lim, and M. A. Mahdi, "Dengue E Protein Detection Using a Graphene Oxide Integrated Tapered Optical Fiber Sensor," *IEEE Journal of Selected Topics in Quantum Electronics*, vol. 25, no. 1, pp. 1-8, 2019.
- [79] A. Baliyan, S. P. Usha, B. D. Gupta, R. Gupta, and E. K. Sharma, "Localized surface plasmon resonance-based fiber-optic sensor for the detection of triacylglycerides using silver nanoparticles," *J Biomed Opt*, vol. 22, no. 10, pp. 1-10, Oct, 2017.
- [80] S. Korposh, S. W. James, S.-W. Lee, and R. P. Tatam, "Tapered Optical Fibre Sensors: Current Trends and Future Perspectives," *Sensors (Basel, Switzerland)*, vol. 19, no. 10, pp. 2294, 2019.
- [81] Y. Tian, W. Wang, N. Wu, X. Zou, and X. Wang, "Tapered optical fiber sensor for label-free detection of biomolecules," *Sensors (Basel)*, vol. 11, no. 4, pp. 3780-90, 2011.
- [82] J. Cao, H. Tu, T. Sun, and K. Grattan, "Wavelength-based localized surface plasmon resonance optical fiber biosensor," *Sensors and Actuators B: Chemical*, vol. 181, pp. 611-619, 05/01, 2013.
- [83] P. Savaliya, and A. Dhawan, "Tapered fiber nanoprobe: plasmonic nanopillars on tapered optical fiber tips for large EM enhancement," *Opt Lett*, vol. 41, no. 19, pp. 4582-4585, Oct 1, 2016.
- [84] K. Hsu, N. Chen, S. Chou, S. Liaw, Y. Lai, and S. Chi, "Bandpass Filter With Variable Bandwidth Based on a Tapered Fiber With External Polymer Cladding," *IEEE Photonics Technology Letters*, vol. 21, no. 13, pp. 935-937, 2009.
- [85] Z. Yu, L. Jin, L.-P. Sun, J. Li, Y. Ran, and B.-O. Guan, "Highly Sensitive Fiber Taper Interferometric Hydrogen Sensors," *IEEE Photonics Journal*, vol. 8, pp. 1-1, 01/01, 2015.
- [86] Q. Liu, Y. Liu, H. Yuan, J. Wang, J. Guang, and W. Peng, "Smartphone based LSPR biosensor." pp. 1-3.
- [87] W. Putzbach, and N. J. Ronkainen, "Immobilization techniques in the fabrication of nanomaterial-based electrochemical biosensors: a review," *Sensors (Basel, Switzerland)*, vol. 13, no. 4, pp. 4811-4840, 2013.
- [88] Q. Zhang, C. Xue, Y. Yuan, J. Lee, D. Sun, and J. Xiong, "Fiber Surface Modification Technology for Fiber-Optic Localized Surface Plasmon Resonance Biosensors," *Sensors (Basel, Switzerland)*, vol. 12, pp. 2729-41, 12/01, 2012.
- [89] S. Srivastava, R. Verma, and B. Gupta, "Surface plasmon resonance based fiber optic sensor for the detection of low water content in ethanol," *Sensors and Actuators B: Chemical*, vol. 153, pp. 194-198, 03/31, 2011.

- [90] S. Unser, I. Bruzas, J. He, and L. Sagle, "Localized Surface Plasmon Resonance Biosensing: Current Challenges and Approaches," *Sensors (Basel)*, vol. 15, no. 7, pp. 15684-716, Jul 2, 2015.
- [91] L. Singh, R. Singh, B. Zhang, B. K. Kaushik, and S. Kumar, "Localized Surface Plasmon Resonance Based Hetero-Core Optical Fiber Sensor Structure for the Detection of L-Cysteine," *IEEE Transactions on Nanotechnology*, vol. 19, pp. 201-208, 2020.
- [92] S. Kumar, R. Singh, B. K. Kaushik, N. Chen, Q. S. Yang, and X. Zhang, "LSPR-Based Cholesterol Biosensor Using Hollow Core Fiber Structure," *IEEE Sensors Journal*, vol. 19, no. 17, pp. 7399-7406, 2019.
- [93] C.-W. Wu, C.-Y. Chiang, C.-H. Chen, C.-S. Chiang, C.-T. Wang, and L.-K. Chau, "Self-referencing fiber optic particle plasmon resonance sensing system for real-time biological monitoring," *Talanta*, vol. 146, pp. 291-298, 2016/01/01/, 2016.
- [94] C. Zhou, H. Zou, M. Li, C. Sun, D. Ren, and Y. Li, "Fiber optic surface plasmon resonance sensor for detection of E. coli O157:H7 based on antimicrobial peptides and AgNPs-rGO," *Biosens Bioelectron*, vol. 117, pp. 347-353, Oct 15, 2018.
- [95] S. Kaushik, U. K. Tiwari, S. S. Pal, and R. K. Sinha, "Rapid detection of Escherichia coli using fiber optic surface plasmon resonance immunosensor based on biofunctionalized Molybdenum disulfide (MoS<sub>2</sub>) nanosheets," *Biosensors and Bioelectronics*, vol. 126, pp. 501-509, 2019/02/01/, 2019.
- [96] A. R. Camara, P. M. P. Gouvêa, A. C. M. S. Dias, A. M. B. Braga, R. F. Dutra, R. E. de Araujo, and I. C. S. Carvalho, "Dengue immunoassay with an LSPR fiber optic sensor," *Optics Express*, vol. 21, no. 22, pp. 27023-27031, 2013/11/04, 2013.
- [97] N. Omar, Y. W. Fen, J. Abdullah, C. Chik, and M. A. Mahdi, "Development of an optical sensor based on surface plasmon resonance phenomenon for diagnosis of dengue virus E -protein," *Sensing and Bio-Sensing Research*, vol. 20, 06/01, 2018.
- [98] S. Kaye, Z. Zeng, M. Sanders, K. Chittur, P. M. Koelle, R. Lindquist, U. Manne, Y. Lin, and J. Wei, "Label-free detection of DNA hybridization with a compact LSPR-based fiber-optic sensor," *Analyst*, vol. 142, no. 11, pp. 1974-1981, 2017.
- [99] W. Yang, J. Yu, X. Xi, Y. Sun, Y. Shen, W. Yue, C. Zhang, and S. Jiang, "Preparation of Graphene/ITO Nanorod Metamaterial/U-Bent-Annealing Fiber Sensor and DNA Biomolecule Detection," *Nanomaterials (Basel, Switzerland)*, vol. 9, no. 8, pp. 1154, 2019.
- [100] Z. Luo, Y. Wang, Y. Xu, X. Wang, Z. Huang, J. Chen, Y. Li, and Y. Duan, "Ultrasensitive U-shaped fiber optic LSPR cytosensing for label-free and in situ evaluation of cell surface N-glycan expression," *Sensors and Actuators B: Chemical*, vol. 284, pp. 582-588, 2019/04/01/, 2019.

- [101] H.-M. Kim, D. Hong Jeong, H.-Y. Lee, J.-H. Park, and S.-K. Lee, "Improved stability of gold nanoparticles on the optical fiber and their application to refractive index sensor based on localized surface plasmon resonance," *Optics & Laser Technology*, vol. 114, pp. 171-178, 2019/06/01/, 2019.
- [102] M. J. McGrath, and C. N. Scanail, "Sensing and Sensor Fundamentals," *Sensor Technologies: Healthcare, Wellness, and Environmental Applications*, M. J. McGrath and C. N. Scanail, eds., pp. 15-50, Berkeley, CA: Apress, 2013.
- [103] S. Unser, I. Bruzas, J. He, and L. Sagle, "Localized Surface Plasmon Resonance Biosensing: Current Challenges and Approaches," *Sensors (Basel, Switzerland)*, vol. 15, no. 7, pp. 15684-15716, 2015.
- [104] K. R. Ryu, and J. W. Ha, "Influence of shell thickness on the refractive index sensitivity of localized surface plasmon resonance inflection points in silver-coated gold nanorods," *RSC Advances*, vol. 10, no. 29, pp. 16827-16831, 2020.
- [105] B. A. Prabowo, A. Purwidyantri, and K.-C. Liu, "Surface Plasmon Resonance Optical Sensor: A Review on Light Source Technology," *Biosensors*, vol. 8, no. 3, pp. 80, 2018.
- [106] R. Trevethan, "Sensitivity, Specificity, and Predictive Values: Foundations, Plabilities, and Pitfalls in Research and Practice," *Frontiers in public health*, vol. 5, pp. 307-307, 2017.
- [107] N. Chen, M. Chang, X. Zhang, J. Zhou, X. Lu, and S. Zhuang, "Highly Sensitive Plasmonic Sensor Based on a Dual-Side Polished Photonic Crystal Fiber for Component Content Sensing Applications," *Nanomaterials*, vol. 9, no. 11, 2019.
- [108] I. E. Sendroiu, M. E. Warner, and R. M. Corn, "Fabrication of silica-coated gold nanorods functionalized with DNA for enhanced surface plasmon resonance imaging biosensing applications," *Langmuir : the ACS journal of surfaces and colloids*, vol. 25, no. 19, pp. 11282-11284, 2009.
- [109] I. Lieberman, G. Shemer, T. Fried, E. M. Kosower, and G. Markovich, "Plasmon-Resonance-Enhanced Absorption and Circular Dichroism," *Angewandte Chemie International Edition*, vol. 47, no. 26, pp. 4855-4857, 2008/06/16, 2008.
- [110] Z. Zhou, Z. Wang, Y. Tang, J. Gao, C. C. Zhang, and Q. Wang, "Multi-modal tracking dopamine using a hybrid inorganic-organic silver nanoparticle and its cellular imaging performance," *Journal of Luminescence*, vol. 204, pp. 394-400, 2018/12/01/, 2018.
- [111] S. Kumar, R. Singh, G. Zhu, Q. Yang, X. Zhang, S. Cheng, B. Zhang, B. K. Kaushik, and F. Liu, "Development of Uric Acid Biosensor Biosensor using Gold Nanoparticles and Graphene Oxide Functionalized Micro-Ball Fiber Sensor Probe," *IEEE Transactions on NanoBioscience*, pp. 1-1, 2019.

- [112] N. Shahbazi, and R. Zare-Dorabei, "Probe for sensitive direct determination of sulphide ions based on gold nanoparticles," *IET Nanobiotechnology*, vol. 12, no. 8, pp. 1140-1143, 2018.
- [113] V. Semwal, and B. D. Gupta, "LSPR- and SPR-Based Fiber-Optic Cholesterol Sensor Using Immobilization of Cholesterol Oxidase Over Silver Nanoparticles Coated Graphene Oxide Nanosheets," *IEEE Sensors Journal*, vol. 18, no. 3, pp. 1039-1046, 2018.
- [114] S. Kumar, B. K. Kaushik, R. Singh, N.-K. Chen, Q. S. Yang, X. Zhang, W. Wang, and B. Zhang, "LSPR-based cholesterol biosensor using a tapered optical fiber structure," *Biomedical Optics Express*, vol. 10, no. 5, pp. 2150-2160, 2019/05/01, 2019.
- [115] P. Dhara, R. Kumar, L. Binetti, H. T. Nguyen, L. S. Alwis, T. Sun, and K. T. V. Grattan, "Optical Fiber-Based Heavy Metal Detection Using the Localized Surface Plasmon Resonance Technique," *IEEE Sensors Journal*, vol. 19, no. 19, pp. 8720-8726, 2019.
- [116] Q. Yang, X. Zhang, S. Kumar, R. Singh, B. Zhang, C.-L. Bai, and X. Pu, "Development of Glucose Sensor Using Gold Nanoparticles and Glucose-Oxidase Functionalized Tapered Fiber Structure," *Plasmonics*, 12/17, 2019.
- [117] Q. Yang, G. Zhu, L. Singh, Y. Wang, R. Singh, B. Zhang, X. Zhang, and S. Kumar, "Highly sensitive and selective sensor probe using glucose oxidase/gold nanoparticles/graphene oxide functionalized tapered optical fiber structure for detection of glucose," *Optik*, vol. 208, pp. 164536, 2020/04/01/, 2020.
- [118] F. Wang, Y. Zhang, Z. Liu, H. Yuan, Z. Wu, D. Zhou, Z. Jing, and W. Peng, "Highly sensitive glucose detection using Au Nanoparticles based fiber optic SPR sensor," *OSA Technical Digest*. p. ThC5.
- [119] C. Zhang, J. Ren, J. Zhou, M. Cui, N. Li, B. Han, and Q. Chen, "Facile fabrication of a 3,4,9,10-perylene tetracarboxylic acid functionalized graphene-multiwalled carbon nanotube-gold nanoparticle nanocomposite for highly sensitive and selective electrochemical detection of dopamine," *Analyst*, vol. 143, no. 13, pp. 3075-3084, Jun 25, 2018.
- [120] V. Semwal, A. M. Shrivastav, R. Verma, and B. D. Gupta, "Surface plasmon resonance based fiber optic ethanol sensor using layers of silver/silicon/hydrogel entrapped with ADH/NAD," *Sensors and Actuators B: Chemical*, vol. 230, pp. 485-492, 2016/07/01/, 2016.
- [121] J. Lao, L. Han, Z. Wu, X. Zhang, Y. Huang, Y. Tang, and T. Guo, "Gold Nanoparticle-Functionalized Surface Plasmon Resonance Optical Fiber Biosensor: In Situ Detection of Thrombin With 1 n-M Detection Limit," *Journal of Lightwave Technology*, vol. 37, no. 11, pp. 2748-2755, 2019.

- [122] G. M. Shukla, N. Punjabi, T. Kundu, and S. Mukherji, "Optimization of Plasmonic U-Shaped Optical Fiber Sensor for Mercury Ions Detection Using Glucose Capped Silver Nanoparticles," *IEEE Sensors Journal*, vol. 19, no. 9, pp. 3224-3231, 2019.
- [123] B. R. Heidemann, I. Chiamenti, M. M. Oliveira, M. Muller, and J. L. Fabris, "Functionalized Long Period Grating—Plasmonic Fiber Sensor Applied to the Detection of Glyphosate in Water," *Journal of Lightwave Technology*, vol. 36, no. 4, pp. 863-870, 2018.
- [124] L. Singh, R. Singh, B. Zhang, S. Cheng, B. Kumar Kaushik, and S. Kumar, "LSPR based uric acid sensor using graphene oxide and gold nanoparticles functionalized tapered fiber," *Optical Fiber Technology*, vol. 53, pp. 102043, 2019/12/01/, 2019.
- [125] K. S. Korshunov, L. J. Blakemore, and P. Q. Trombley, "Dopamine: A Modulator of Circadian Rhythms in the Central Nervous System," *Frontiers in Cellular Neuroscience*, vol. 11, no. 91, 2017-April-03, 2017.
- [126] R. Mittal, L. H. Debs, A. P. Patel, D. Nguyen, K. Patel, G. O'Connor, M. h. Grati, J. Mittal, D. Yan, A. A. Eshraghi, S. K. Deo, S. Daunert, and X. Z. Liu, "Neurotransmitters: The Critical Modulators Regulating Gut-Brain Axis," *Journal of cellular physiology*, vol. 232, no. 9, pp. 2359-2372, 2017.
- [127] H. Juárez Olguín, D. Calderón Guzmán, E. Hernández García, and G. Barragán Mejía, "The Role of Dopamine and Its Dysfunction as a Consequence of Oxidative Stress," *Oxidative Medicine and Cellular Longevity*, vol. 2016, pp. 9730467, 2015/12/06, 2016.
- [128] S. Korposh, James, S.-W. Lee, and R. Tatam, "Tapered Optical Fibre Sensors: Current Trends and Future Perspectives," *Sensors*, vol. 19, pp. 2294, 05/17, 2019.
- [129] E. Petryayeva, and U. Krull, "Localized Surface Plasmon Resonance: Nanostructures, bioassays and Biosensing—A Review," *Analytica chimica acta*, vol. 706, pp. 8-24, 11/07, 2011.
- [130] N. Lou, R. Jha, J. L. Domínguez-Juárez, V. Finazzi, J. Villatoro, G. Badenes, and V. Pruneri, "Embedded optical micro/nano-fibers for stable devices," *Optics Letters*, vol. 35, no. 4, pp. 571-573, 2010/02/15, 2010.
- [131] N. Agrawal, B. Zhang, C. Saha, C. Kumar, B. K. Kaushik, and S. Kumar, "Development of Dopamine Sensor Using Silver Nanoparticles and PEG-Functionalized Tapered Optical Fiber Structure," *IEEE Transactions on Biomedical Engineering*, vol. 67, no. 6, pp. 1542-1547, 2020.
- [132] H. Li, H. Li, F. Meng, X. Lou, and L. Zhu, "All-fiber MZI sensor based on seven-core fiber and fiber ball symmetrical structure," *Optics and Lasers in Engineering*, vol. 112, pp. 1-6, 2019/01/01/, 2019.
- [133] H. Hatakeyama, H. Akita, and H. Harashima, "The Polyethyleneglycol Dilemma: Advantage and Disadvantage of PEGylation of Liposomes for Systemic Genes and Nucleic Acids Delivery to Tumors," *Biological & pharmaceutical bulletin*, vol. 36, pp. 892-899, 06/01, 2013.

- [134] J.-W. Shin, J. Yoon, M. Shin, and J.-W. Choi, "Electrochemical Dopamine Biosensor Composed of Silver Encapsulated MoS<sub>2</sub> Hybrid Nanoparticle," *Biotechnology and Bioprocess Engineering*, vol. 24, no. 1, pp. 135-144, 2019/02/01, 2019.
- [135] D. S. Kim, E. S. Kang, S. Baek, S. S. Choo, Y. H. Chung, D. Lee, J. Min, and T. H. Kim, "Electrochemical detection of dopamine using periodic cylindrical gold nanoelectrode arrays," *Sci Rep*, vol. 8, no. 1, pp. 14049, Sep 19, 2018.
- [136] P. Suresh Kumar, S. Megarajan, G. Rajendra Kumar Reddy, and V. Anbazhagan, "Facile synthesis of gold nanoparticles using carbon dots for electrochemical detection of neurotransmitter, dopamine in human serum and as a chemocatalyst for nitroaromatic reduction," *IET Nanobiotechnol*, vol. 12, no. 7, pp. 909-914, Oct, 2018.
- [137] E. Kazuma, and T. Tatsuma, "Localized surface plasmon resonance sensors based on wavelength-tunable spectral dips," *Nanoscale*, vol. 6, no. 4, pp. 2397-2405, 2014.
- [138] E. B. Kurutas, "The importance of antioxidants which play the role in cellular response against oxidative/nitrosative stress: current state," *Nutrition journal*, vol. 15, no. 1, pp. 71-71, 2016.
- [139] J.-H. Heo, H. Lee, and K.-M. Lee, "The Possible Role of Antioxidant Vitamin C in Alzheimer's Disease Treatment and Prevention," *American journal of Alzheimer's disease and other dementias*, vol. 28, 01/09, 2013.
- [140] F. Chiavaioli, F. Baldini, S. Tombelli, C. Trono, and A. Giannetti, "Biosensing with optical fiber gratings," *Nanophotonics*, vol. 6, no. 4, pp. 663-679, 2017.
- [141] R. Bogue, "Fibre optic sensors: A review of today's applications," *Sensor Review*, vol. 31, pp. 304-309, 09/13, 2011.
- [142] S. Kumar, R. Singh, Q. Yang, S. Cheng, B. Zhang, and B. K. Kaushik, "Highly Sensitive, Selective and Portable Sensor Probe Using Germanium-Doped Photosensitive Optical Fiber for Ascorbic Acid Detection," *IEEE Sensors Journal*, vol. 21, no. 1, pp. 62-70, 2021.
- [143] M. Soliman, P. del Pino, W. Parak, and B. Pelaz, "Synthesis and Surface Engineering of Gold Nanoparticles, and Their Potential Applications in Bionanotechnology," 2017.
- [144] A. T. Smith, A. M. LaChance, S. Zeng, B. Liu, and L. Sun, "Synthesis, properties, and applications of graphene oxide/reduced graphene oxide and their nanocomposites," *Nano Materials Science*, vol. 1, no. 1, pp. 31-47, 2019/03/01/, 2019.
- [145] G. Zhu, N. Agrawal, R. Singh, S. Kumar, B. Zhang, C. Saha, and C. Kumar, "A novel periodically tapered structure-based gold nanoparticles and graphene oxide – Immobilized optical fiber sensor to detect ascorbic acid," *Optics & Laser Technology*, vol. 127, pp. 106156, 2020/07/01/, 2020.

- [146] R. Shukla, V. Bansal, A. Basu, R. Bhonde, and M. Sastry, "Biocompatibility of Gold Nanoparticles and Their Endocytotic Fate Inside the Cellular Compartment: A Microscopic Overview," *Langmuir : the ACS journal of surfaces and colloids*, vol. 21, pp. 10644-54, 12/01, 2005.
- [147] A. Sabir, M. Wasim, M. Shafiq, and T. Jamil, "Chapter 14 - Carbon Nanotube and Graphene Oxide Based Membranes," *Nanoscale Materials in Water Purification*, S. Thomas, D. Pasquini, S.-Y. Leu and D. A. Gopakumar, eds., pp. 361-381: Elsevier, 2019.
- [148] D. Yue, Y. Huang, J. Zhang, X. Zhang, Y. Cui, Y. Yang, and G. Qian, "A Two-Dimensional Metal–Organic Framework as a Fluorescent Probe for Ascorbic Acid Sensing," *European Journal of Inorganic Chemistry*, vol. 2018, no. 2, pp. 173-177, 2018/01/23, 2018.
- [149] C. Mu, H. Lu, J. Bao, and Q. Zhang, "Visual colorimetric 'turn-off' biosensor for ascorbic acid detection based on hypochlorite-3,3',5,5',-Tetramethylbenzidine system," *Spectrochim Acta A Mol Biomol Spectrosc*, vol. 201, pp. 61-66, Aug 5, 2018.
- [150] L. Fu, Y.-H. Zheng, and Z.-X. Fu, "Ascorbic acid amperometric sensor using a graphene-wrapped hierarchical TiO<sub>2</sub> nanocomposite," *Chemical Papers*, vol. 69, no. 5, pp. 655-661, 2015.
- [151] M. Ganiga, and J. Cyriac, "An ascorbic acid sensor based on cadmium sulphide quantum dots," *Analytical and Bioanalytical Chemistry*, vol. 408, no. 14, pp. 3699-3706, 2016/05/01, 2016.
- [152] Y. Wang, Y. Yang, W. Liu, F. Ding, P. Zou, X. Wang, Q. Zhao, and H. Rao, "A carbon dot-based ratiometric fluorometric and colorimetric method for determination of ascorbic acid and of the activity of ascorbic acid oxidase," *Microchimica Acta*, vol. 186, no. 4, pp. 246, 2019/03/16, 2019.
- [153] Y.-C. Ko, T.-L. Lin, C.-T. Yeh, N.-K. Sun, J.-J. Shyue, G.-Y. Liu, S.-W. Chou, Y.-C. Liu, C.-H. Hsu, and M.-L. Ho, "Silver nanoprism-based paper as a ratiometric sensor for extending biothiol detection in serum," *New Journal of Chemistry*, vol. 41, no. 24, pp. 15120-15126, 2017.
- [154] G. Rushworth, and I. Megson, "Existing and potential therapeutic uses for N-acetylcysteine: The need for conversion to intracellular glutathione for antioxidant benefits," *Pharmacology & therapeutics*, vol. 141, 09/27, 2013.
- [155] E. Klantsataya, P. Jia, H. Ebendorff-Heidepriem, T. M. Monroe, and A. François, "Plasmonic Fiber Optic Refractometric Sensors: From Conventional Architectures to Recent Design Trends," *Sensors*, vol. 17, no. 1, 2017.
- [156] S. Kumar, B. K. Kaushik, R. Singh, N. K. Chen, Q. S. Yang, X. Zhang, W. Wang, and B. Zhang, "LSPR-based cholesterol biosensor using a tapered optical fiber structure," *Biomed Opt Express*, vol. 10, no. 5, pp. 2150-2160, May 1, 2019.
- [157] N. Agrawal, C. Saha, C. Kumar, R. Singh, B. Zhang, R. Jha, and S. Kumar, "Detection of L-Cysteine Using Silver Nanoparticles and Graphene Oxide Immobilized Tapered SMS Optical Fiber Structure," *IEEE Sensors Journal*, vol. 20, no. 19, pp. 11372-11379, 2020.

- [158] I. Sanskriti, and K. K. Upadhyay, "Cysteine, homocysteine and glutathione guided hierarchical self-assemblies of spherical silver nanoparticles paving the way for their naked eye discrimination in human serum," *New Journal of Chemistry*, vol. 41, no. 11, pp. 4316-4321, 2017.
- [159] Q. Xiao, L. Zhang, and C. Lu, "Resonance light scattering technique for simultaneous determination of cysteine and homocysteine using fluorosurfactant-capped gold nanoparticles," *Sensors and Actuators B: Chemical*, vol. 166-167, pp. 650-657, 2012/05/20/, 2012.
- [160] P. K. Sudeep, S. T. S. Joseph, and K. G. Thomas, "Selective Detection of Cysteine and Glutathione Using Gold Nanorods," *Journal of the American Chemical Society*, vol. 127, no. 18, pp. 6516-6517, 2005/05/01, 2005.
- [161] C. Lu, and Y. Zu, "Specific detection of cysteine and homocysteine: recognizing one-methylene difference using fluorosurfactant-capped gold nanoparticles," *Chemical Communications*, no. 37, pp. 3871-3873, 2007.
- [162] K. Watanabe, K. Tajima, and Y. Kubota, "Macrobending characteristics of hetero-core splice fiber optic sensor for displacement and liquid detection," *IEICE Trans. Electron.*, vol. E83-C, 03/01, 2000.
- [163] K. Takagi, and K. Watanabe, "Near Infrared Characterization of Hetero-Core Optical Fiber SPR Sensors Coated with Ta<sub>2</sub>O<sub>5</sub> Film and Their Applications," *Sensors*, vol. 12, no. 2, 2012.
- [164] "Cholesterol," *Clinical Veterinary Advisor*, J. Mayer and T. M. Donnelly, eds., pp. 613-614, Saint Louis: W.B. Saunders, 2013.
- [165] K. Bhowmik, and G.-D. Peng, "Polymer Optical Fibers," pp. 1-51, 2019.
- [166] T. Osuch, A. Anuszkiewicz, K. Markowski, A. Filipkowski, D. Pysz, R. Kasztelan, R. Stepień, M. Klimczak, and R. Buczyński, "Inscription of Bragg gratings in nanostructured graded index single-mode fibers," *Optics Express*, vol. 27, no. 10, pp. 13721-13733, 2019/05/13, 2019.
- [167] R. Sardar, and J. S. Shumaker-Parry, "Spectroscopic and microscopic investigation of gold nanoparticle formation: ligand and temperature effects on rate and particle size," *J Am Chem Soc*, vol. 133, no. 21, pp. 8179-90, Jun 1, 2011.
- [168] M. Grzelczak, J. Perez-Juste, P. Mulvaney, and L. M. Liz-Marzan, "Shape control in gold nanoparticle synthesis," *Chem Soc Rev*, vol. 37, no. 9, pp. 1783-91, Sep, 2008.
- [169] J. D. Wilton-Ely, "The surface functionalisation of gold nanoparticles with metal complexes," *Dalton Trans*, no. 1, pp. 25-9, Jan 7, 2008.
- [170] J. Shah, R. Purohit, R. Singh, A. S. Karakoti, and S. Singh, "ATP-enhanced peroxidase-like activity of gold nanoparticles," *Journal of Colloid and Interface Science*, vol. 456, pp. 100-107, 2015/10/15/, 2015.

- [171] H. V. Xu, Y. Zhao, and Y. N. Tan, "Nanodot-Directed Formation of Plasmonic-Fluorescent Nanohybrids toward Dual Optical Detection of Glucose and Cholesterol via Hydrogen Peroxide Sensing," *ACS Applied Materials & Interfaces*, vol. 11, no. 30, pp. 27233-27242, 2019/07/31, 2019.
- [172] X. Jiang, Z. Tan, L. Lin, J. He, C. He, B. D. Thackray, Y. Zhang, and J. Ye, "Surface-Enhanced Raman Nanoprobes with Embedded Standards for Quantitative Cholesterol Detection," *Small Methods*, vol. 2, no. 11, pp. 1800182, 2018/11/01, 2018.
- [173] J. Tang, Y. Lu, Z. Tseng, and S. Chu, "Growth of Dual-Layer Nanorods and Nanowalls Using Al Reaction Layer For Cholesterol Biosensor," *IEEE Sensors Journal*, vol. 17, no. 6, pp. 1584-1589, 2017.
- [174] S. Immanuel, V. Elakkiya, M. Alagappan, and R. Selvakumar, "Development of colorimetric cholesterol detection kit using TPU nanofibre/cellulose acetate membrane," *IET Nanobiotechnol*, vol. 12, no. 5, pp. 557-561, Aug, 2018.
- [175] H. Mohd Yusof, R. Mohamad, U. H. Zaidan, and N. A. Abdul Rahman, "Microbial synthesis of zinc oxide nanoparticles and their potential application as an antimicrobial agent and a feed supplement in animal industry: a review," *Journal of animal science and biotechnology*, vol. 10, pp. 57-57, 2019.
- [176] S. Jain, S. Verma, S. Singh, and S. Sharma, "An electrochemical biosensor based on novel butylamine capped CZTS nanoparticles immobilized by uricase for uric acid detection," *Biosensors & Bioelectronics*, vol. 127, pp. 135-141, 02/15, 2019.
- [177] M. A. Breshears, and A. W. Confer, "The Urinary System," *Pathologic Basis of Veterinary Disease*, pp. 617-681.e1, 2017.
- [178] D. Yuan, Y. Dong, Y. Liu, and T. Li, "Mach-Zehnder Interferometer Biochemical Sensor Based on Silicon-on-Insulator Rib Waveguide with Large Cross Section," *Sensors*, vol. 15, no. 9, 2015.
- [179] X. Chen, G. Wu, Z. Cai, M. Oyama, and X. Chen, "Advances in enzyme-free electrochemical sensors for hydrogen peroxide, glucose, and uric acid," *Microchimica Acta*, vol. 181, no. 7, pp. 689-705, 2014/06/01, 2014.
- [180] N. Misra, V. Kumar, L. Borde, and L. Varshney, "Localized surface plasmon resonance-optical sensors based on radiolytically synthesized silver nanoparticles for estimation of uric acid," *Sensors and Actuators B: Chemical*, vol. 178, pp. 371-378, 2013/03/01/, 2013.
- [181] M. M. Alam, A. M. Asiri, M. T. Uddin, M. A. Islam, M. R. Awual, and M. M. Rahman, "Detection of uric acid based on doped ZnO/Ag<sub>2</sub>O/Co<sub>3</sub>O<sub>4</sub> nanoparticle loaded glassy carbon electrode," *New Journal of Chemistry*, vol. 43, no. 22, pp. 8651-8659, 2019.

- [182] J. Lv, C. Li, S. Feng, S.-M. Chen, Y. Ding, C. Chen, Q. Hao, T.-H. Yang, and W. Lei, "A novel electrochemical sensor for uric acid detection based on PCN/MWCNT," *Ionics*, vol. 25, no. 9, pp. 4437-4445, 2019/09/01, 2019.
- [183] W. Qi, M. Zhao, Y. Fu, H. He, X. Tian, D. Wu, Y. Zhang, and P. P. Hu, "Fluorescent detection of uric acid through photoinduced electron transfer using luminol-terbium(III) nanoparticles synthesized via aggregation-induced fluorescence strategy," *Dyes and Pigments*, vol. 172, pp. 107797, 2020/01/01/, 2020.
- [184] N. E. Azmi, N. I. Ramli, J. Abdullah, M. A. Abdul Hamid, H. Sidek, S. Abd Rahman, N. Ariffin, and N. A. Yusof, "A simple and sensitive fluorescence based biosensor for the determination of uric acid using H<sub>2</sub>O<sub>2</sub>-sensitive quantum dots/dual enzymes," *Biosensors and Bioelectronics*, vol. 67, pp. 129-133, 2015/05/15/, 2015.
- [185] A. Göçenoğlu Sarıkaya, B. Osman, T. Çam, and A. Denizli, "Molecularly imprinted surface plasmon resonance (SPR) sensor for uric acid determination," *Sensors and Actuators B: Chemical*, vol. 251, pp. 763-772, 2017/11/01/, 2017.
- [186] Y.-C. Cheng, Y.-J. Chang, Y.-C. Chuang, B.-Z. Huang, and C.-C. Chen, "A plasmonic refractive index sensor with an ultrabroad dynamic sensing range," *Scientific Reports*, vol. 9, no. 1, pp. 5134, 2019/03/26, 2019.

# LIST OF PUBLICATIONS

## Papers in Refereed Journals

- I. N. Agrawal, L. Singh, C. Saha, C. Kumar, S. Kumar, "Developments of SPR/ LSPR Phenomenon Based Biosensors During 2015-2020: A Review and Present State of the Art", *Optics and Laser Technology (Elsevier)* (communicated- under review)
- II. N. Agrawal, C. Saha, C. Kumar, R. Singh, B. Zhang, S. Kumar, "Development of Uric Acid Sensor Using Copper Oxide/Silver – Nanoparticles Immobilized SMSMS Fiber-Based MZI Probe", *IEEE Transactions on Instrumentation and Measurement (TIM)*, vol. 69, issue 11, pp. 9097-9104, Nov 2020 (<https://doi.org/10.1109/TIM.2020.2998876>).
- III. N. Agrawal, C. Saha, C. Kumar, R. Singh, B. Zhang, R. Jha, S. Kumar, "Detection of L-Cysteine using Silver Nanoparticles and Graphene Oxide immobilized Tapered SMS Fiber Structure," *IEEE Sensors Journal*, vol. 20, issue 19, pp. 11372-11379, Oct 2020 (<https://doi.org/10.1109/JSEN.2020.2997690>).
- IV. G. Zhu, N. Agrawal, R. Singh, S. Kumar, B. Zhang, C. Saha, C. Kumar, "A novel periodically tapered structure-based gold nanoparticles and graphene oxide – Immobilized optical fiber sensor to detect ascorbic acid", *Optics & Laser Technology (Elsevier)*, vol. 127, p. 106156, 2020/07/01/ 2020 (<https://doi.org/10.1016/j.optlastec.2020.106156>).
- V. N. Agrawal, B. Zhang, C. Saha, C. Kumar, X. Pu, S. Kumar, "Ultra-Sensitive Cholesterol Sensor Using Gold and Zinc-Oxide Nanoparticles Immobilized Core Mismatch MPM/SPS Probe", *IEEE/OSA- Journal of Lightwave Technology (JLT)*, vol. 38, pp. 2523-2529, Feb 2020 (<https://doi.org/10.1109/JLT.2020.2974818>).

- VI. N. Agrawal, B. Zhang, C. Saha, C. Kumar, B. K. Kaushik, S. Kumar, “Development of Dopamine Sensor Using Silver Nanoparticles and PEG-Functionalized Tapered Optical Fiber Structure”, *IEEE Transactions on Biomedical Engineering (TBME)*, vol. 67, pp. 1542-1547, Sept 2019 (<https://doi.org/10.1109/TBME.2019.2939560>).